UNIVERSITY OF CALIFORNIA

Santa Barbara

High Q Terahertz Photonic Crystal Microcavities

A Dissertation submitted in partial satisfaction of the

requirements for the degree Doctor of Philosophy

in Physics

by

Cristo Manuel Yee Réndon

Committee in charge:

Professor Mark S. Sherwin, Chair

Professor S. James Allen

Professor Leon Balents

December 2009

The dissertation of Cristo Manuel Yee Rendon is approved.

Professor Leon Balents

Professor S. James Allen

Professor Mark S. Sherwin, Committee Chair

September 2009

High Q Terahertz Photonic Crystal Microcavities

To my parents:

Manuel Yee Gonzales

and

Manuela Rendon Sanchez

ACKNOWLEDGEMENTS

I like to start thanking my advisor Professor Mark S. Sherwin for his patience, support and resourceful guidance through all the five years that I worked under his supervision, for all the personal meeting in which he always no only encourage me but also point out the most efficient and elegant way to solve problems.

Then I would like to thanks the member of my committee, Dr. James Allen and Dr. Leon Balents for helping to improve my thesis project.

I also want to thanks my colleagues Nathan Jukam who him I work during my first year in the group and from whom I learned most of the fine details of clean room processing. Susumu Takahashi who has a extraordinary ability to completely construct an lab from the floor to the ceiling, and who makes a complicated subject looks simple. To Dominik Sther from who I learn that loot can be done in single afternoon if you know what you are doing. Also I would like to thank to Stephen Parham who help in the lab in work in which I am not particular patient.

I would like to thanks to the present and former members of my research group from who I spend quite nice lab time. Sangwoo Kim, Christopher Morris, Ben Zacks and Dan Allen. Also a very special mention to Dr. Louis Claude Brunel from whom I share my office but we also share a lot of good conversations from history to family issues an extraordinary experience I always will remember he shown that there is also a “Sueño Mexicano”. Special thanks to Michael Champion and George Kontsevich for proofreading my thesis.

Thanks to the undergrad students that worked with me during different research projects, Stephen Parham, Kayla Nguyen and George Kontsevich.

I want to thanks to Clean room staff, Jack Whaley, Luiz Zunuaga, Brian Thibeault and specially to Donald Freeborn for recovering my shatter samples from inside the etching chambers. Thanks to Physics machine shop staff Mike Deal, Mike Wrocklage and Jeff Dutter. Thanks to the FEL staff David Enhart and Gerry Ramian.

I would like to take a lot to the staff in the ITST, to chief Marlene Rifkin, to Kate Ferrian for it sweets moments. To Rita Makogon, Elizabeth Strait, Jose and Rob Marquez. To the staff member in the physics department, to Jennifer Farrar, Shilo Tucker and Kerri O'Connor. To the people at UC-MEXUS program Dr. Wendy DeBoer, Susana Hidalgo and Clara Quijano. And to the staff member at CONACYT Veronica Barrientos and Samuel Manterola.

I also want to thanks to the Mexican National Council of Science and Technology, to University of California Institute for Mexico and United States, to the National Science foundation and to Keck foundation for their generous support.

Thanks to Dr. Maximo Lopez Lopez my former adviser in Mexico City, to Dr. Juan Antonio Nieto Garcia my advisor as undergrad student. To Dr. Miguel Angel Perez Angon. Thanks to Hector Uriarte, Dr. Servando Aguirre, Dr. Maribel Loaiza and Carlos Valencia.

Finally but not least important I would like to thanks to persons to who I dedicated not only work but my life as well, to my parents Manuel Yee Gonzalez and Manuela Rendon Sanchez from wh always inspired me and push me forward, to my brothers and sisters Ana, Zumey, Bruce and Arturo Yee Rendon. To my grandparents Manuel Yee Lam, Ruperta Gonzalez, Bernabe Rendon and Julia Lopez. Thanks to my wife Lorena Ruiz de Yee who inspired me and help me to reach higher altitudes that I will definitively never will have done alone, and thanks to my beautiful daughter Sarah Sophia Yee Ruiz who changed my life completely and give me a powerful reason to complete my goals.

Thanks you all for helping me to the complete my academic education.

VITA OF CRISTO MANUEL YEE RENDON

September 2009

EDUCATION

September 1995 – August 2000

Bachelor of Sciences in Physics

School for Physics and Mathematics, Autonomus University of Sinaloa

Culiacan, Sinaloa, Mexico.

August 2000 – March 2003

Master of Sciences in Physics

Physics Department, Center for research and advanced studies, IPN.

Mexico City, Mexico.

March 2005 – September 2009

Doctor of Philosophy in Physics

Physics Department, University of California

Santa Barbara, California, USA.

PROFESSIONAL EMPLOYMENT

September 2003 – December 2004

Teaching Assistant

Department of Physics, University of California, Santa Barbara

December 2004 – September 2009

Graduate Student Researcher

Terahertz Dynamics and Quantum Information in Semiconductors Lab.,

Department of Physics and Institute for Terahertz Science and Technology,

University of California, Santa Barbara

PUBLICATIONS

[1] Cristo M. Yee and Mark S. Sherwin, "High-Q terahertz microcavities in silicon photonic crystal slabs.", *Applied Physics Letters*, vol. **94** , p. 154104 , (2009).

[2] Cristo Yee, Nathan Jukam, and Mark Sherwin, "Transmission of single mode ultrathin terahertz photonic crystal slabs.", *Applied Physics Letters*, vol. **91** , no. 19, pp. 194104-3, nov (2007).

[3] Nathan Jukam, Cristo Yee, Mark S. Sherwin, Ilya Fushman, and Jelena Vučković, "Patterned femtosecond laser excitation of terahertz leaky modes in GaAs photonic crystals.", *Applied Physics Letters*, vol. **89** , no. 241112, (2006).

[4] C. M. Yee-Rendón, A. Pérez-Centeno, M. Meléndez-Lira, G. González de la Cruz, M. López-López, Kazuo Furuya, Pablo O. Vaccaro. “Interdiffusion of Indium in piezoelectric InGaAs/GaAs quantum wells grown by molecular

beam epitaxy on (11n) substrates.", *Journal of Applied Physics* **96**, 3702 (2004).

[5] C.M. Yee-Rendón, M. López-López, and M. Meléndez-Lira, "Influence of Indium segregation on the ligth emission of piezoelectric InGaAs/GaAs quantum wells grown by molecular beam epitaxy.", *Revista Mexicana de Física* vol**. 50,** 193 (2004).

[6] J.A. Nieto, M.P. Ryan, O. Velarde and C.M. Yee, "Duality symmetry in Kaluza-Klein (n + D + d)-dimensional cosmological model.", *International Journal of Modern Physics A*, vol. **19**, 2131 (2004).

[7] J.A. Nieto and C.M. Yee, "p-brane action from gravidilaton effective action", Modern *Physics Letters A*, vol. **15**, 1611 (2000).

CONFERNCE PRESENTATIONS

[1] Materials Research Society (MRS) Spring meeting, San Francisco, CA (talk, 2009)

[2] International Workshop on Optical Terahertz Science and Technology (OTST), Santa Barbara, CA (talk, 2009)

[3] American Physical Society (APS) March meeting, New Orleans, LA (talk, 2008)

[4] American Physical Society (APS) March meeting, Denver, CO (talk, 2007)

HONORS

[1] Mexican National Council of Science and Technology – University of California Institute for Mexico and United States Scholarship, September 2003 to August 2008.

[2] Mexican National Council of Science and Technology Scholarship, August 2000 to August 2002.

[3] Telmex Foundation Scholarship, September 1997 to August 2002.

[4] Autonomous University of Sinaloa Academic Scholarship, September 1998 to August 2000.

ABSTRACT

High Q Terahertz Photonic Crystal Microcavities

by

Cristo Manuel Yee Rendon

We present a study of terahertz photonic crystal structures consisting of photonic crystal slabs, photonic crystal waveguides and photonic crystal cavities. The structures were fabricated from high resistivity silicon wafers using deep reactive ion etching. The photonic crystals were based on a triangular array of hole for which for hole size $r=0.30a$ has a photonic gap for transversal electric polarization and for hole size $r=0.45a$ it has a optical gap for transversal magnetic polarization, where a is the lattice constant.

We fabricated samples to operate at 1 THz for transversal electric and transversal magnetic polarizations which were intended to be coupled to quantum transitions in nanostructures or hydrogen like transitions of impurities in semiconductors which lie near 1 THz. The optical gaps for the photonic structures were measured using far infrared spectroscopy and time domain spectroscopy. Cavities were constructed and inserted into a waveguide forming a narrow band Lorentzian filter. For transversal electric (transversal magnetic) polarization we used an L3 (L2) which consist in

three (two) holes missing along the ΓJ orientation. The transmittance measurements using a narrow band source present sharp resonances associated with the resonant modes of the cavity. A quality factor as high a 1020 for transversal electric and 1560 for transversal magnetic were found.

We also studied the 240 GHz range. Here the cavity is intended to be incorporated into a 240 GHz electron spin resonance setup. Here we used the L3 cavity for transversal electric polarization. The photonic crystal cavity was coupled to a waveguide using the Lorentzian coupling and channel drop scheme. Transmittance measurements and scattering into free space by the cavity employing a narrow band source reveals a Q factor as high as 3800.

Frequency domain and finite time domain measurements using the experimental parameter of the structures accurately predict the values found in the experiment.

TABLE OF CONTENTS

1 Motivation and overview

The terahertz domain is located at the heart of the electromagnetic spectrum. It is commonly accepted to cover the range from 0.3 to 30 THz. This region marks a transition zone where electronic and photonic technologies converge, a place that up to now has been considerably challenging due to the non trivial way to produce and detect radiation but also a place where significant improvements could be made.

Science at terahertz frequencies is a very active region of research as many physical phenomena are in its scope. The black body radiation of an object with temperature above 10K emits in the terahertz region. Collective modes in polar liquids, like water, absorb at terahertz frequencies. Biological systems are also in this range as collective motions in proteins occur at terahertz frequencies Quantum transitions in nanostructure like intersubband transitions in quantum wells and quantum dots lie in the terahertz regime [1,2,3,4,5]

A. Motivations

Among the interesting research topics studied at terahertz frequencies is the proposal for a quantum information scheme based in a terahertz quantum system. In particular the proposal that motivated the present work is the one formed by the 1s-2p transition of shallow donors in GaAs as a qubit and a terahertz photonic crystal cavity as the resonator.

Photonic crystal cavities have the properties that they could reach extremely high Q values and very small modal volume, properties required in order to reach the strong coupling regime needed for the implementation of quantum information schemes. A high Q cavity is also useful not only for quantum information but also for applications where strong localized fields are needed, as in the case of compact sensors and filters and low-threshold lasers [6,7].

The quantum transition 1s-2p for an ensemble of shallow donors in GaAs has a typical energy of 4mev and a inhomogeneous line width of $\gamma_Q = 15$ GHz and for a moderate Q=1000 we have that the linewidth $\gamma_C = 1\ GHz$. The coupling strength of an ensemble of donors to a cavity mode is given by $\Omega = \sqrt{N} g_0$, where N is the number of donors coupled in the cavity and g_0 is the coupling strength for a single donor. For a moderated doping of $n = 4 \times 10^{20}\ m^{-3}$ the cavity strength coupling is given by $\Omega = 175\ \mu eV \approx 42\ GHz$. With these values the condition for strong coupling $\Omega \geq (\gamma_Q - \gamma_C)/4$ is satisfied.

High Q cavity could lead to produce extremely low threshold lasers by using the intersub-level transition in quantum dots. Recently quantum posts [8], have been proven to have intersub-level transitions at terahertz frequencies. Quantum posts have the advantage their energy transitions could be tuned by changing the size of the post. The integration of a quantum post into a terahertz photonic crystal opens the opportunity to produce an extremely low threshold lasers. In particular we explore the possibility of constructing a photonic crystal cavity that will couple to quantum posts. A quantum post transition has a strong dipole along the growth axis and therefore requires a cavity with electric field polarized in the same direction. According to the conventions of photonic crystals, such a cavity has a transverse magnetic (TM) polarization. Most of the work has been done for transverse electric (TE) polarized cavities and therefore a high Q TM cavity is worth exploring.

A high Q cavity with small mode volume will be beneficial to a high frequency electron spin resonance (ESR). High fields enhance the sensitivity of this technique, and in particular we look to integrate a photonic crystal cavity to the UCSB 240 GHz ESR spectrometer. Electron spins in Si are of particular interest. The lifetime of donor electron spins in phosphorus-doped silicon is extremely large [9,10], and it's been proposed as a qubit.bFor this particular quantum system, the line width of the transition is $\gamma_C \approx 7MHz$ and for a doping density $n = 1 \times 10^{21} m^{-3}$ an ensemble of spins has a coupling strength $\Omega \approx 8.85\ MHz$. For reaching the regime of strong coupling it will be required to have a cavity with a line width of 25 MHz or less which at 240 GHz correspond to a cavity with a quality factor *Q=9600,* a Q value that is within the reach of a photonic crystal cavity.

The construction of photonic crystal cavities that couple to the three THz schemes that we mentioned before, shallow impurities in GaAs, terahertz quantum nanostructures, in particular quantum posts, and electron spin resonances are the motivation behind our work.

Photonic crystals at terahertz frequencies has been constructed mainly intended to be used for terahertz quantum cascade lasers; here the mode is lateral confined by a two dimensional photonic crystal while the vertical confinement is produced by double wall metal waveguide; using this simple structure very small threshold laser have been constructed. However a real photonic cavity in which the modes are strongly confined will push even further the laser threshold, this dielectric cavity has not been constructed yet. The main obstacle is not the construction of the cavity itself, as there a lot of examples of photonic crystal structures and applications based on THz photonic crystals [11,12,13,14,15,16,17,18], but in its characterization. One way to characterize a photonic crystal cavity is by having a source inside the cavity [19], however there is not a THz emitter that could be used for this purpose. Another way to measure a photonic crystal cavity is by coupling the cavity to a waveguide [20], however at THz frequencies there a very few tunable sources that could employed for this purpose; as for measuring high-Q cavities a very narrow lines are required.

Recently there is been an effort to construct a terahertz photonic crystal cavity for sensing purposes, these type of photonic crystal are based on metallic waveguides and have prove to produce cavities with a $Q \approx 100$ [21]. In these metallic cavities the fields are confined in air; which have a severe effect of the maximum quality factor that can be reached with this scheme. A $Q \approx 100$ factor is also very close to the resolution limit for terahertz time domain spectroscopy which typically is used to characterize THz photonic crystals.

B. Objectives

The objective of the present thesis work is the study of dielectric photonic crystal cavities at terahertz frequencies. This work covers the construction of a terahertz photonic crystal to the construction of a high Q photonic crystal cavity. The characterization of the photonic crystal cavities was done by coupling the cavity to a waveguide; we explore two different waveguide coupling schemes which together with a high resolution tunable source enable us to measure cavities with a Q factor as high as 3800 limited by carrier absorption at room temperature. Is worth to mention that these high-Q THz photonic crystal cavities have the highest Q factor reported and in fact the very first constructed and measured at THz frequencies.

C. Thesis structure

The thesis is dived in eight chapter and seven appendixes. The first chapter corresponds to a brief background and an overview of the material covered by the thesis. In chapter two we introduce the basic concept of a photonic crystal, including photonic crystal waveguides and photonic crystal cavities. Only the main ideas are presented here with detailed explanation presented in appendices A and B. Chapter three explains the design and construction of the photonic crystal samples with the detailed recipes for each set of samples presented in appendix D. The central part of the present work corresponds to chapter 4 to chapter 7 in which each one corresponds to a different project which involves design, construction, experimental measurement and theoretical modeling for a specific photonic crystal structure. Finally in chapter eight we present the conclusion of the present work and we outline further development in the area. We expect the present work to be a useful starting point for future development that will help to bridge the terahertz technological gap.

2 Theoretical Foundations

A. Photonic crystals

The blue resplendent reflection of opal or intricate iridescence colors in butterfly wings scales are some of the most prominent examples of naturally occurring photonic crystals.

The optical properties of photonic crystals are products of the application of Maxwell's equations to a symmetric macroscopic media. Light propagating through a periodic medium[1] undergoes scattering if the wavelength is comparable to the periodicity of the medium. This phenomenon is similar to electrons that undergo scattering by the periodical potential of the atomic cores constituting a crystal, and similarly the solution for the equation governing the behavior of a stream of photons are planes waves modulated by a periodic function in the lattice, i.e. Bloch functions. The representation of the wave function of electrons as Bloch functions is one of the foundations of semiconductor theory in solid state physics. The analogy is emphasized by borrowing terms like optical band gap or point defects.

Perhaps the simplest and most know example of a photonic crystal is the quarter wavelength dielectric mirror or Bragg reflector, as shown in Figure 2.1. A Bragg reflector consists in a one dimensional stack of two dielectrics with different indices of refraction. The dielectric mirror is normally designed to operate at a given

[1] Here we are considering a periodic medium as one in which the index of refraction is not constant.

frequency and near normal incidence. As the name suggests a quarter wavelength dielectric mirror consists of a series of dielectric layers with the thickness for each layer chosen to be a quarter of the wavelength of light in the medium. The interference of reflections from each interface causes for a normal or near normal incident beam to be strongly reflected; normally very few periods are need to obtain a reflection coefficient that exceeded that obtained by metal coated surfaces. These mirrors are widely used of the fabrication of laser cavities [22].

The high reflection of the dielectric mirror produces a very low transmittance for a frequency range around a target frequency. This low transmittance region is called photonic crystal gap, and an equivalent definition of a photonic gap is a frequency range for which there are no propagating modes in the structure; the photonic gap is the key property of a photonic crystal on which all the applications are based.

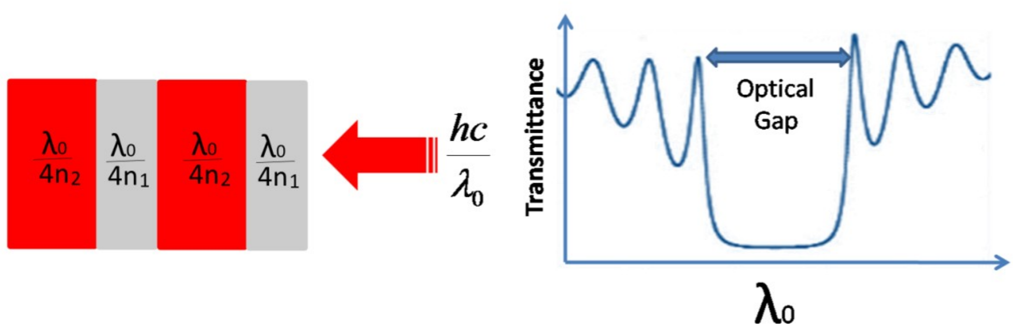

Figure 2.1 A quarter wavelength dielectric mirror is an example of a one dimensional photonic crystal. For a specific wavelength a very high reflection or very low transmittance is obtained by the constructive interference of the reflection at each interface.

The principle behind the optical gap for the one dimensional dielectric stack is index of refraction periodicity as was explained by Lord Raleigh in 1887 [23]. Using this principle to extend this idea to higher dimensional systems is straightforward, like the examples shown in Figure 2.2, which are just examples of structures with a two or three dimensional periodicity.

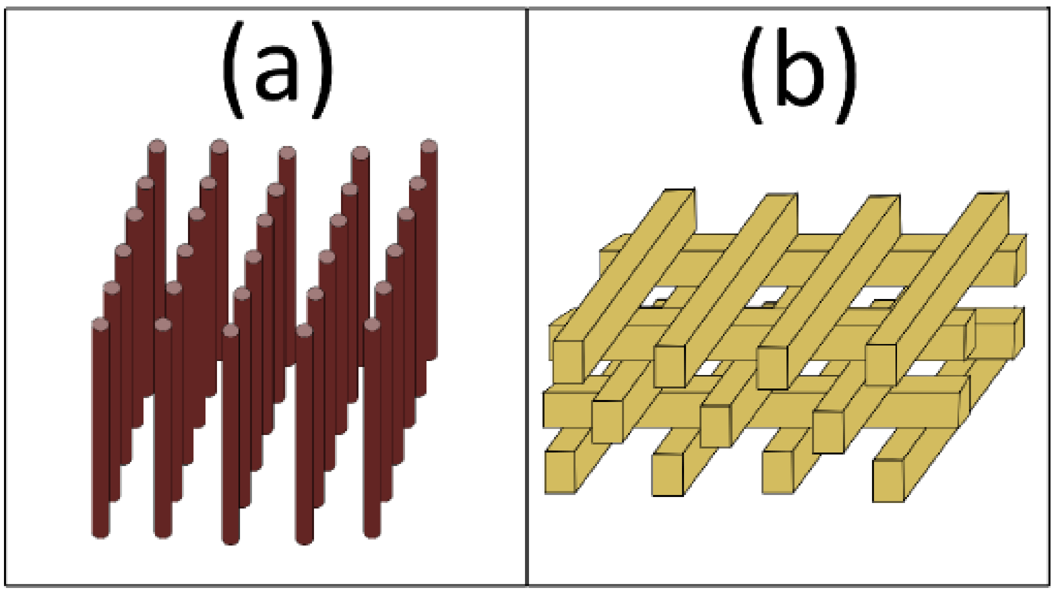

Figure 2.2 (a) shows a two dimensional array of dielectric rods in which the distance between rods is negligible compared with size of the rods. The system is periodic in two dimensions and homogeneous in the third. An optical gap could be created for a beam propagating in the plane perpendicular to rod axis. (b) Shows a three dimensional photonic crystal in which there is a three dimensional periodicity, an optical gap could be found for beam propagation along any direction in the crystal.

The three dimensional photonic crystal is particularly difficult to incorporate into standard silicon and GaAs technology. In practice there is a hybrid approach which is more convenient. A photonic crystal slab is a structure with a two dimensional periodicity and with a finite thickness in the third direction. The confinement mechanism is given by a total internal reflection of the propagating vector by a 2 dimensional photonic crystal in the plane of the slab. As shown in Figure 2.3.

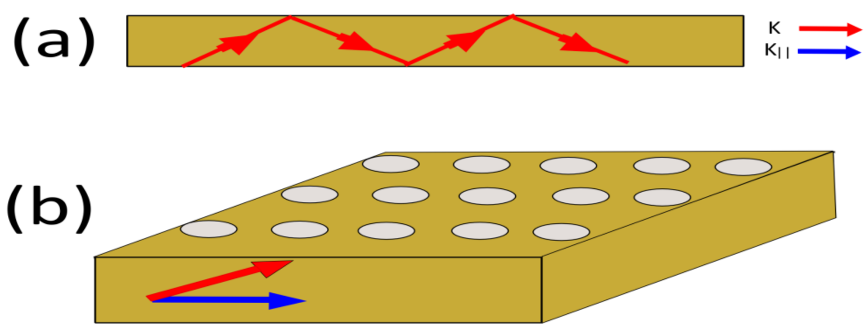

Figure 2.3 Confined modes in a photonic crystal slab. (a) The vertical confinement of a mode in a slab if produced by total internal reflection. (b) An inplane confinement is produce by a two dimensional photonic crystal.

The modes in a photonic crystal slab can be classified according to the z=0 mirror symmetry plane of the E field as Transversal Electric (TE) if the E field has an even symmetric or Transversal Magnetic (TM) if the field as an odd symmetry, as is illustrated in figure 2.4. Strictly speaking only in the middle plane the modes are pure TE or TM which is exact for a two dimensional photonic crystal. The distinction between TE and TM is important since the photonic crystal gap is polarization dependent.

Most part of our work was done using a photonic crystal slab with a triangular lattice, so we will emphasize the concepts using this lattice. The details of the mathematical treatment of photonic crystals are reports in appendices A and B. Here we will be only repeating the material which is strictly necessary.

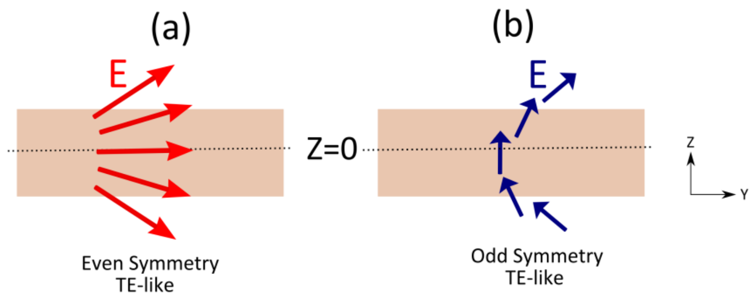

Figure 2.4 The polarization of the mode deepens on the mirror plane symmetry obeyed by the E field. (a) TE-like for even mirror symmetry. (b) TM-like for odd symmetry.

As in solid state physics the concept of band diagrams is useful for the understanding of the properties of a crystal. A band diagram or dispersion relation is a plot of frequency as a function of the wave vector, usually along a high symmetric direction in the reciprocal space. Using the property that a Bloch function for an arbitrary vector in the reciprocal space could be mapped into the first Brillouin zone, the band diagram is only plotted in the reduced scheme zone, and is along a high symmetry orientation in the Brillouin zone due to this being where the Brag conditions could be satisfied; therefore, these are the only places where $\omega = \omega(k)$ could be discontinuous.

The band diagram for the photonic crystal slab is the projection of the band diagram into a two dimensional triangular reciprocal lattice, i.e. is a plot of frequency as a function of the in plane k vector. For a silicon photonic crystal slab with hole radius r=0.30 and thickness t=0.6 the band diagram for TE polarization is shown in Figure 2.3. This plot has been calculated using the program MPB. The detail of the code is found in the appendix F. MPB is a frequency domain solver code that computes the harmonic modes for Maxwell's equations reformulated as an eigenvalue problem (see appendix A).

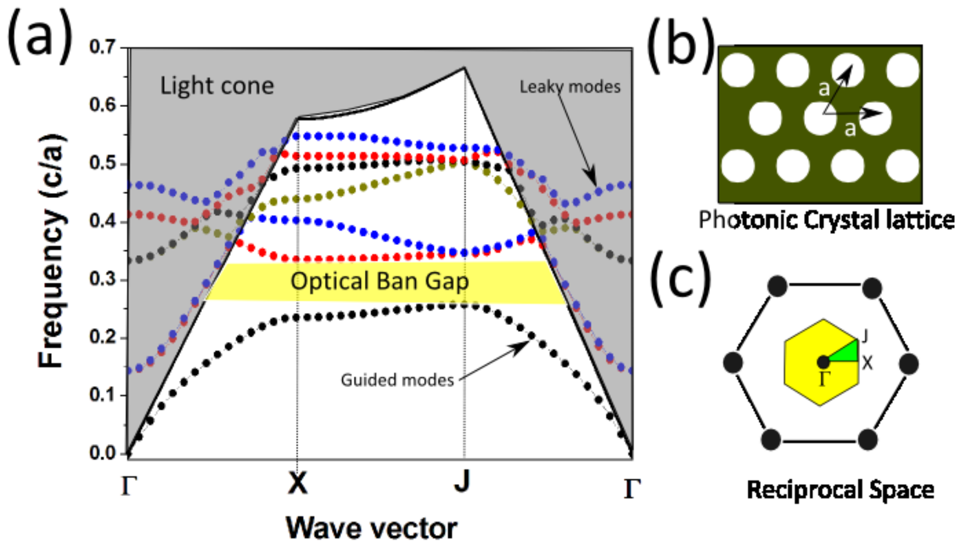

Figure 2.5 (a) The band diagram for a photonic crystal slab with thickness t=0.6 a and hole radius r=0.3a, where a is the lattice constant. An photonic crystal gap for guided modes is found from 0.256 to 0.320 (c/a). (b) The photonic crystal triangular lattice. This 2-d lattice is responsible for the confinement of the guided modes in the plane of the slab. (c) The reciprocal space for the triangular lattice, in yellow is the First Brillouin zone, the irreducible zone is in green and the high symmetric points in the Brillouin zone are highlighted.

The solid line here is the "light line", the dispersion relation of light in vacuum projected onto the Brillouin zone. Any mode above this line will not be guided through the slab because its k vector does not satisfy the condition of total internal reflection. The region between 0.256 (c/a) to 0.320 (c/a) where there are no modes is called photonic crystal gap. For this range of frequencies light will not propagate through the slab.

In some cases the transmission through the structure is more important that the band structure itself. Take for example the quarter wavelength dielectric mirror where the transmission and reflection characteristics of the structure are essential. In those cases there are alternatives like the Transfer Matrix Method (TMM) and the Finite Difference Time Domain (FDTD) method. In our work we will be using the latter. Time domain methods start from initial field configurations, and then the fields are updated using the central difference approximations to the space and time partial derivatives. An excitation or driven term is included, normally as a field component that we are interested in, which could be a pulse or a continuous source. The field updating process continues until a steady state is reached for a continuous source or else the time scale is large enough so all the desired interactions have already finish as in a pulse excitation. For calculating the transmittance we use short pulses, i.e. pulses with a non-zero frequency width. The source is located opposite to the point where the transmittance is to be calculated. The flux is then monitored at the measuring point as a function of time and by Fourier transform the frequency response is obtained

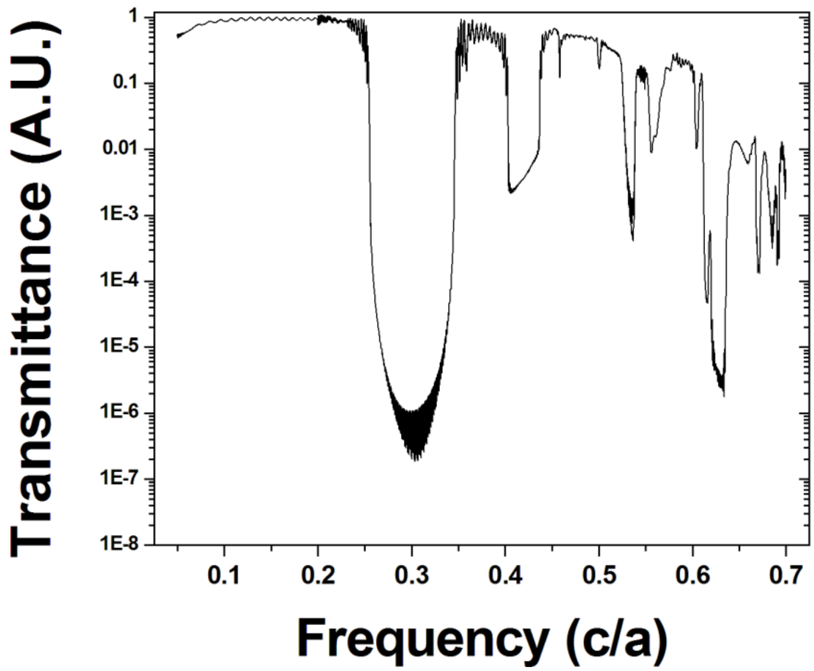

Figure 2.6 The transmittance spectra for a photonic crystal slab with a triangular lattice calculated using finite difference time domain calculation. . As expected, the region of low transmittance (optical band gap) corresponds to the photonic crystal bandgap that is found using frequency domain methods (Fig. 2.4).

To calculate the transmission through the sample we use the free available software called MEEP. Using MEEP the transmittance along the ΓJ orientation in the crystal is computed, the detailed code used by MEEP is shown in appendix F. The computed transmittance for a photonic crystal slab with radius *r=0.30a* and with thickness *t=0.6a* is shown in Figure 2.6. Here we used a symmetric pulse along the ΓJ. The most prominent feature of the transmittance is the zone with very small transmittance center a 0.30 (c/a) which corresponds to the gap between band 1 and bands 2. The second smaller gap correspond to gap between bands 3 and 5. It can be proved that band 4 does to couple to a symmetric beam and therefore is not shown in the transmittance.

B. Photonic crystal cavities

The optical gap for a photonic crystal could be used for far more that just making an excellent mirror. The optical gap could also lead to the construction of the ultimate cavity by creating a space inside this high quality mirror; this is the idea behind a photonic crystal cavity. Light trapped inside the cavity will be confined between the mirrors; the better the mirrors the better the cavity. The simplest way to produce a cavity in a photonic crystal is by creating a defect.

A photonic crystal defect is analogous to an impurity in a semiconductor in solid state physics. It is a state created with a defined frequency in the otherwise forbidden gap of the structure; the state is localized around the defect. The introduction of a defect creates a local zone in which the discrete translation symmetry is broken and eigenstates of k constant are not permitted, and therefore it cannot couple to the bulk modes of the photonic crystal, where the modes are defined by a reciprocal vector and a defined frequency.

In our particular case we considered the photonic crystal slab with a triangular lattice in which three holes are removed along the ΓJ orientation in the lattice. This is a well know cavity known as the L3 defect in the literature. It has been reported that for visible and optical telecommunications frequencies Q values as high as 500000 [24,25]are possible by carefully tuning the parameters of a L3 cavity.

Figure 2.7 (a) shows the geometry of the cavity with its three holes missing. Figure 2.7 (b) and (c) shows the Hz and Ey field components of the resonant mode of the cavity. As expected the mode is well confined around the defect. FDTD simulation of the L3 defect shows that it has a Q=4600 and its resonant frequency is f=0.27 (c/a).

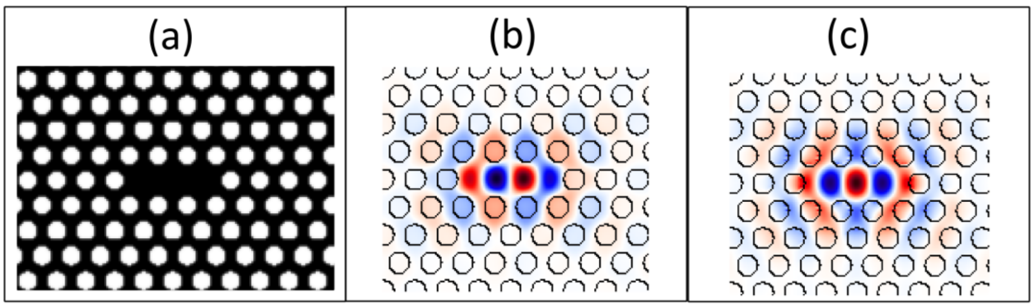

Figure 2.7 The photonic crystal L3 cavity. (a) The structure of the L3 cavity consists in three holes missing along the ΓJ orientation. (a) Hz mode profile of the resonant mode of the L3 cavity. (b) Ey mode profile of the resonant mode of the L3 cavity.

C. Photonic crystal waveguide

A photonic crystal waveguide is another fundamental structure used by the photonic crystal community. The transport of radiation from one part of the device to another would be impossible without waveguides.

A photonic waveguide is a type of defect similar to the photonic crystal cavity but with a great difference; a waveguide supports states with a well-defined value of k and frequencyω. These Bloch states propagate in the structure and are localized around the waveguide. One easy way to produce such kinds of systems is by introduction of line defect as shown in Figure 2.8(a).

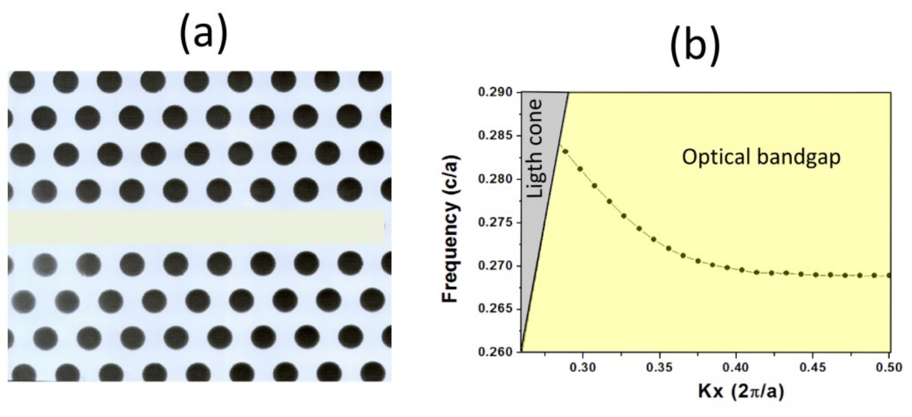

Figure 2.8 (a) Photonic crystal waveguide. (b) Photonic crystal waveguide dispersion.

By removing a line of holes the effective index is increased and therefore modes from the second band in the band diagram shown in Figure 2.8(a), are pushed into the optical gap forming a defined band. As shown in Figure 2.8(b).

Waveguides will play a very important role for characterizing our photonic crystal cavities; all our samples will rely on coupling a cavity with a waveguide to measure and determine the quality factor of the cavity.

3 Photonic crystal Design and Fabrication

In this chapter we describe the process of design and fabrication of the photonic crystal samples. The overall process will be described in some detail with the complete recipes reported in the appendix D.

The first part of the design process is to compute the frequency response of the structure using FDTD. There are three parameter that could change the optical properties of a given photonic crystal: lattice constant, hole radius, and slab thickness, provided that the index of refraction stays constant.

In the process of choosing the right parameter for the samples we decided to set the thickness and the hole radius to specific values and work only with the lattice constant. Employing FDTD the structure is simulated to verify that the frequency response that we are interested in, usually a cavity frequency resonance, falls into the range of our source of THz radiation. In order to access the entire dimensionless frequency range of interest, we tune the frequency of our source over its entire range, and also create structures which are geometrically identical but scaled in size.

With the parameters of the structure known, we used a cad program, LEDIT, to design a mask.. When we designed the mask we tried to maximize the space to include several designs to be able to fabricate them in a single batch. An example of the photomask is shown in Figure 3.1

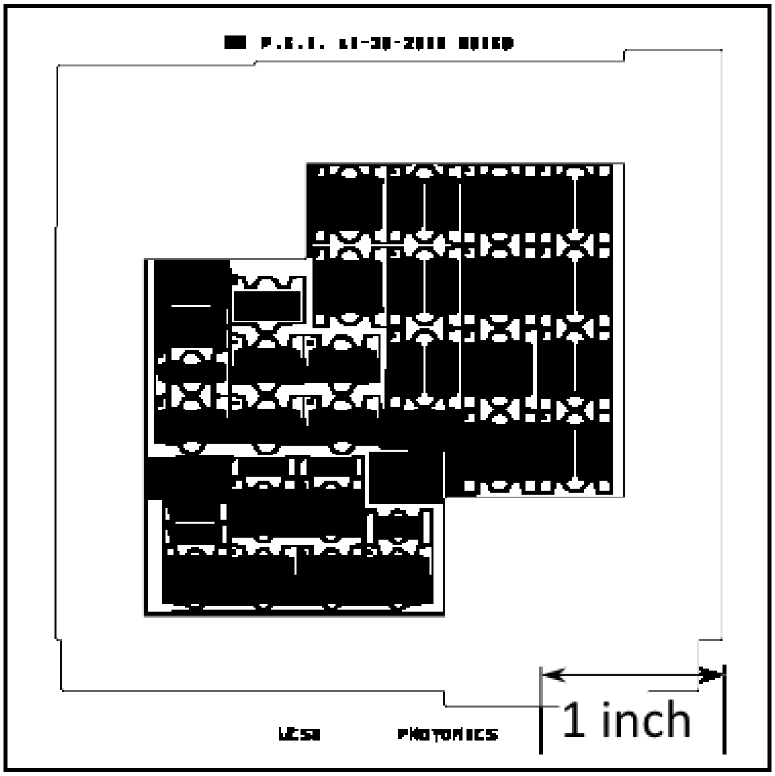

Figure 3.1 Typical photomask employed in the sample fabrication. Here a set of photonic crystal structure with different variation parameters. The space is maximized in order to have the largest number of samples in the smallest area of the mask aiming to have uniform fabrication conditions for a particular set of samples.

We fabricate a set of samples in a single batch looking to simplify the process and also looking to have the same parameter for all the structures. We did not preprocess the wafer to a specific thickness thus the thickness of the wafer could vary from wafer to wafer. By fabricating an entire set of samples from a single wafer, we can ensure that all the samples will have the same thickness and the results could be compared more directly than if we had samples made from a different wafer.

In the case of photonic crystal cavities the absorption coefficient can change from wafer to wafer making it harder to compare the quality factor from two different sets.

In our first designs, we made our own photomask using a Heidelberg DWL 200. Later it turned out to be most cost effective to purchase the photo mask from a vendor. We use the company Photosicence,inc. Once the photomask is fabricated we continue the fabrication process in the cleanroom.

All our samples were fabricated at Nanotech UCSB. In Figure 3.2 we present the basic flow chart of the clean room fabrication processing. The process starts by coating a 4-inch silicon wafer with 2.00 to 6.00 μm $Si0_2$. This wafer is used as a carrier wafer. We need to coat the carrier wafer due to the fact that the etching rate of Reactive Ion Etching (RIE) strongly depends on the area of Silicon exposed to the reactive ions. The ratio of the etching rate of $Si:Si0_2$ is 200:1 and since our wafers are at most 400 μm thick a few microns of $Si0_2$ is all that is needed.

The samples are made from high resistivity silicon from 2-3 KOhm-cm up to 10-20 KOhm-cm. The wafer preparation starts with a standard solvent cleaning procedure. After the cleaning we process the sample using ultraviolet lithography. The next step is to mount the sample on the carrier wafer[2] using either a thin layer of photoresist A4110 or Santovac; the etching step was done using the Si Deep-Reactive Ion Etching using a Bosch Plasma-Therm 770 SLR.

[2] In the case of the samples with thickness 50 μm it was first glued to an extra carrier wafer coated with Si02 to facilitate manipulation during the lithography process.

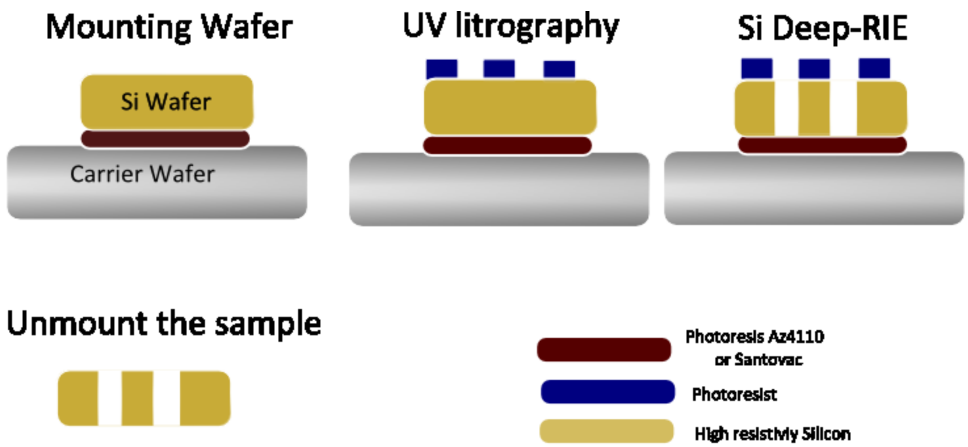

Figure 3.2 Fabrication flow chart.

After completing the etching cycles the samples are inspected under an optical microscope. If the etch is incomplete, the sample is returned to the etching chamber to continue an extra etching cycles. The initial time that the sample stays in chamber is determined by the etching rate of the RIE. The nominal etching rate is 2 μm per minute, which implies a time of about 25 minutes to half hour for a 50 μm thick sample and 2 hours and 10 minutes for a thicker 380 μm sample. Usually more time than the nominal rate implies was required. Finally after the etch step is finished the samples are soaked in acetone to be removed from the carrier wafer. If photoresist was employed to glue the samples to the carrier wafer an overnight bath in acetone is required.

4 Terahertz Photonic crystal slab

In the present chapter we're covering the basic structure of a photonic crystal; in particular the triangular holes photonic crystal slab (PCS) which have a transverse electric (TE) photonic crystal gap. We characterized the photonic structure by transmission measurement, and used finite difference time domain [26] and frequency domain code [27]to model the PCS optical properties.

Terahertz photonic crystals slabs have been studied using Fourier Transform Infrared (FTIR) measurements [28] and time domain techniques [29]. In the previously reported works the thickness of the slab was several times the lattice constant, and therefore supported multiple slab waveguide modes. In contrast our fabricated samples were slightly more than half wavelength in the material of the center frequency gap and therefore our slabs are single mode.

The multimode slabs also have the inconvenience that the extra modes are pushed into the optical gap decreasing its size and in some case completely covering the gap. Such thick PCSs are not suitable for fabricating PC waveguides and high-Q resonators due to the possibility of having effects such as mode conversion and dispersive guiding. The photonic crystal optical gap is the basis for more complicated photonic structures that will be explored in the following chapters.

The first objective was to construct a photonic crystal with its frequency response in the 1 THz frequency range. The selected design was a photonic crystal slab with a triangular lattice of holes. We selected the triangular lattice due to it having a substantial optical gap for TE polarization[3].

A. . Experimental setup

We used the Fourier Transform Infrared (FTIR) spectroscopy to characterize the frequency response of the photonic crystal. FTIR spectroscopy is a broad band measurement technique that covers the range from the ultraviolet to well into the terahertz regime. It consists of a broad band thermal emission source that passes through a Michelson interferometer with a fixed mirror and a movable mirror. The beam is focused into a sample by an off-axis parabolic mirror, transmitted through the sample and then collected by another set of off-axis parabolic mirrors to be finally measured by a detector. The detector measures the output of the interferometer as a function of the path difference between two mirrors. This path difference is equivalent to time difference and so the interferogram measure is the autocorrelation of the source. By taking its Fourier transform the frequency spectrum of the source is obtained. In general it's more complicated as the effect of the beam splitter and the detector itself needs to be considered.

The transmittance is taken from dividing the spectrum of the sample with respect to the spectrum of the reference.

[3] The results from this section appeared published in Applied Physics Letters "Transmission of single mode ultrathin terahertz photonic crystal slabs", Cristo M. Yee, Nathan Jukam and Mark Sherwin, *Appl. Phys. Lett*. **91**, 194104 (2007).

In our case we use a Bruker I66-V with a mercury lamp and employed a 4 K Silicon composite bolometer. The schematic of our setup is shown in figure 4.1.

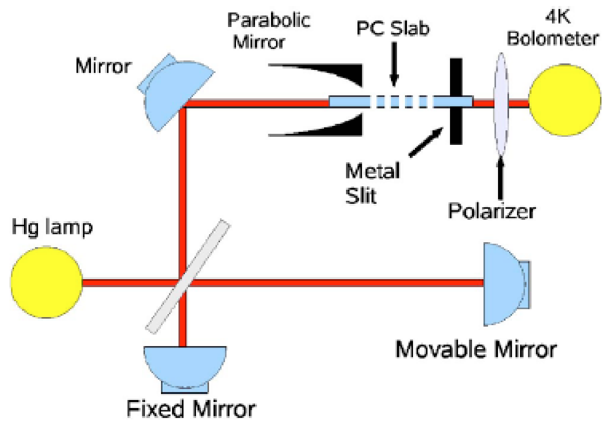

Figure 4.1 Experimental FTIR setup

We employed a 50 μm Mylar beam splitter. We employed a 2-dimensional parabolic mirror to further focus the beam into the sample. On the edge of the sample we use a metal slit to block the light which is not guided through the sample. Then a polarizer is used to select the appropriate linear polarization. At the end a Liquid helium Silicon composite detector is used to record the signal.

The frequency spectrum of FTIR with no sample is shown in Figure 4.2 using the 50 μm thick beam splitter. The first minimum in this beam splitters reflectance is at 2 THz, and the first maximum is at 1.4 THz. Using FDTD simulations, we designed a photonic crystal slab with its optical band gap centered near 1.4 THz to achieve the best possible signal to noise ratio in our measurements.

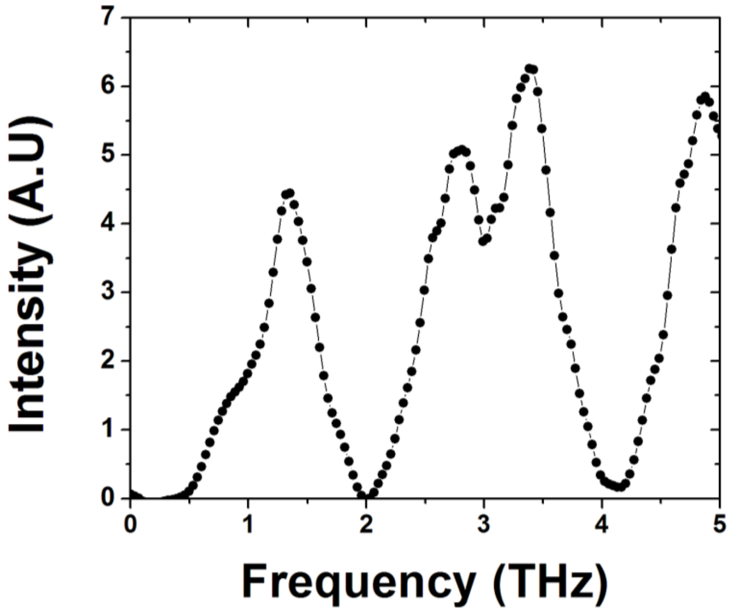

Figure 4.2 Frequency spectrum of the FTIR using a mercury lamp, a 50 μm Mylar beam splitter and a silicon composite bolometer

The sample design is a simple photonic crystal slab 50 μm thick with a triangular lattice with lattice constant a=64 μm. The sample contained 5 lines of holes along the ΓJ orientation of the crystal as seen in figure 4.5, each hole with radius r=0.3 a. We selected only 5 holes as the length of the photonic crystal because even with this short length it still has a clear optical gap.

B. Sample fabrication

The photonic crystal slab structure was fabricated following the procedure explained in chapter 3. A scanning electron microscopy photograph is shown Figure 4.3. The samples show good quality interfaces and smooth sidewalls characteristics of the Deep Silicon RIE.

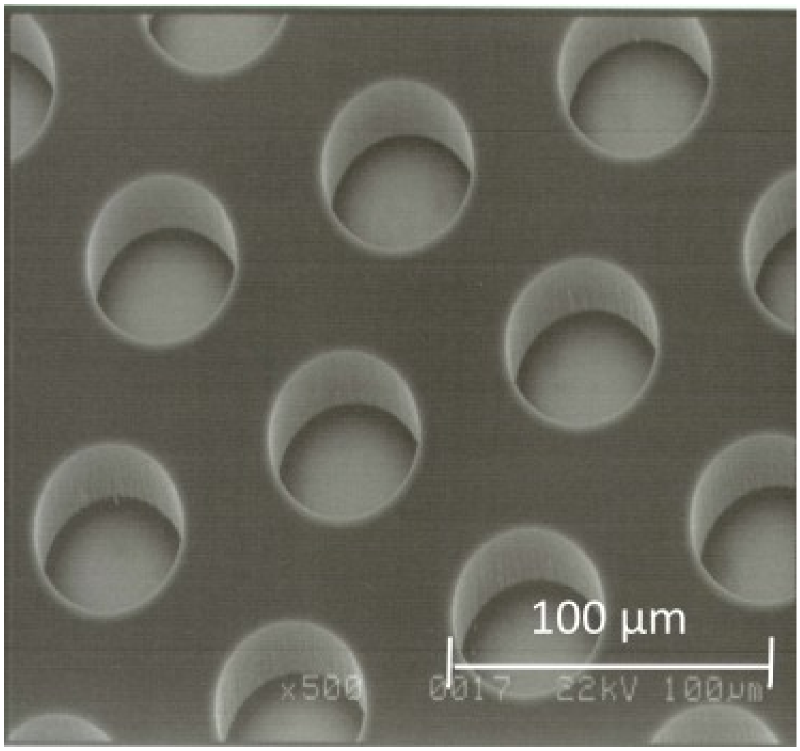

Figure 4.3 Scanning electron microscopy photograph of a photonic crystal slab with a triangular lattice

The sizes of the holes were estimated from optical microscopy photographs and were found to be $r/a = 0.3075 \pm 0.003$, where a is the lattice constant. This value is slightly larger than the nominal 0.3; we estimate that these values were either the product of the lithography process or from an overetch during the fabrication process.

The sample was too thin to measure by mechanical means, so we measured its thickness using the FTIR as described in Appendix E. The experimental of slab thickness was $t = 48.56 \pm 0.03\ \mu m$.

C. Experimental results and discussion

The optical gap for the triangular PCS have TE polarizations which are the modes with the Electric field in the plane of the slab. In our experiment we measure, using transmission, the optical gap along the ΓJ orientation. The configuration which shows the transmission direction and the beam polarization is shown explicitly in Figure 4.4.

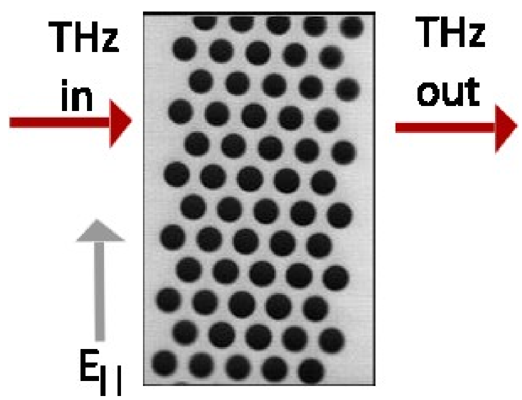

Figure 4.4 The transmission is along the ΓJ orientation in the triangular lattice and the polarization is with the E field in the plane of the slab.

The FTIR transmittance experiment for the photonic crystals was realized using a resolution of 15 GHz; as a reference transmission spectrum we used the transmittance through a piece of unprocessed silicon wafer with equal thickness. As shown in Figure 4.5 it is clear that there is a region of low transmittance from 1.16 to 1.65 which is centered around 1.4 THz as expected from the design of the sample. This low transmittance is associated with the photonic crystal optical gap.

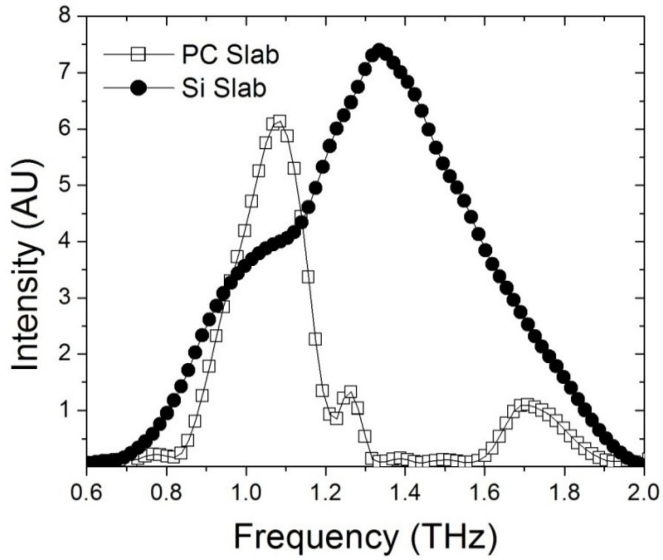

Figure 4.5 FTIR transmittance through the photonic crystal compared with the transmittance from a reference wafer. A low transmittance region from 1.16 to 1.65 THz is measured. In the spectra the transmittance through the photonic crystal is multiplied by an arbitrary constant.

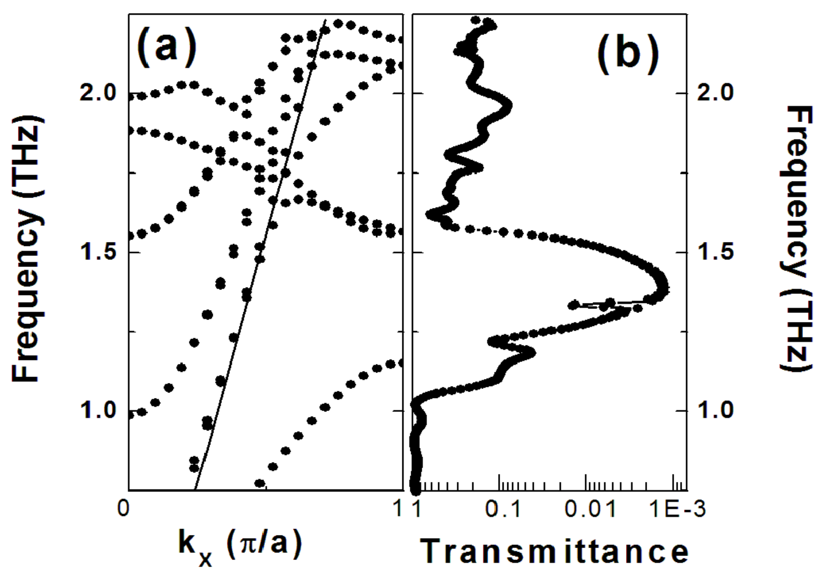

Figure 4.6 **(a)** Frequency domain calculations of the band diagram for TE modes of the PCS; here the PCS is considered to be infinite on the plane of the slab. (b) Finite difference time domain calculation of the transmittance for TE modes of the PCS

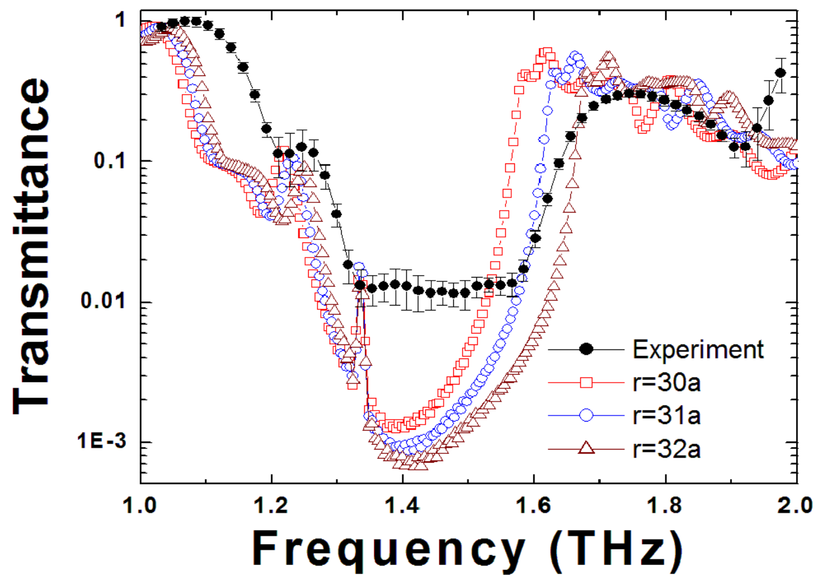

Figure 4.7 Experimental spectrum compared with FDTD simulations. The maximum in the transmittance in normalized to 1. The spectra with radius r=0.31 is the best fit for the experimental setup and in consisted with the hole size measured experimentally.

We realized frequency domain (FD) simulation of the structure photonic crystal slab. Figure 4.6 (a) shows the band diagram considering that the structure is infinite in the plane of the slab. The band diagram shows an optical bandgap with frequency region that matches the region of low transmission found experimentally. However FD simulation cannot be directly compared to the transmittance because it only shows the allowed mode but it does not take into account the coupling for each mode. A more direct comparison between and experiment is given by a full 3-D FDTD simulation as shown in Figure 4.6 (b). The FDTD simulation used the parameters of the structure including its thickness, hole radius, lattice constant and finite size along the direction of propagation (5 rows of holes). The FDTD spectrum shows a low transmittance that matches the optical gap of the FD simulations and also agrees with the experiment.

The FDTD transmittance prediction matches very well the transmittance found in the experiment. As a verification of how well theory matches with the experiment we calculated the transmittance for different values of the hole size. Figure 4.7 shows a detailed comparison of the experimental transmittance and the FDTD calculation for the ΓJ orientation for different radii, as we expected the best match is given by the experimentally measured parameters of the slab.

The FDTD calculations for different radii agree with one another and the experiment at the lower frequency part of the bandgap (dielectric band). The higher frequency part (air band), however, is extremely sensitive to changes in the parameters of the PCS. For the measured parameters of the structure (r=0.31) the FDTD shows a region of low transmittance whose width matches the experiment. The experimental transmission floor is limited by leakage around the PCS and thus higher than the calculated value.

D. Conclusion: optical gap for a THz TE photonic crystal slab

From Figure 4.5 and Figure 4.7 we conclude that for silicon photonic crystal slab with triangular lattice of holes with lattice constant $a = 64\,\mu m$, radius $r = 0.3075\,a = 19.68\,\mu m$ and thickness $t = 0.759\,a = 48.56$ the transmission spectrum has an optical gap for TE polarized guided modes propagating along the ΓJ orientation in crystal. The transmittance is well modeled by FDTD using the experimentally-measured dimensions of the sample.

Single mode PCSs are the foundation for waveguides and resonators, structures that will be explored in the following chapters. The present work however shows that it is possible to have these structures work at terahertz frequencies and thus enabling another tool that helps to close the terahertz technology gap.

5 Transversal Electric Photonic Crystal Cavity

After successfully fabricating and measuring a photonic crystal slab at terahertz frequencies our next goal was to construct a photonic crystal cavity that operated in the vicinity of 1 THz[4]. The main motivation for constructing a photonic crystal cavity with a resonance near 1 THz was to incorporate the cavity into a quantum information processing scheme [30]. However, small cavities with high quality factors Q are also fundamental to the implementation of devices such as compact sensors and filters [20,6], low-threshold lasers [3] and studies of strong coupling between light and matter [31].

Photonic crystal structures are important components of the toolbox for manipulating terahertz radiation. Silicon is an excellent material for the construction of photonic crystals because it has extremely low loss [32] and silicon processing technology is well developed. Silicon and GaAs PCSs have been demonstrated with band gaps near 1 THz [33,34] Metallic photonic crystal cavities coupled to metallic photonic crystal waveguides [21] have been shown to have multiple resonances with Q≈100. An approach that has been widely implemented at telecommunications and near-infrared wavelengths is based on two-dimensional 2D photonic crystal slabs PCS [35,36] such as the one we studied in chapter 4.

For this work we kept the photonic crystal slab with a triangular lattice, and we select the L3 cavity which is a cavity formed by filling three holes along the ΓJ

[4] The preset work is published in Cristo M. Yee and Mark S. Sherwin, "High-Q terahertz microcavities in silicon photonic crystal slabs.", *Applied Physics Letters*, vol. **94** , p. 154104 , (2009)

orientation in the triangular lattice. Cavities with this geometry have been widely studied at optical and near IR frequencies. This cavity has a particularly high Q value estimated to be 4700 for an isolated cavity. The L3 cavity could reach Q factors as high as 500 000 and mode volume of order $(\lambda/n)^3$ by carefully adjusting the diameter and position of the surrounding holes [37,38,39]. Such cavities have been coupled to waveguides to create compact optical circuits.

For measuring the quality factor of the L3 cavity we use a photonic crystal waveguide to pump power into the cavity. We also employed a waveguide for measuring the frequency spectrum of the light leaking from the cavity. We employed a Lorentzian filter configuration (see appendix C). In this configuration the cavity is embedded inside a waveguide. The resonant mode of the cavity is shown in the transmittance as a Lorentzian line in the transmission through the sample.

For the purpose of characterizing the structure we were interested in the conduction of the photonic crystal waveguide and also in the resonant frequency of the cavity so silicon photonic crystal slab waveguides with and without embedded L3 photonic crystal cavities were designed and fabricated.

We based our samples in a photonic crystal slab with a triangular lattice and with the parameters $r = 0.30a$ and $t = 0.60a$, where r is the radius of the hole, a is the lattice constant and t the thickness of the slab. This structure is known to provide an optical bandgap for transverse electric (TE) polarization. We constructed samples with lattice constant $a=80$ µm and *76* µm. For each lattice constant we fabricated a waveguide and a Lorentzian filter. The fabrication process was carried out at the

UCSB Nanofabrication facility. Ultraviolet lithography on a 44 μm thick silicon double-side polished wafer with a nominal resistivity 4kOhm-cm was followed by silicon deep reactive ion etching using a Plasma-Therm 770 SLR using the process described in chapter 4.

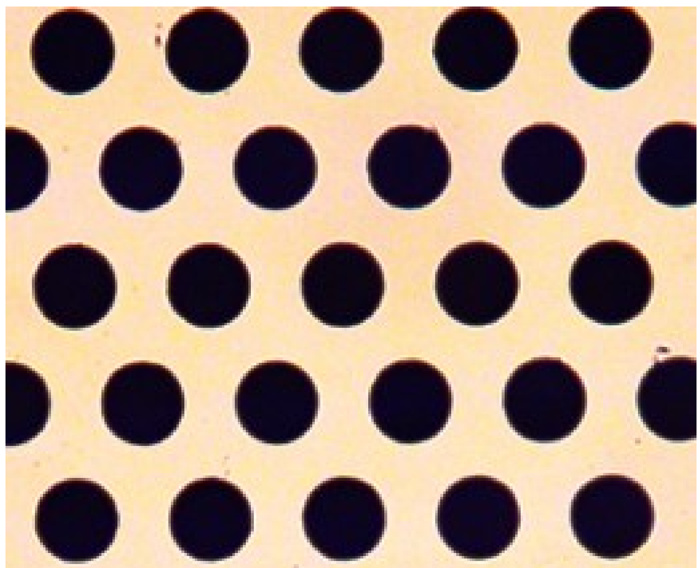

Figure 5.1 Optical photograph of the photonic crystal slab

We learned from chapter 4 that for a correct characterization of our samples we require the parameters of the structure. The lattice constant and the hole size are well controlled by the lithography process, as verified by optical microscopy as shown in Figure 5.1. The thickness of the slab was measured prior to fabrication using far infrared Fourier transform spectroscopy (see Appendix E), and it was found to be $t = 44 \pm 2$ μm.

Due to the spot size of the source (2 mm) and the size of the waveguide (≈ 100 μm) the coupling of terahertz radiation from free space into a waveguide is small. To enhance the coupling into the waveguide entrance we incorporate into the structure a 2-D solid immersion lens.

Each immersion lens consists of a semicircle with diameter of 2 mm which is integrated into the photonic crystal waveguide structure as shown in Figure 5.2. The samples with a = 80 μm (76 μm) have length of the waveguide of 5.44 mm (5.472 mm) with a total length (including the lenses) along the direction of the waveguide of 8.04 mm (8.072 mm) while the width of the sample is 9 mm.

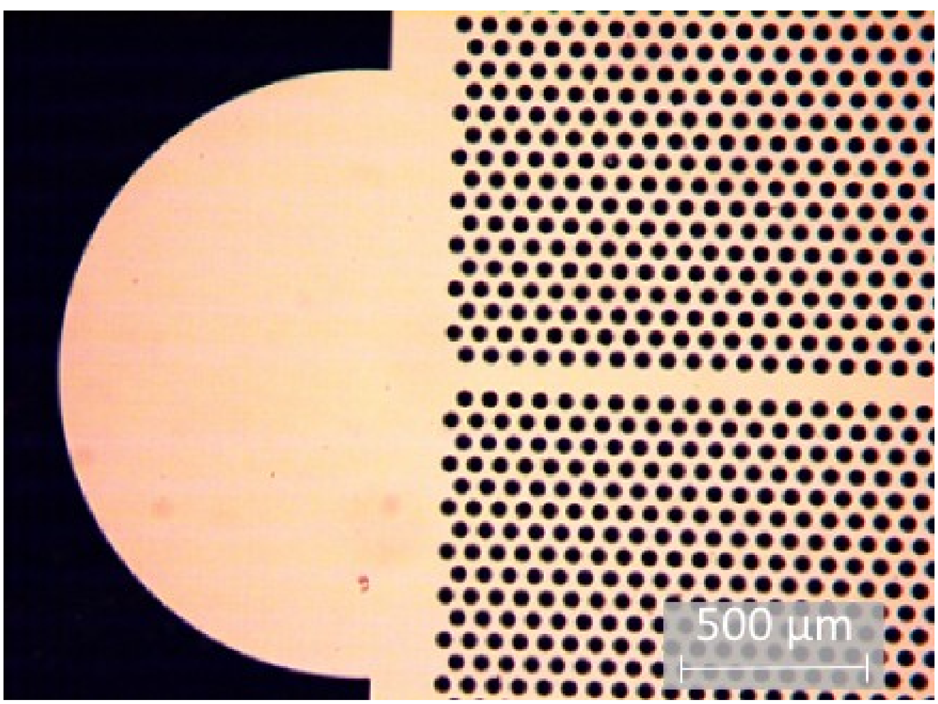

Figure 5.2 Optical photograph of a photonic crystal waveguide with an integrated 2D solid immersion lens with lattice constant a = 80 μm and thickness t=0.55 a.

To estimate the effect of the immersion lenses in the transmission we realize FDTD simulation of the whole structure. Figure 5.3(a) shows the calculation cell used in a full 3D FDTD simulation for the waveguide with immersion lenses; the figure corresponds to a plane centered in the middle of the slab. The corresponding theoretical transmittance for the waveguide with immersion lenses is reported in Figure 5.3(b). The structure for the waveguide without the immersion lenses and it corresponding transmittance are shown in Figure 5.3(c) and Figure 5.3(d) respectively.

From the FDTD simulation we have that the transmittance increased by as much as factor 10 for the structure without the immersion lenses. The reason is very simple: we have that the spotsize, 2mm, is larger than the input of the waveguide , about 100 μm, for the present structures. On the other hand the immersion lenses are about the same size of the spotsize. The factor of 10 comes from the bigger cross section of the beam that the lenses are able to focus into the entry of the waveguide.

In figure 5.4(d) the lower frequency edge of optical gap is located at 1.03 THz and is clearly visible in the spectrum. A high transmittance is observed below the edge of the optical gap for the sample without lenses which is clearly not seen in the waveguide with immersion lenses.

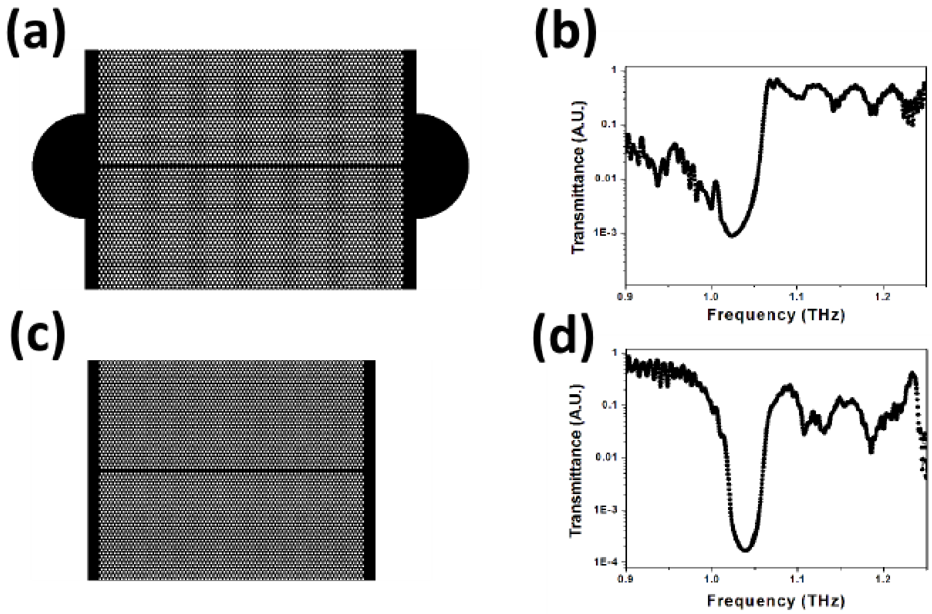

Figure 5.3 Transmittance in a Photonic crystal slab waveguide with and without immersion lenses. The photonic crystal slab waveguide with an immersion lenses structure (a) and its FDTD transmission through the structure (b). The photonic crystal slab waveguide structure (c) and the transmission through the structure (d) respectively. By comparing the transmittance (b) and (d) we have the immersion lenses improves significantly through the optical gap compared with the waveguide without immersion lenses.

The low transmittance below the gap for the samples with lenses is produced by the diffraction from the focusing point in the entry of the waveguide; if it is below the optical gap of the photonic crystal the beam focused is no longer confined to the waveguide and low transmittance is the final result. We can increase the power into the waveguide by increasing the size of the lenses but it will increase also the size of the sample. We estimated that with the parameters of the structure the transmittance was large enough to characterize the photonic crystal cavities.

We first characterized our waveguides by realizing transmission measurements. Figure 5.4 shows the experimental setup. The source is a continuous tunable source manufactured by Virginia Diodes inc., the source consists of a frequency synthesizer with a frequency span from 13.3 to 15 GHz. This is followed by a cascade of three frequency doublers and two frequency triplers. The final output is tunable from 0.9576 to 1.08 THz in steps as small as 72 KHz. The output launches a Gaussian beam with a 2mm beam diameter and 5μW average power. The sample is put in front of the source output and held in position by a metal slit to block the light which is not guided through the sample. Once the beam is transmitted through the sample a pair of of-axis parabolic mirrors collects the light and focuses into a 4K Silicon composite bolometer. A wire grid polarizer is located between the two parabolic mirrors to select the appropriate polarization.

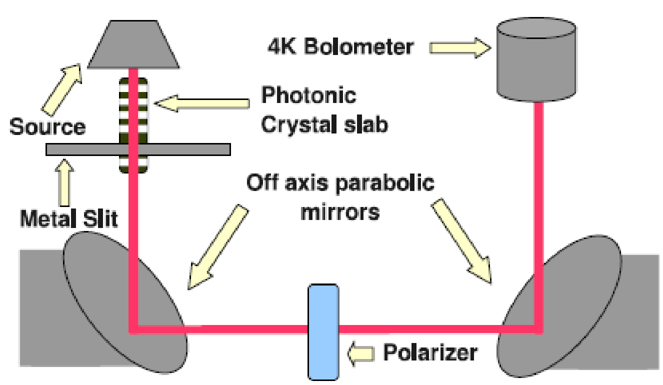

Figure 5.4 Transmission experimental setup.

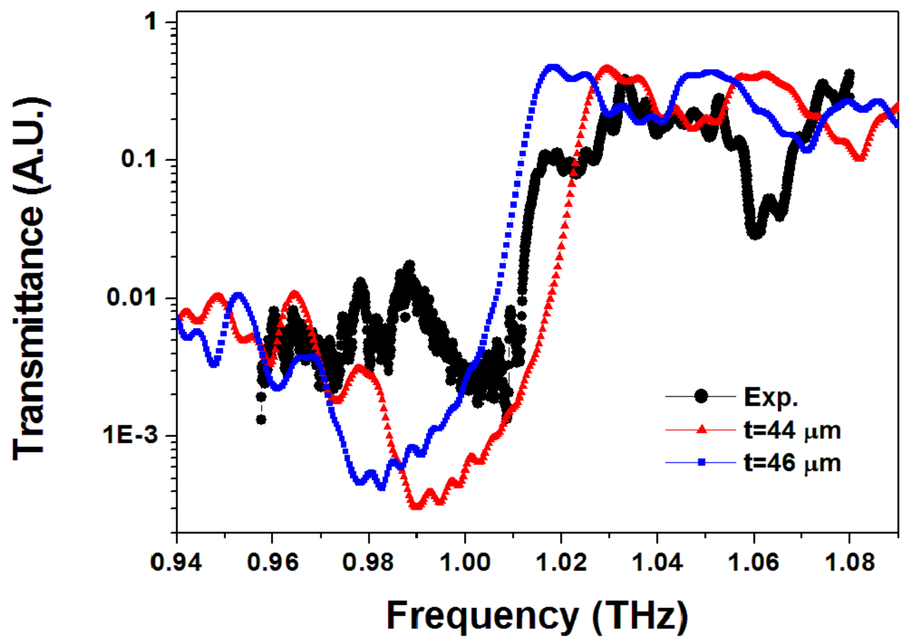

Figure 5.5 Experimental data is shown and compared with the FDTD simulation for t = 46 μm and t = 44 μm for the 80 μm sample.

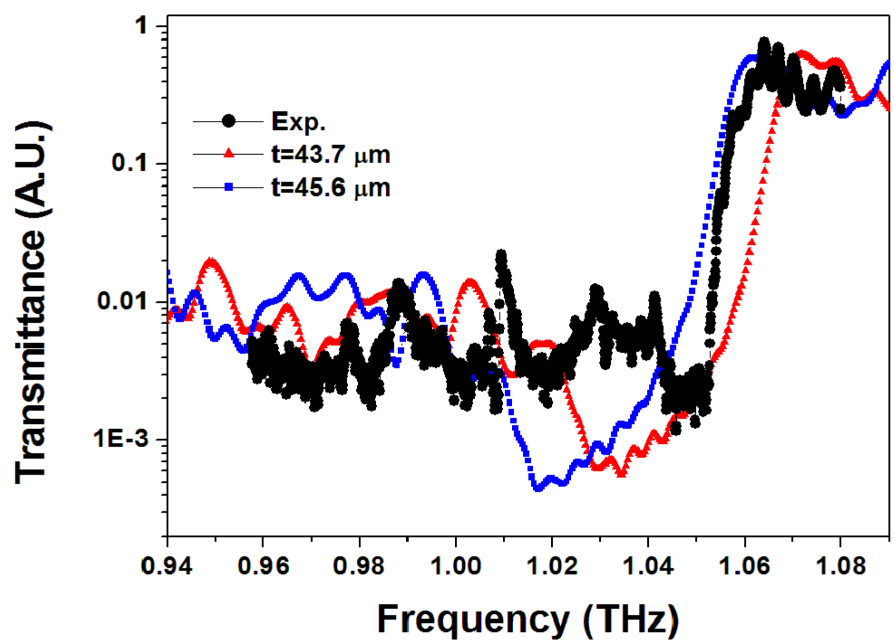

Figure 5.6 Experimental data is shown and compared with the FDTD simulation for t = 45.6 μm and t = 43.7 μm for the 76 μm sample.

The experimental transmittance measurements are reported in Figure 5.5(Figure 5.6) for the 80μm (76 μm) sample. We normalize the transmittance using the spectrum of the source and scaled to set the maximum in the waveguide transmission equal to one for each lattice constant.

The results for the samples with lattice constant 80 μm are shown in Figure 5.5. The waveguide starts transmitting at 1.015 THz. In Figure 5.6 we present the transmittance for the sample with lattice constant a = 76 μm. We observe that the edge of the transmission shifts to higher frequencies 1.053 THz as is expected for a sample with a smaller lattice constant. The frequency position of the edge of the transmission in both cases is less than 10 GHz, or within 1 % of the predicted value.

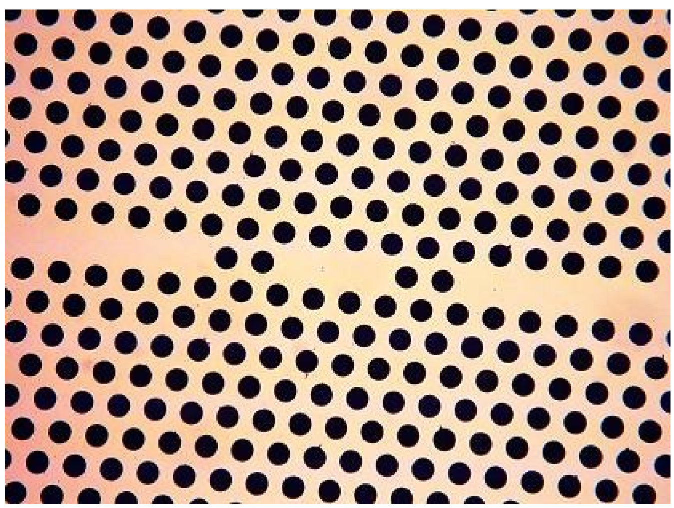

Figure 5.7 The Lorentzian filter formed by inserting a cavity in a photonic crystal waveguide. The cavity consists of three holes missing along the J orientation in a single mode photonic crystal slab with a triangular lattice of holes

The photonic crystal samples have the same dimensions as the waveguide samples. The Lorentzian filter is formed by inserting the L3 cavity into the waveguide and is delimited by two holes at each side of the cavity as is shown in Figure 5.7.

The Lorentzian filters were also characterized using the same transmittance setup. The transmittances for each lattice constant are shown in Figure 5.8 and Figure 5.9. For comparison we have also plotted the transmittance for the waveguide with the corresponding lattice constant.

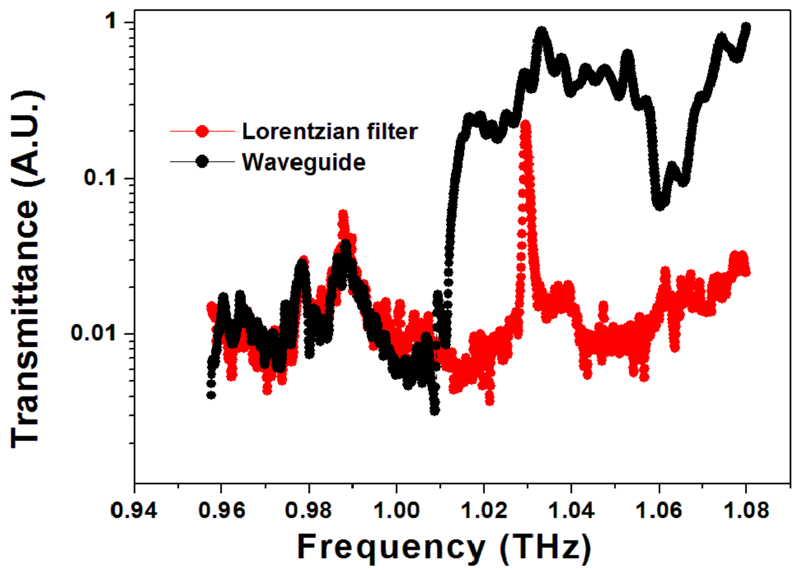

Figure 5.8 Transmittance through the waveguide and the Lorentzian filter for the sample with a=80 μm, a sharp resonance at 1.0296 THz in the Lorentzian filter, is associated with the resonance mode of the L3 cavity.

We observe that for the sample with a=80 μm the transmittance for the Lorentzian filters presents a sharp resonance at 1.0296 THz that corresponds to the frequency of the cavity mode as shown in Figure 5.7. For the 76 μm shown in Figure 5.8 the transmittance has the cavity resonance shift to 1.0724 THz, again consistent with the scalability property of photonic crystals.

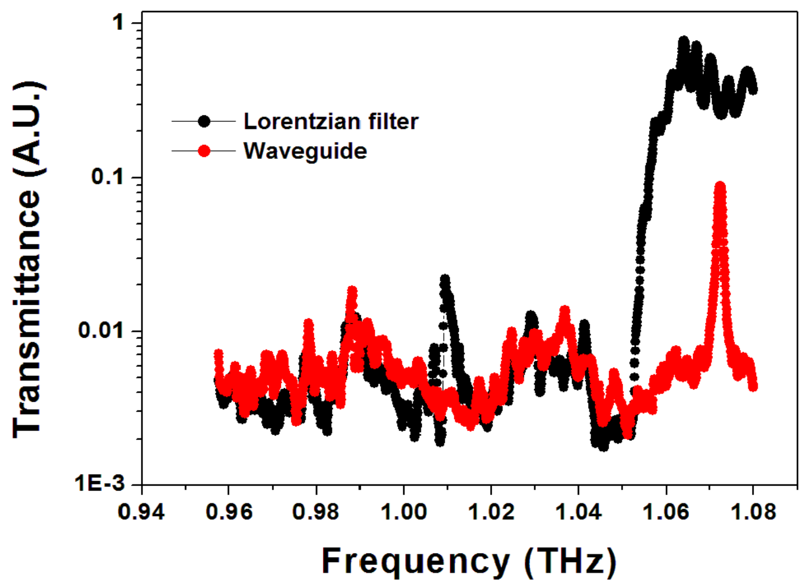

Figure 5.9 Transmittance through the waveguide and the Lorentzian filter for the sample with a=76 μm, a sharp resonance at 1.0724 THz in the Lorentzian filter, is associated with the resonance mode of the L3 cavity.

The resonances for the Lorentzian filters are fitted using a Lorentzian line shape. Figure 5.10 and Figure 5.11 shows the transmittance spectrum of the Lorentzian filter. Here we normalize the transmission spectrum of the filter using the transmission spectrum of the waveguide with the corresponding lattice constant.

For the sample with lattice constant 80 μm the resonance frequency is 1.0296 THz with a frequency width of 1.13 GHz which gives a Q value of 910 as shown in Figure 5.10. The resonance frequency for the 76 μm sample is located at 1.0724 THz with a frequency width 1.05 GHz or a Q value of 1020 as reported in Figure 5.11.

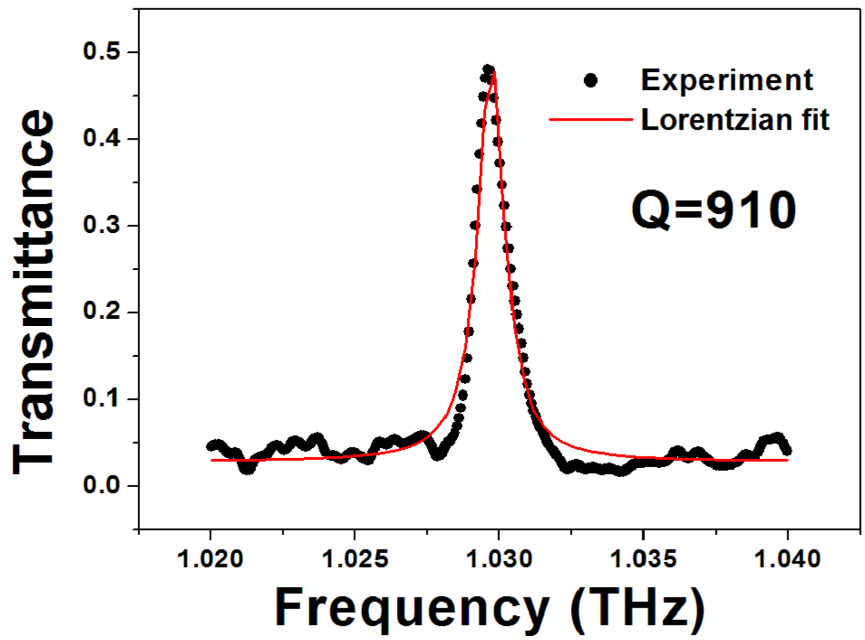

Figure 5.10 The transmittance through the filter is fit by a Lorentzian line center at 1.0296 THz with Q=910 for the 80 μm sample.

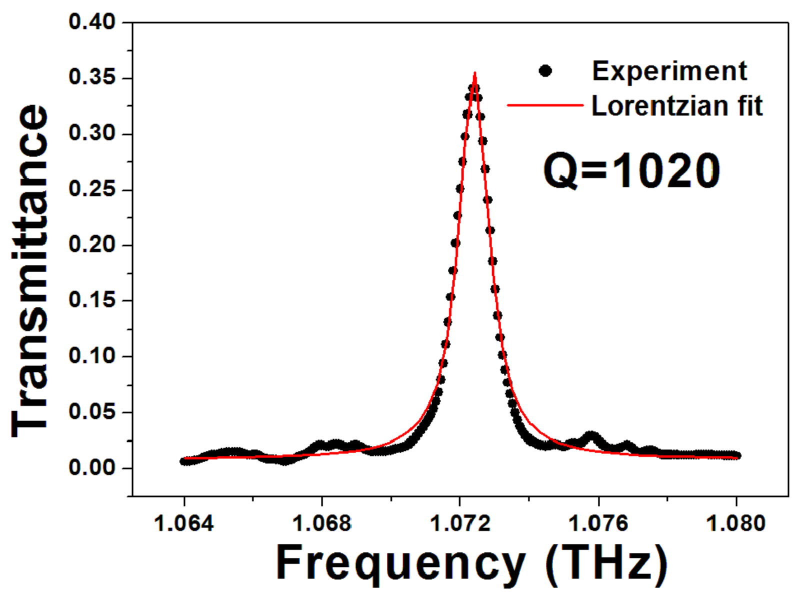

Figure 5.11 The transmittance through the filter is fit by a Lorentzian line center at 1.0724 THz with a Q=1020 for the 76 μm sample.

The resonant modes of the photonic crystal were analyzed using FDTD calculations for the resonant frequency and the quality factor of the structure. Temporal mode coupling theory [40] predicts that the quality factor Q_T for the Lorentzian filter is given by:

$$\frac{1}{Q_T} = \frac{1}{Q_R} + \frac{1}{Q_W} + \frac{1}{Q_M}$$

Where $1/Q_R$ is the radiative loss of the cavity, $1/Q_W$ is the loss associated with coupling to the waveguide, and $1/Q_M$ is the material loss.

Assuming that the material loss $1/Q_M$ is zero, FDTD predicts that the quality factor for the Lorentzian filter $(Q_R + Q_W)^{-1} = 1500$. Using these values we can estimate the material loss for the Lorentzian filter $1/Q_M$ to be 432 and 313 μradians for the 80 and 76 μm lattice samples respectively.

Lattice (μm)	Frequency (THz)	Quality Factor Q
	Experiment	
80	1.0296	910
76	1.0724	1020
	3D-FDTD	
80	1.0293	960
76	1.0742	1065

Table I. Experimental frequency and Q values for the L3 cavity resonance mode and the 3D-FDTD simulated values for the structure. A loss of 432(313) μrad is included for the 3D-FDTD simulation for the 80(76) μm sample.

As a consistency check, FDTD calculations where performed with the estimated material losses, given a total Q value of 960 and 1065, which are close to those found in the experiments (see Table I).

The absorption coefficient α can be calculated using the expression:

$$\alpha = \frac{2\pi n f}{c} Tan(\delta)$$

Here we have that $Tan(\delta)$ is the loss tangent corresponding to the material loss, f is the frequency and c is the velocity of light. With these values the absorption coefficients are 0.318 and 0.240 cm^{-1} for the samples with 80 and 76 μm, respectively. These values are higher than 0.01cm^{-1}, the reported value for intrinsic absorption in high quality silicon with resistance higher than 10 kΩ-cm [32] . The higher losses we observe indicate that our wafer has a lower resistivity than 10 kΩ-cm (nominal resistivity 4 kΩ-cm) and there may also be small additional loss of unknown origin.

6 Transversal Magnetic Photonic crystal cavity

In parallel to the fabrication and measurement of the TE photonic crystal slab we also studied the possibility of the construction for a Transversal Magnetic (TM) photonic crystal cavity. The search for a TM cavity is motivated by the fact that, for some applications, a small resonant cavity with electric field normal to the surface of a semiconductor wafer is desirable [17].

We employed FDTD to test different design until we finally chose the cavity shown in Figure 6.1. The cavity consists in two holes missing along the ΓJ orientation in a triangular lattice of air holes in a silicon slab. The cavity is embedded in a waveguide and delimited by two holes at each side of the waveguide, forming a Lorentzian filter. The characterization of these structure was done by transmission and to enhance the coupling into the waveguide we used solid immersion lenses that we incorporate into the structure [41].

Because of the fragility of this structure, which is only 21% Silicon in the bulk of the photonic crystal, we chose a Si slab much thicker than the 50 μm slab used in the TE samples discussed in the chapters 4 and 5. The slab supports several transverse modes, up to five modes for the used thickness. High-Q cavity modes are observed experimentally. The assignment of the experimentally-observed modes to particular modes supported in the structure turned out to be significantly more complicated than anticipated at the beginning of this project.

The work plan for this chapter starts with the fabrication of the samples and the measure of the photonic crystal parameters. . We will start our measurements by measuring the single most important feature of photonic crystal structure: its photonic crystal gap because within where a photonic crystal cavity mode could be found. The quality factor and frequency resonance of the cavity will we measure through a high frequency resolution transmittance using a narrow band tunable source. Then we will go through a heavy theoretical description of the cavity-waveguide coupling, which ultimate goal is to indentify the resonant peak in the transmittance as a resonant mode of the cavity. The identification process strongly relies in the two dimensional picture of the cavity, i.e. the structure considering that thickness is infinite, in which the identification of the modes is simpler. Employing the symmetry set by the excitation pulse used in the experiment a single cavity mode is positively identifies as the one observed in high frequency resolution transmittance for the Lorentzian filter

A. Sample Fabrication

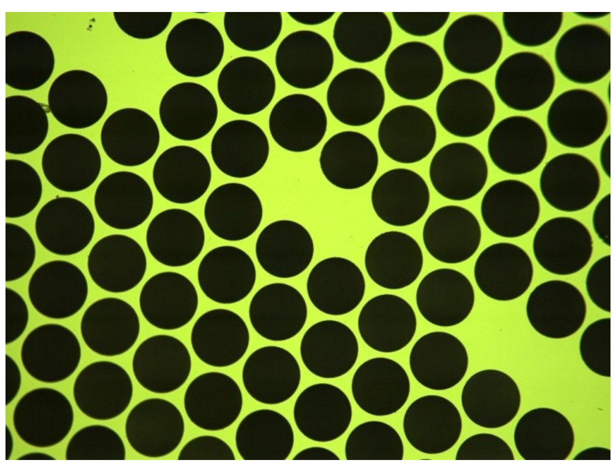

Figure 6.1 Optical photograph of the cavity embedded in the photonic crystal waveguide. The lattice constant is a=135 μm, the thickness t=2.81 a and the hole radius r=0.46 a.

The fabrication process was done at Nanotech UCSB Nanofabrication Facility. The process starts by using ultraviolet lithography to transfer a designed pattern to a single side polish 20 kΩ-cm high resistivity silicon wafer with nominal thickness of 380 μm. The etching of the holes in the pattern was done using Deep Reactive Ion Etching (RIE) with a Plasma-Therm 770 SLR. The details of the fabrication are described in chapter 3 and the detailed recipes are in Appendix D.

The thickness of the slab was thick enough to be measured with a thickness gauge. The average values found was 380 μm and the flatness specified by the vendor was 2μm thus the thickness of the slab is $t=380\pm2$ μm. The hole radius was specified to be $r=0.45$ however the optical microscopy measurements on the fabricated samples found a value of $r/a = 0.465 \pm 0.005$ for the size of the hole, we attribute the discrepancy with a overetch and a macroloading effect (large exposed areas etch faster) in the RIE.

B. Photonic crystal gap measurements

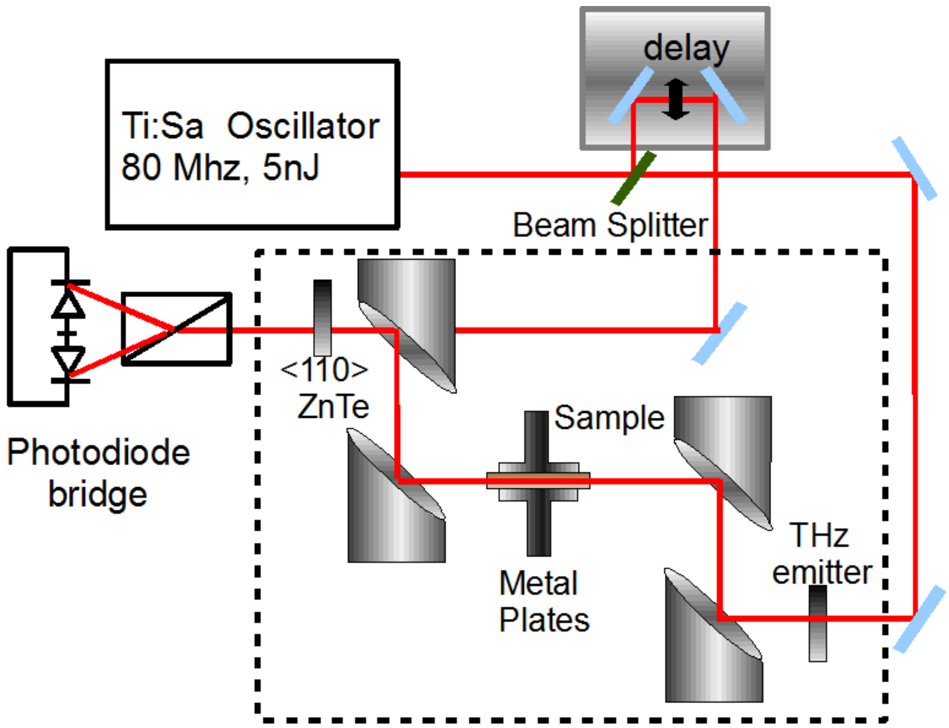

Figure 6.2 Terahertz time domain setup. A photoconductive switch is used as a broadband source and it is detected by electro-optic effects using a ZnTe crystal and balance photodiode bridge.

Our first step was to measure the photonic crystal gap of our strcutre; for this purpose we employed a THZ-time-domain spectrometer (TDS); The THZ-TDS system that we employed in the experiment has significant better signal to noise in 1 THz region compared with FTIR. THz-TDS technique relies on the fact that short time pulses are formed by a large superposition of frequencies. The typical setup consists in an ultra-short pulse typically around 100fs. The femtosecond pulse is divided into two beams. One beam is used as a probe beam while the other is used to excite an emitter. The emitter generates terahertz with bandwidth of a couple terahertz depending of the generation scheme. In most conventional systems the exciting beam before striking the emitter goes through a Michelson interferometer, while the optical path of beam is kept fixed. Once the terahertz beam is generated it goes through the sample and then is focused into a detector together with the probe beam. The detector generates a signal that is a function of the electric field in the terahertz beam. The probe pulse, being shorter that the Terahertz beam, maps the electric field in the terahertz pulse as a function of the time delay of the excitation pulse. This creates a time trace of the electric field that could be Fourier transform to obtain the frequency information carried by the terahertz pulse.

Our THz-TDs system is based on a Ti:Sa laser with a photoconductive switch as a source and detecting the signal through electro-optical. Single cycle terahertz pulses were produced when 70 fs pulses with a wavelength of 800 nm from a A Ti:Sa oscillator were delivered to a photoconductive switch. The femtosecond pulse with energy above the bandgap generates carriers in the semiconductor substrate. The carriers are then accelerated by a bias produced by a metal pattern in a semiconductor substrate. The bandwidth of the produced Terahertz is determined by the applied voltage and the pulse duration. In our setup as shown in Figure 6.2 the switch consisted in an interdigitated structure [32] with a gap of 1.5 μm constructed on a semi-insulating GaAs substrate. The bias voltage was set to 1.5 V which results in an electric field of 10 kV/cm and the pulse energy of 2.5 nJ. With these values the THz fields were a few tens of V/cm.

The beam was collimated and then refocused on to the sample with a spot size of about 500 μm using off-axis parabolic mirrors (OAPMs). The transmitted pulse is then analyzed by electro-optic detection in a 500 μm thick <110> oriented ZnTe crystal and Lock-In detection to the frequency of the modulated bias voltage was employed. The path of the THz radiation can efficiently be purged with dry nitrogen to avoid water absorption. For the transmission, the TEM polarized THz pulses are edge-coupled into the photonic crystal that was mounted in-between metal plates without further focusing elements beside the OAPMs. The beam was focus in the photonic crystal at a point locate around 2000 μm from the entry of the waveguide. Although better coupling methods have been developed [42], the coupling efficiency was large enough for our system.

In Figure 6.3 we show the time trace of the pulse traveling in the purged empty box, a single cycle pulse is generated and it has a time width of a few picoseconds. In Figure 6.4 we show the Fourier transform of the time trace. Here for the Fourier analysis we only considering the time window before the second pulse is measured, the second pulse is produces by the backside reflection inside the semiconductor substrate.

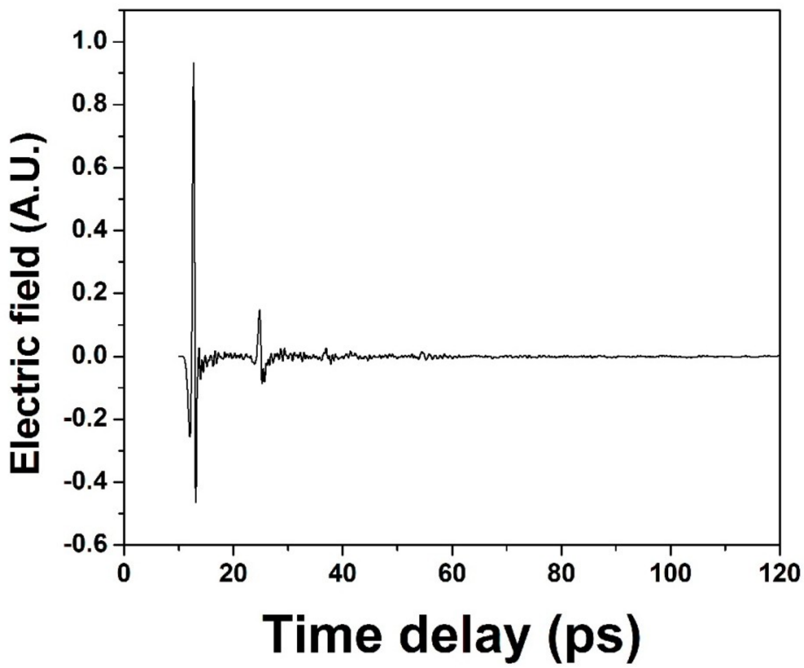

Figure 6.3 Time domain trace of the reference

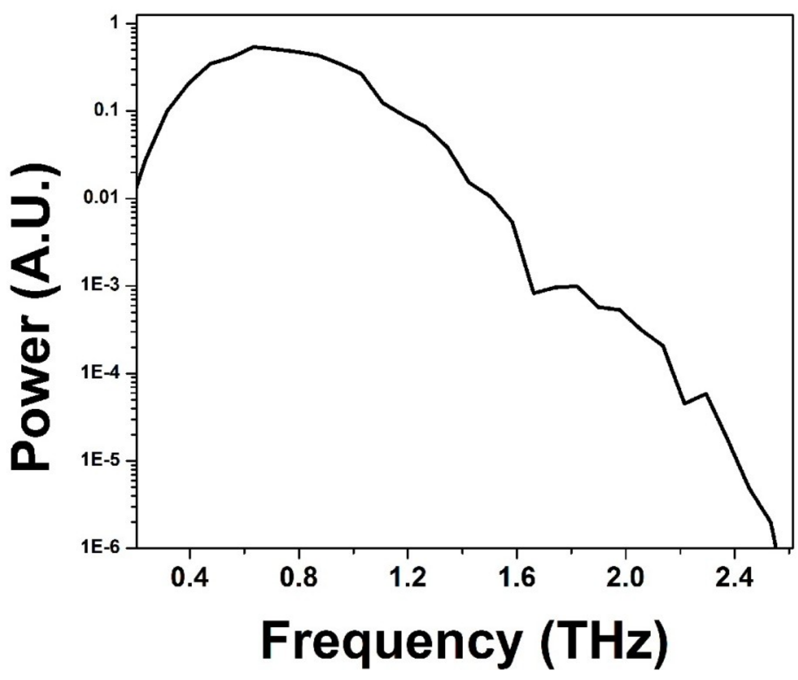

Figure 6.4 Fourier transform of the time domain trace.

From Figure 6.5 to Figure 6.7 we show the time domain trace and its corresponding transmittance for samples with lattice constant 140, 135 and 150 µm respectively; we use as a reference the transmittance of the single pulse in the empty box shown in Figure 6.3 and Figure 6.4. For the three samples a large dispersion from the single cycle reference is seen as is expected for a photonic crystal structure, especially for the frequencies components that are close to the stop bands of the structure where band dispersion in nearly flat.

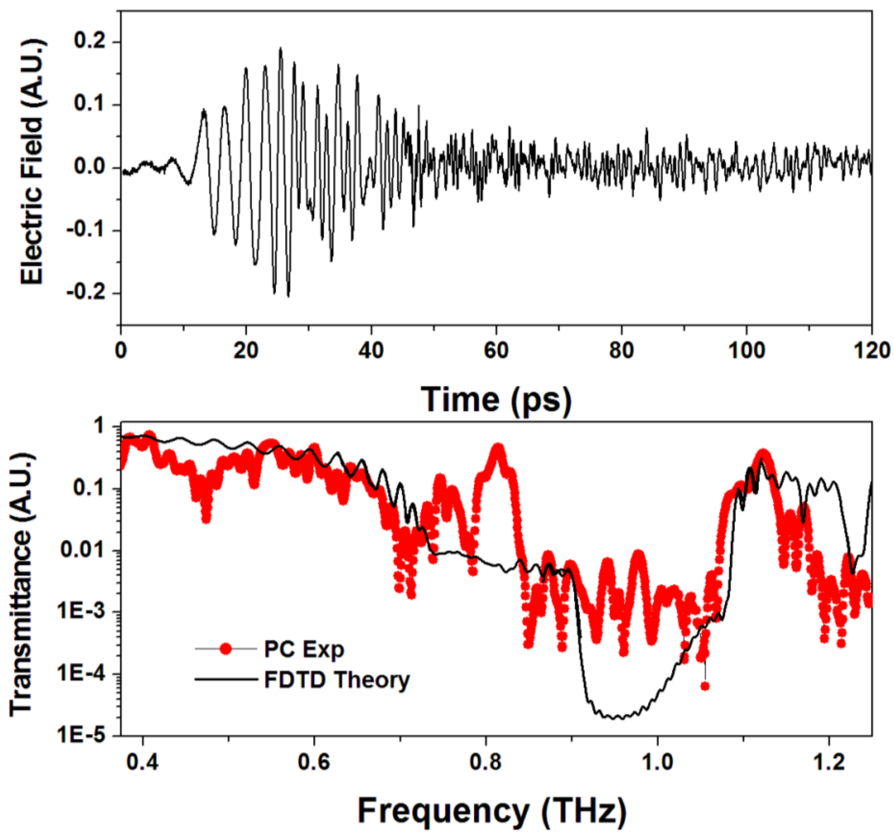

Figure 6.5 Terahertz time domain measurement. Time trace of the Electric field and THz pulse transmitted through the samples with lattice constant a=135 µm. A low transmittance from 0.835 to 1.074 THz shows a good agreement with the FDTD calculations.

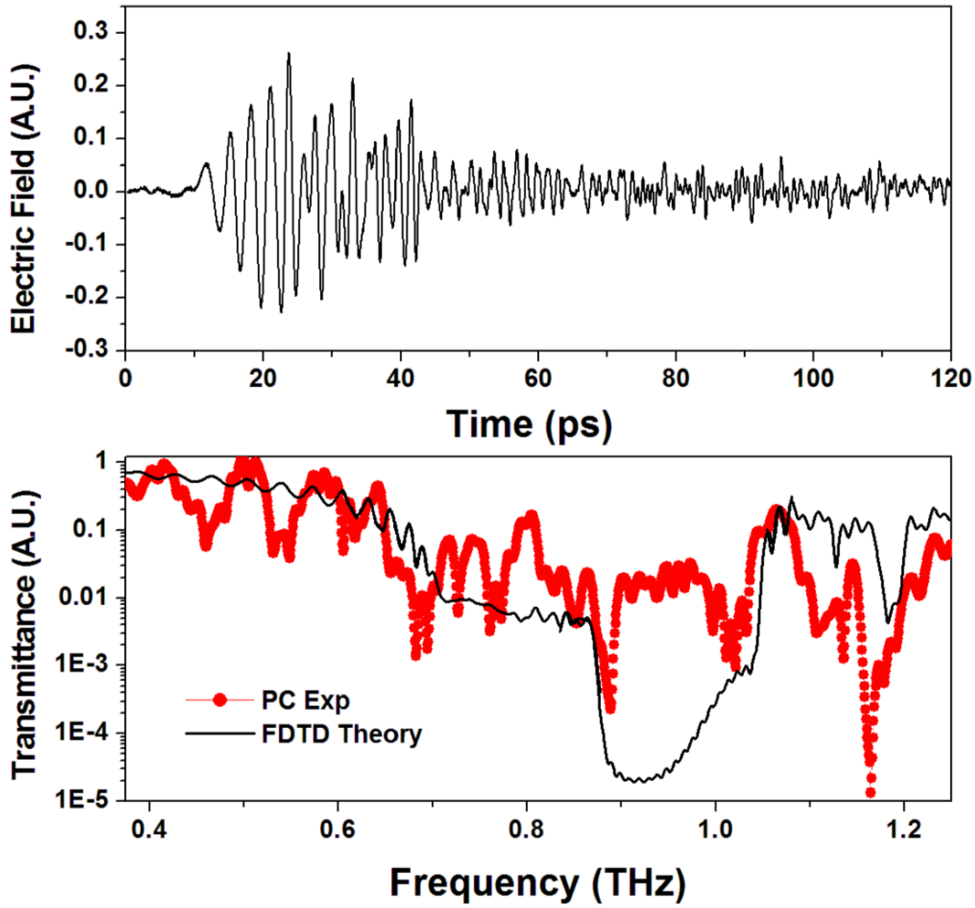

Figure 6.6 Terahertz time domain measurement. Time trace of the Electric field and THz pulse transmitted through the samples with lattice constant a=140 µm. A low transmittance from 0.808 to 1.036 THz shows a good agreement with the FDTD calculations.

Figure 6.5 to 6.7 shows a low transmittance region that is well matched by using FDTD simulations of the structure which for the three figures are shown in solid line. The values for the low transmittance predicted by FDTD and found are shown in Table 6.1. The code used for calculating the transmittance in shown in Appendix F.

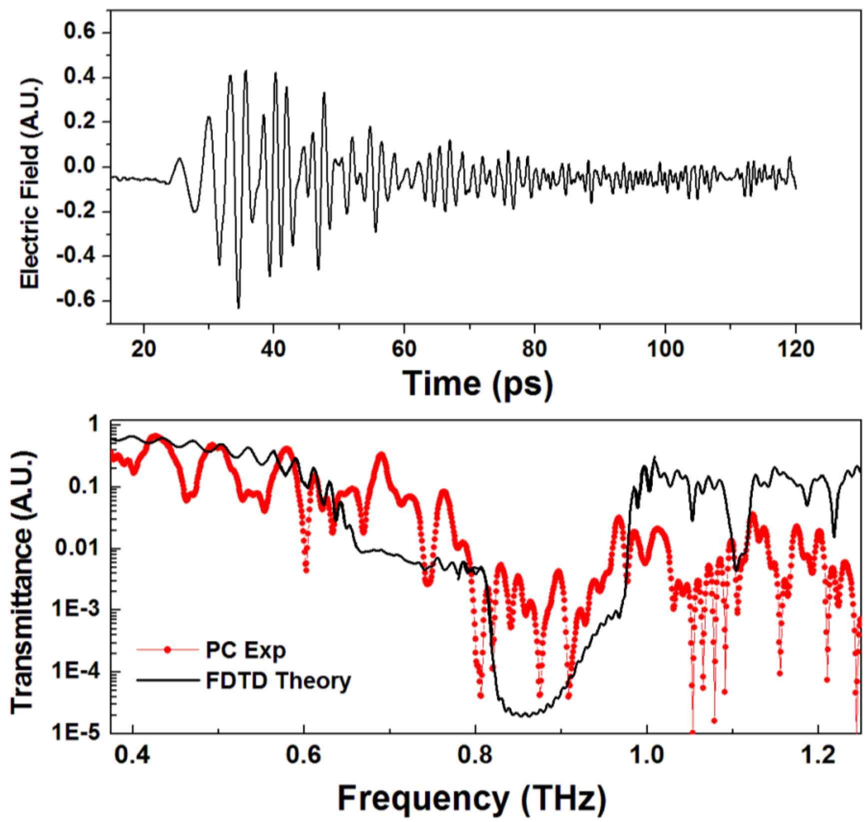

Figure 6.7 Terahertz time domain measurement. Time trace of the Electric field and THz pulse transmitted through the samples with lattice constant a=150 µm. A low transmittance from 0.795 to 0.961 THz is consistent with the FDTD calculations.

Lattice constant (μm)	Start frequency (THz)	End frequency (THz)	Width (THz)	Gap to midgap (THz)
Experiment				
150	0.795	0.961	0.166	0.189
140	0.809	1.036	0.227	0.246
135	0.835	1.074	0.239	0.251
3d FDTD				
150	0.8265	0.9692	0.1427	0.1589
140	0.8754	1.0356	0.1602	0.168
135	0.9091	1.0877	0.1786	0.179

Table 6-1 Photonic crystal frequencies experimental and theoretical values, the experimental error for the frequency is ± 10 GHz, corresponding to the resolution of the THz-TDS

C. *Photonic crystal gap theoretical calculation*

The next step is to compare the transmittance with the theoretical model for the photonic crystal. The thickness of the sample is several times the lattice constant and therefore the slab is not single mode. In principle there is not a complete gap. We will show that product of symmetry imposed by the THz beam used in our experiment produces a low transmittance frequency region that for all practical purposes works as an optical gap. This gap is the product of a stronger coupling to the lower mode in the slab compared to the higher slab modes. We will base our argument in symmetries and in fact we will verify by using FDTD to calculate the transmittance through the photonic crystal as the ones shown in figure 6.5 to figure 6.7. We will show that the coupling higher modes of the modes slab are negligible.

1. Two dimensional calculation

Let start our analysis by considering the two dimensional (infinitely thick) triangular photonic crystal. Figure 6.8 shows the band diagram calculated using MPB; with the code shown in Appendix F. We show the Ez profile for several points along the ΓJ direction in the triangular lattice. We have that band 1, 3 and 5 have their fields symmetric with respect to the ΓJ orientation and therefore could be coupled to a plane wave (or any symmetric beam) traveling along this direction while bands 2 and 4 with antisymmetric field do not couple to a plane wave. For a symmetric in plane excitation we have that modes in bands 1, 3 and 5 will show a transmittance, while modes in bands 2 and 4 will not.

From the band diagram we expect high transmittance up to 0.306, corresponding to the first band. There is an optical gap from 0.306 to 0.484 (c/a), correspond to the gap between band 1 and band 3. Then comes another small window of transmittance from 0.484 to 0.520 (c/a), corresponding to band 3. These optical gaps are confirmed by FDTD simulation as shown in Figure 6.9.

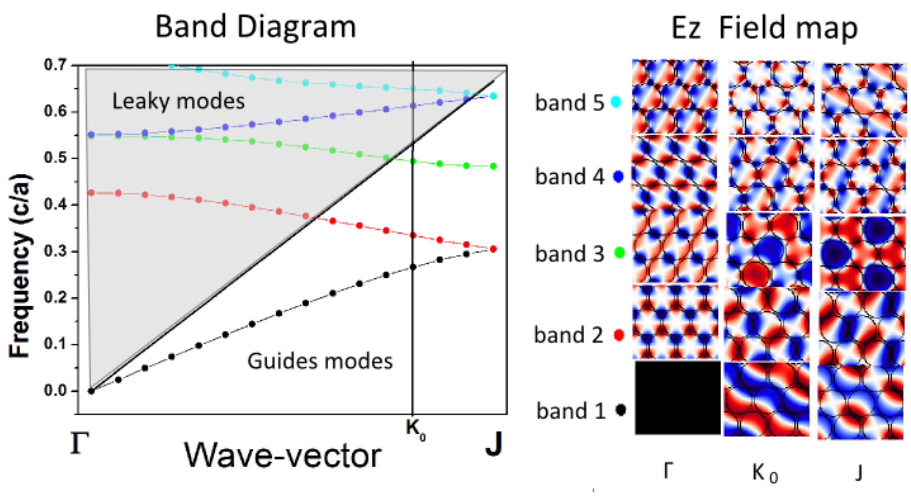

Figure 6.8 Two dimensional photonic crystal band diagram and Ez field for a specific point in the GJ orientation in the First Brillouin Zone

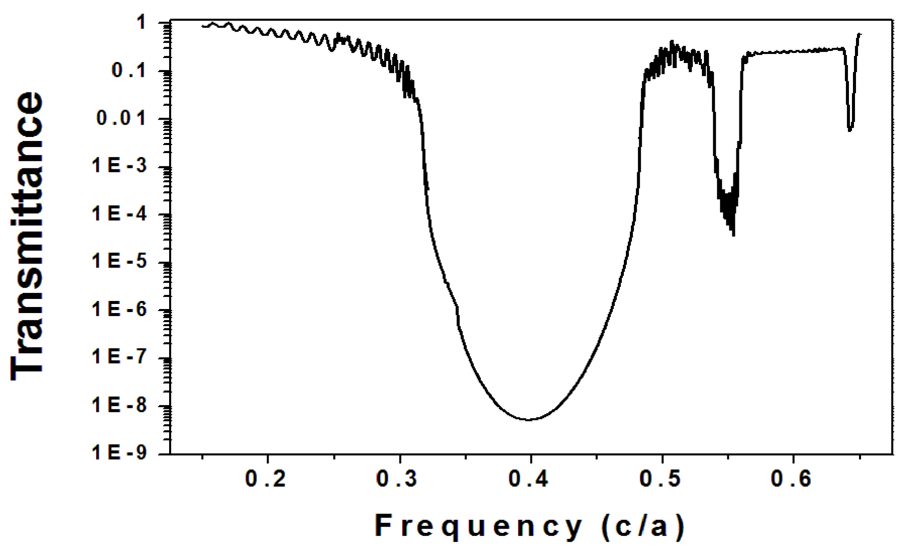

Figure 6.9 Transmittance along the ΓJ orientation in the two dimensional triangular lattice of holes r=0.465a for a TM polarization.

2. Three dimensional calculation

With the information obtained from the 2d case now we confront more easily the highly more complicated band diagram of the 3d photonic slab structure. We realize full 3D simulation of the photonic crystal slab using the parameters corresponding to the 135 μm sample (the qualitative description will be the same for all the samples). The code used is in Appendix F.

The band diagram for the finite thickness photonic crystal slab is shown in Figure 6.10. Here we immediately notice the increase of the number bands in comparison with two dimensional structures as a consequence of the finite thickness.

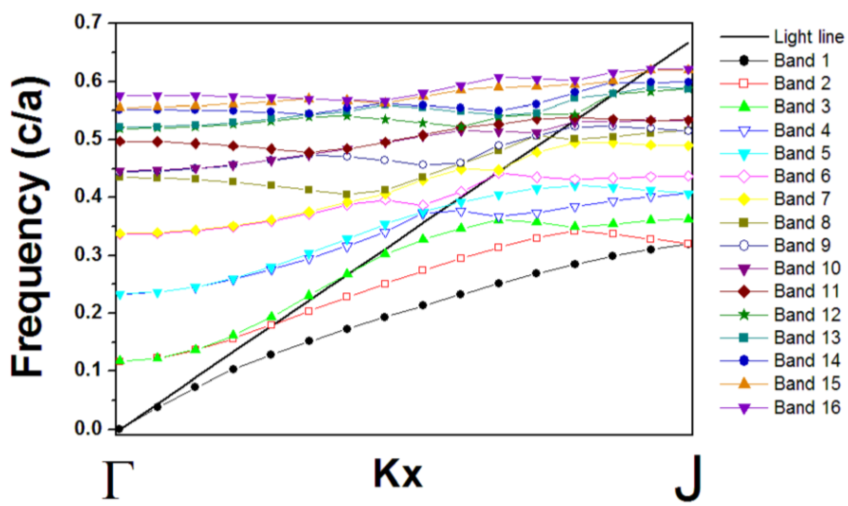

Figure 6.10 Three dimension Band diagram structure for the triangular lattice of holes

Above the light line the modes are leaky i.e. they do not satisfy total internal reflection and therefore are not guided through the slab; these modes are for our purposes completely ignored.

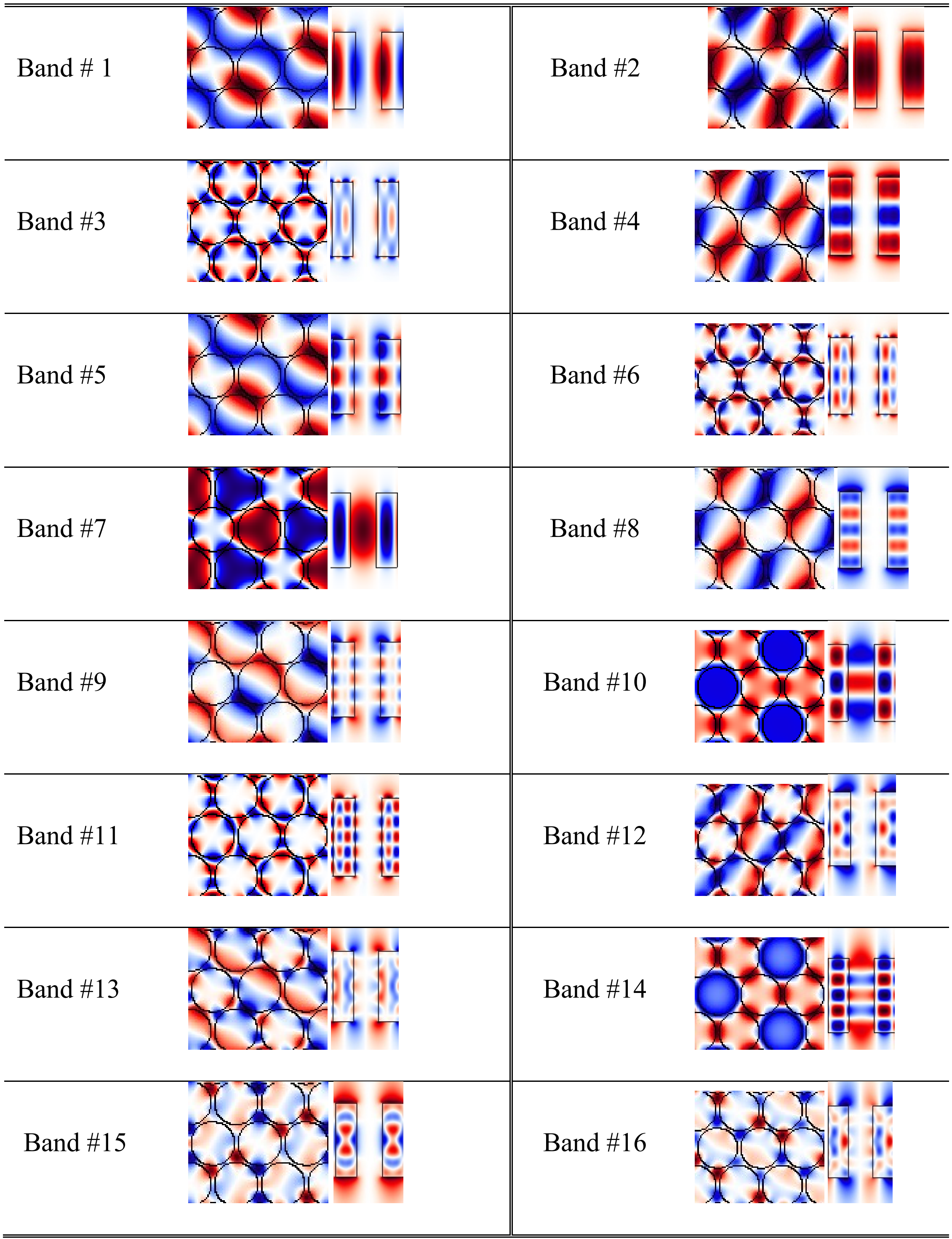

Figure 6.11 Ez field profile for the photonic crystal slab with thickness t=2.81a and hole radius r=0.465a.

The modes below the light line are guided modes. In our experiment we excited the system with a THz Gaussian beam; the symmetry imposed by the excitation selects which modes are able to be excited and also the relative prominence of each mode in the transmittance spectrum.

Our first selection rule is that modes which are not symmetric in the plane of the slab will not be exited. This rule is the same as the two dimensional case in which bands 3 and 4 in Figure 6.8 are not coupled.

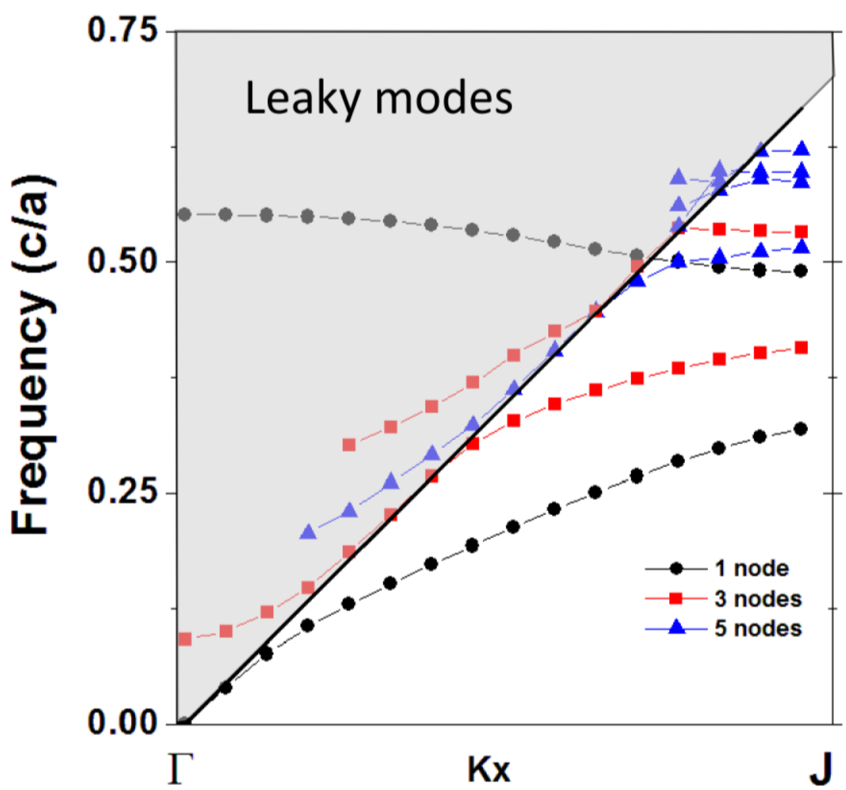

Figure 6.12 Band diagram for the in plane symmetric modes. Below the light line the modes are guided through the slab. Modes in the leaky region are not couple in the transmittance and are omitted here.

The second rule is a quantitative estimate of the relative intensity when there are more than one mode at the same frequency. This is a simple rule of thumb: the higher the harmonic the weaker the coupling is; i.e. a mode which has a higher number of nodes will couple weaker than a mode with a lower number nodes and that the coupling strength is proportional to the overlap between the field of the excitation beam and the field profile of the mode.

To explain this selection of a hierarchy of the modes we show the Ez field profile at the J point in the Brillouin zone in Figure 6.11. The modes 1, 5, 7, 9, 10, 13, 14 and 16 are symmetric with respect to the ΓJ orientation and they could be exited in a transmittance experiment. After eliminating the bands which are not symmetric and keeping only the symmetric modes we have the band diagram show in Figure 6.12.

In Figure 6.12 we marked with ● (solid circle) the band which has a single node, for example field mode in band 7 in Figure 6.11. These bands are the analogues for the two dimensional case. These bands will be very strongly coupled by a Gaussian beam, providing strong transmittance from 0 to 0.3195 (c/a) for the first one node band and from 0.4899 to 0.5025 (c/a) for the second single node band.

Bands marked with a ■ (solid square) in Figure 6.12 are bands with three nodes in the Ez field in the z direction, for example field mode in band 5 in Figure 6.11. They have a lower coupling relative to the single node bands. We expect a low transmittance when coupling to the modes in these bands. The three node bands dominate the transmittance from 0.3195 to 0.40751 (c/a), and from 0.5328 to 0.5371.

Finally bands marked with ▲ in Figure 6.12 are band with modes with 5 nodes in Ez field in the z directions, for example field mode in band 14 in Figure 6.11. These bands have the lowest coupling of all the bands shown in Figure 6.12. They dominate the transmittance where neither the single node nor the three nodes are present. They are dominant from 0.4792 to 0.4899 (c/a), 0.5025 to 0.51585 (c/a) and above 0.57831 (c/a).

We have that there is an optical gap in the symmetric modes from 0.40751 to 0.4792. Another small gap spans from 0.5371 to 0.57831. These gaps found from the band diagram of the bright modes are confirmed by FDTD simulation of the transmittance as shown in Figure 6.13.

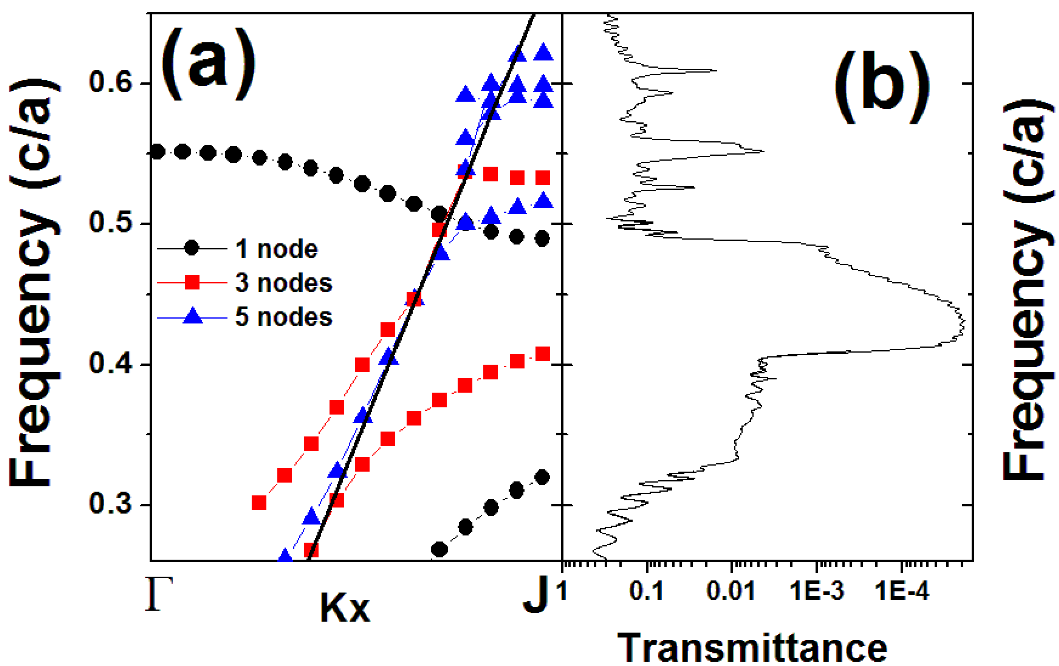

Figure 6.13 (a) Band structure of the in plane symmetric modes (b) transmittance along the ΓJ orientation.

The two dimensional model is extremely useful for understanding the properties of the more complicated three dimensional slab. Our argument is that the excitation beam selects the modes that we are able to couple and the lower modes (modes with a single node in the Z direction) with a symmetric field along the propagation direction are strongly dominant. If we just keep these single node modes we have a description that matches very well the two dimensional case as shown in Figure 6.14. However the match between the single node and the two dimensional is not surprising since the three dimensional band structure should asymptotically approximate to the two dimensional case as the slab increase it thickness. For the present parameter the three dimensional bands structure for single node symmetric modes are a few GHz higher that the corresponding two dimensional. The approximation of using the two dimensional case for explaining the more complex interaction between the THz beam and the 3D photonic crystal structure will be the warhorse for analyzing the frequency response of the filter structure presented in the present chapter.

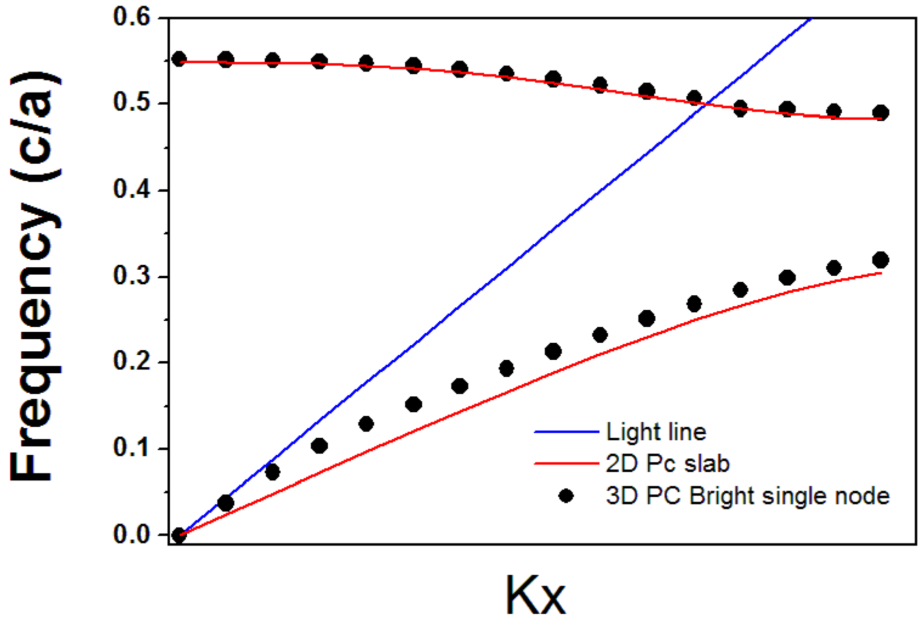

Figure 6.14 Three dimensional bright modes compared with the two dimensional photonic crystal band structures.

The optical transmittance found in the experiment allows working in the optical gap which is in dimensionless frequency range of 0.40751 to 0.4792 (c/a). It is in this frequency range where the resonant cavity modes are located.

D. Cavity mode measurements

Our purpose is to create a cavity with resonant frequency is the vicinity of 1THz for transverse electric polarization. Once we have selected it we need a way to characterize the cavity i.e. we want to know its resonant frequencies and its quality factor. We need either to produce light inside the cavity or couple radiation into the cavity. We use the later approach

For characterizing experimentally the resonant cavity of the photonic crystal we inserted the cavity into a photonic crystal waveguide forming a narrow band Lorentzian filter as shown in Figure 6.1. We expected that from this configuration the peaks in the transmittance through the filter structure contained information on the resonance frequency of the cavity and its quality factor.

Looking for resonant modes with high quality means narrow lines. For a quality factor of 1000 at 1 THz for good characterization we require a frequency resolution at least 0.1 GHz. This resolution is not accessible by using THz-TDS. However it is easily obtained with our high resolution spectroscopy as shown in Figure 6.15.

The Terahertz spectroscopy setup shown in Figure 6.15 is based on a solid state source made by Virginia Diodes inc., with a spectrum range from 0.9576 - 1.080 THz tunable in 72Khz steps. It outputs a polarized Gaussian beam with an average power of 5 μW with a spot size of about 2 mm. The samples were located at the output of the source and held in place by a metal plate. The output of the waveguide then is focused into a 4k silicon composite bolometer using two off-axis parabolic mirrors. A wire grid polarizer is positioned between the two parabolic mirrors to select the polarization of the electric field normal to the plane of the slab (TM).

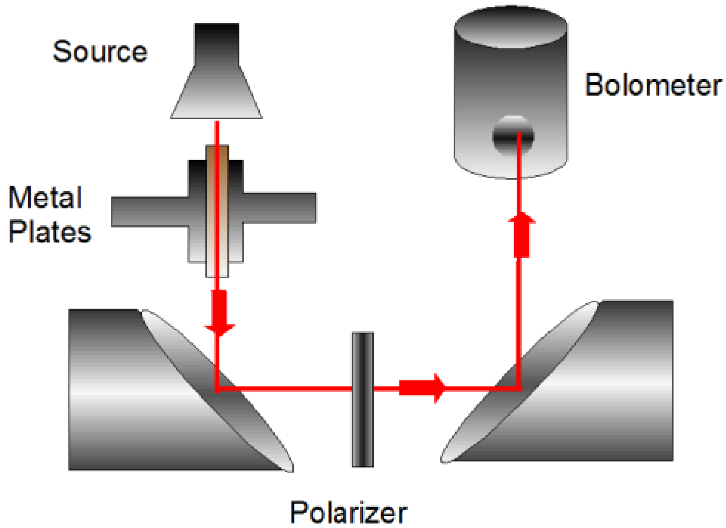

Figure 6.15 Terahertz frequency domain setup. A 0.957 to 1.080 narrow band tunable source couples into sample. The signal is measured using a bolometer.

The transmittance is measured across the range of the source. The results are shown in Figure 6.16. It's worth mentioning that all the peaks that appear in the spectrum are somehow a resonance of the cavity; among the peak that appear in the spectrum we focus our attention on the isolate peak that appears around 0.99 THz for the 140 and at 1.020 for the 135 μm sample. These peaks are well defined and isolated from the rest which makes them more favorable for applications.

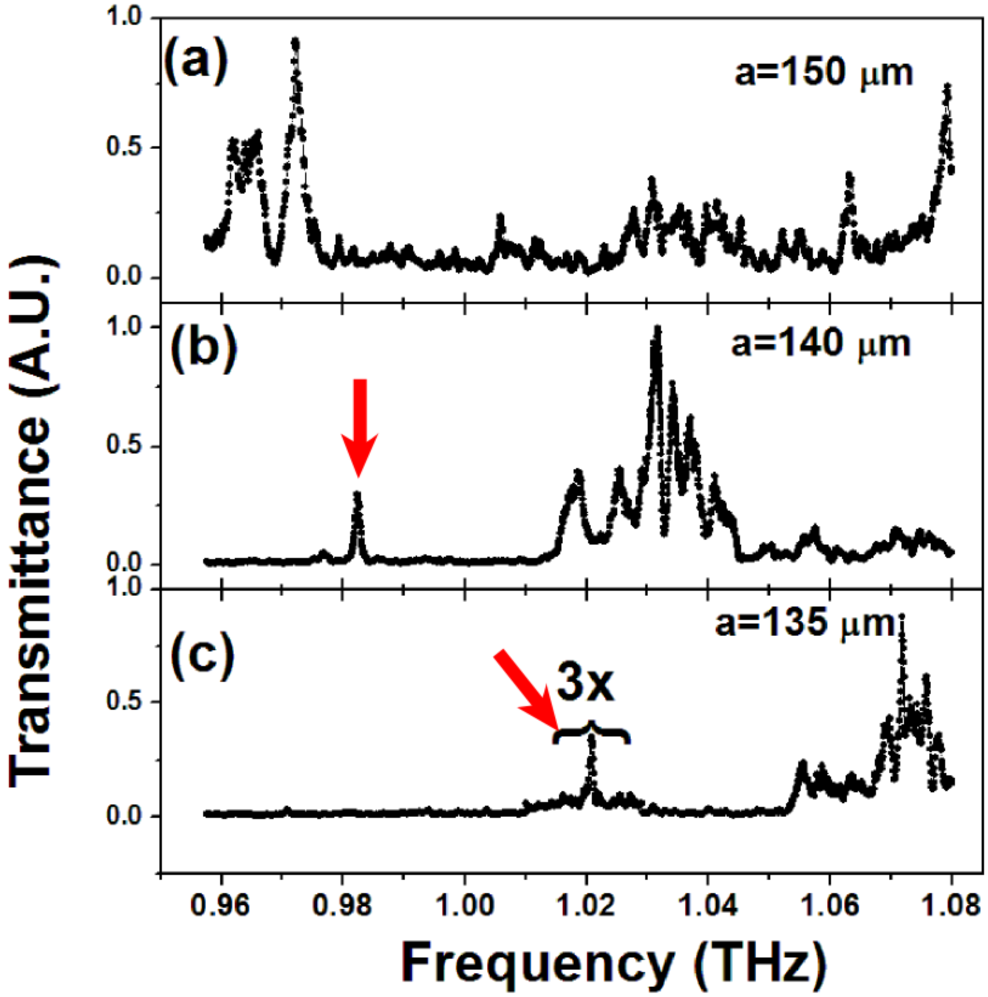

Figure 6.16 Frequency domain measurements for the Lorentzian filter. An isolated peak (signaled with an arrow) well inside the region of low transmittance of the photonic crystal is associated with a resonant mode for the cavity.(a) Here we only observe a high transmission region near 0.960 GHz (b) A resonant mode at located is 0.982 for the 140 μm sample. (c) A resonant mode is located at 1.020 for the 135 μm sample.

To verify that the isolated peaks that appear in Figure 6.16 are resonant modes we need to show that their frequencies and quality factors matches with the theoretical predictions.

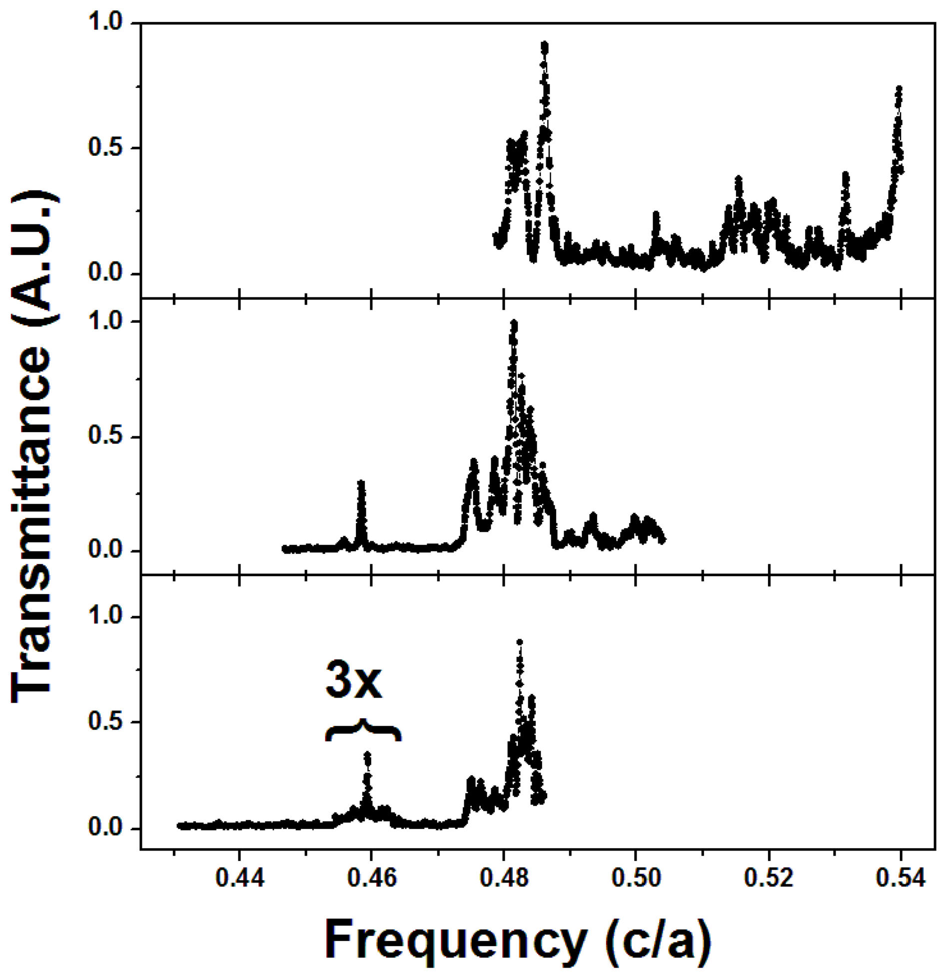

Figure 6.17 Frequency domain measurements for the Lorentzian filter in dimensionless units. An isolated peak located at 0.46 (c/a) is observed for sample with lattice constant a=140 μm and a=135 μm as shown in (b) and (c) respectively. A high transmittance center at 0.48 (c/a) is observed for the three samples.

Our first step is to plot the data from Figure 6.12 using dimensionless units as shown in Figure 6.13. We recognize that the features located at 0.48 (c/a) are similar for the three samples; however these features are not the most interesting part of the spectrum. The most significant feature is the lower frequency peak in the transmittance within the stop band of the photonic crystal, which is associate with a cavity resonant mode and is located at 0.982 (1.020) THz for the 140 (135) μm sample. The transmittance also exhibits a high transmittance window, above 1.015(1.053) THz for the 140(135) μm sample, that corresponds to the upper edge of stop band and in this region there are also several peaks corresponding to modes which are pushed into the stop band by the cavity. These modes however have smaller quality factors and are very close each other and to the band edge, making these modes less useful than the more isolate lower frequency mode.

The location of the peaks in the transmittance for the filter with respect to the stops bands are more clearly observed by comparing them to the THz-TDS measurements of the photonic crystal.

Figure 6.18 shows the comparison of the broad band THZ-TDS of the photonic crystal transmittance (solid line) and the narrow band frequency domain transmittance (dotted line). For this sample with lattice constant a=150 μm we have that the edge of the gap, measured by THZ-TDS, is located at 0.960 THz. This feature is also observed in the frequency domain measurement.

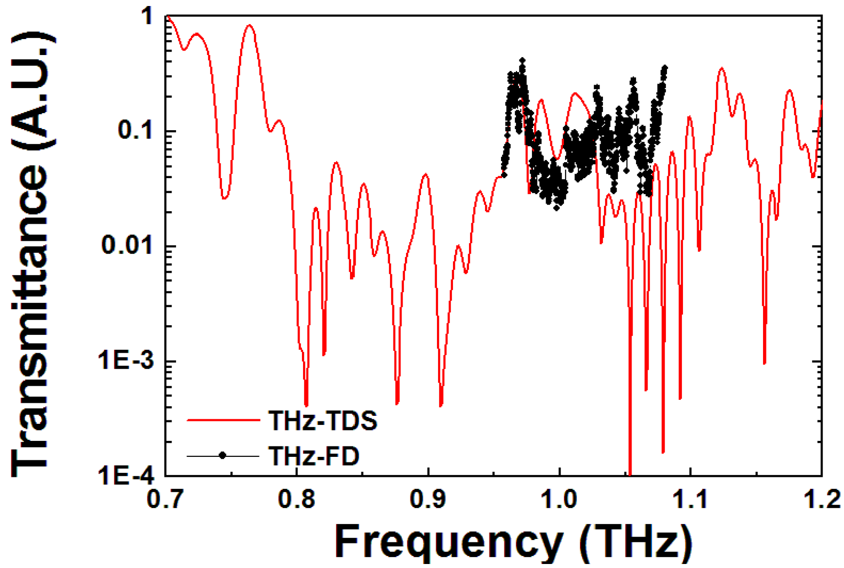

Figure 6.18 Time domain and Frequency domain measurements for the 150 μm sample. Here we have that the edge of the stop band located at 0.960 THz matches with the high transmittance in the filter. Both measurements suggest that the edge is located precisely at 0.960 THz or in dimensionless units at 0.48 (c/a).

Figure 6.19 also shows the edge of the optical gap shifted to higher frequency and located at 1.030 measured by THz-TD (solid line) for the 140 μm sample; above this frequency there is region of transmittance which is corroborated by the frequency domain (dotted line); in the spectrum it is clear that the peak at 0.9824 THz in the transmittance for the filter is inside the optical gap; a unequivocal signature of a cavity resonance.

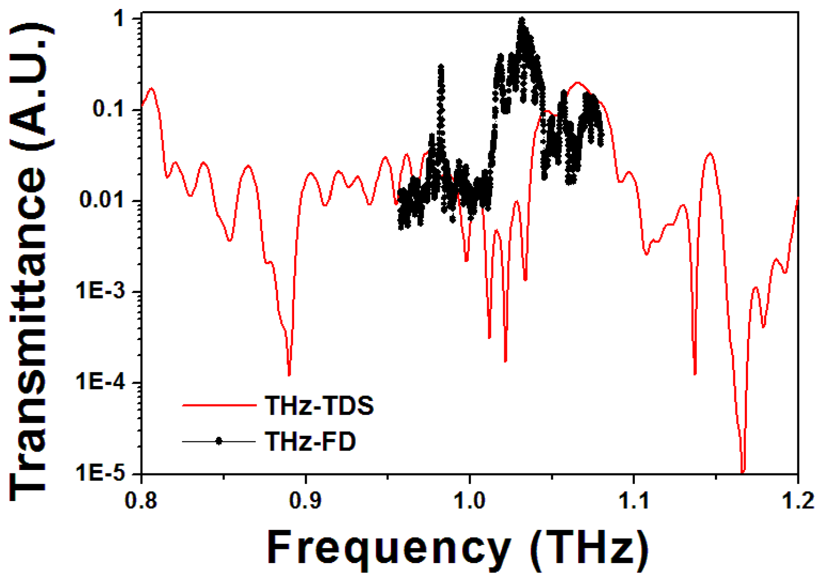

Figure 6.19 Time domain and Frequency domain measurements for the 140 μm. Here we have that the edge of the stop band located at 1.038 THz overlaps with a high transmittance in the filter. However the peak located at 0.9824 is well inside the low transmittance region of the photonic crystal.

Figure 6.20 shows the edge of the photonic gap shifted to 1.074 measured by THz-TD (solid line) for the 135 μm sample; above this frequency there is region of transmittance which is corroborated by the frequency domain (dotted line); in the spectrum it is clear that the peak at 1.0209 THz in the transmittance for the filter is inside the optical gap; again an unequivocal signature of a cavity resonance.

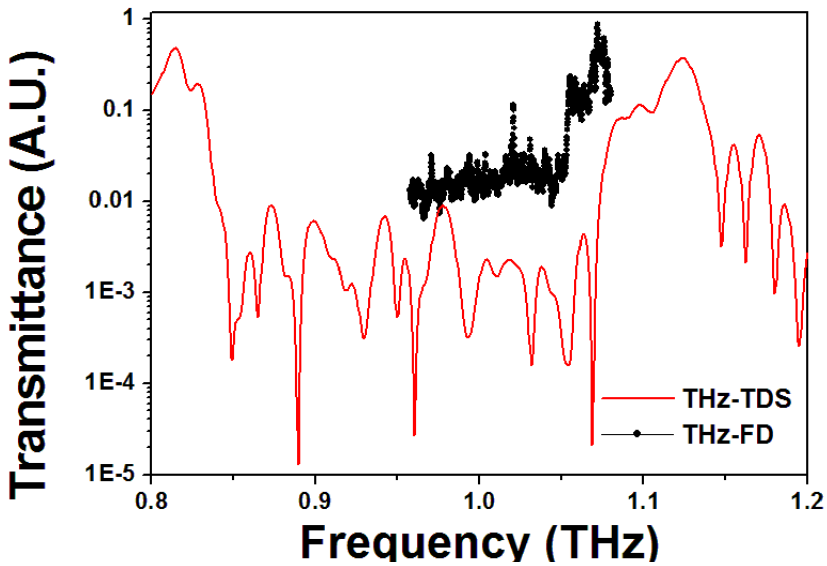

Figure 6.20 Time domain and Frequency domain measurements for the 135 μm. Here we have that the edge of the stop band located at 1.074 THz overlaps with a high transmittance in the filter. However the peak located at 1.0209 is well inside the low transmittance region of the photonic crystal.

The peaks in the transmittance located well inside the optical gap for the transmittance are the resonant modes for the cavity. For now we can fit them to a Lorentzian line shape. Figure 6.21 shows the Lorentzian fit of the resonances found by THz-FD. The fit reveals a resonant frequency at 0.9824 and a Q factor 1190 for the 140 μm sample; while for the 135 μm the resonance is located at 1.0209 and it has a Q factor of 1540.

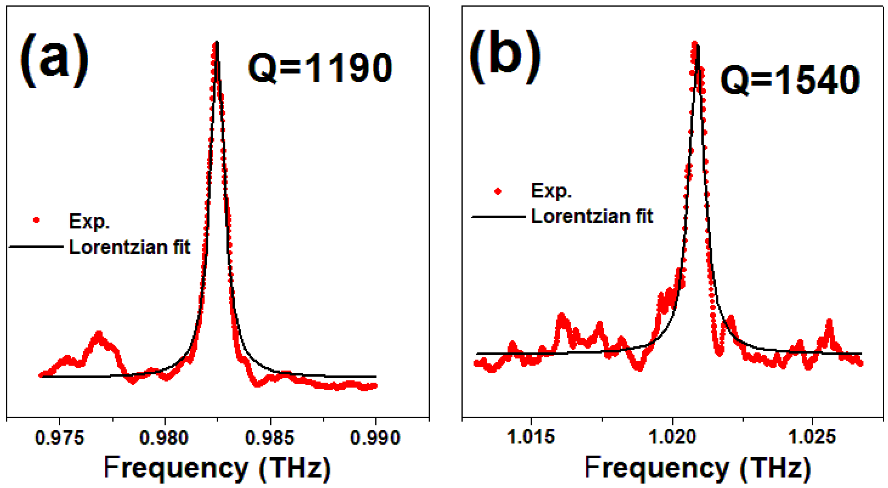

Figure 6.21 Experimental data is fitted using a Lorentzian function. (a) For the 140 μm sample the frequency mode is located at 0.9824 and has a Q value of 1190. (b) for the 135 μm sample the frequency mode is located at 1.0209 with a Q value of 1540.

E. Cavity mode theoretical calculation

To analyze the results from the experimental measurements we realize FDTD simulation for structure. The full 3D simulation reveals three cavity resonances in the vicinity of the experimental peaks. The profiles of the modes are shown in Figure 6.22.

In the transmittance experiment only on peak appears in the spectrum when there are three modes predicted by FDTD. The explanation relies in the actual coupling to the waveguide-cavity; a peak in the transmittance will only show in the spectrum if it can be couple to a waveguide mode.

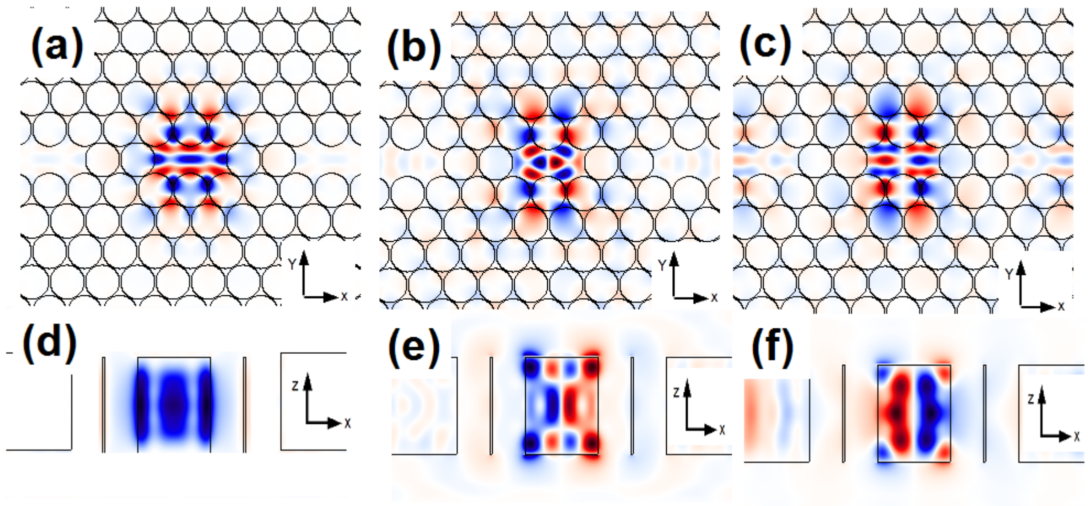

Figure 6.22 The Ez field profile predicted by FDTD corresponding to three resonant modes located near the resonant transmittance peak for the Lorentzian filter. Figure (a) and (d) correspond to a cavity mode located at 0.4569 (c/a) with a Q=6900; which correspond to a frequency 1.0153 (0.9791) for the 135(140) μm sample. Figure (b) and (e) correspond to a cavity mode located at 0.46075 (c/a) with a Q=1300 corresponding to 1.0239 (0.9873) THz for the 135(140) μm sample. Figure (c) and (f) correspond to a cavity mode located at 0.46437 (c/a) with a Q=1630; which correspond to 1.0319 (0.9951) THz for the 135(140) μm sample.

1. Two dimensional cavity modes

We need to discard two of the three modes. We start first by calculating the waveguide modes for the more simple two dimensional photonic structure.

In the case of the triangular lattice we have that the translation symmetry perpendicular to the slab (y-axis) is broken by the waveguide; however, we have that it has discrete translation symmetry along the axis of the waveguide, as shown in Figure 6.23. The modes for the waveguide could be divided in two main categories: continuous extended bulk modes and discrete localized modes.

Continuous extended modes are modes propagating along the waveguide but not exclusively bound to it; they extend into the bulk of the photonic crystal and therefore they coupled to the bulk photonic crystal modes and as a consequence the frequency spectrum for these modes is continuous.

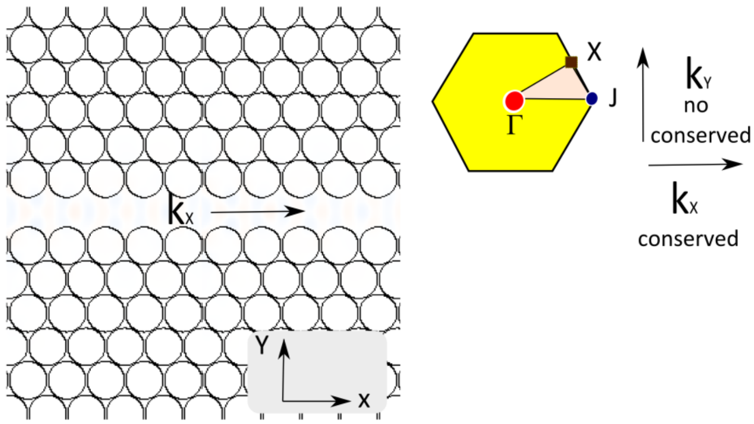

Figure 6.23 In a photonic crystal waveguide the translation perpendicular to the axis of the waveguide (y-axis) is broken; therefore the momentum in this direction is not conserved. The translation symmetry along the axis of the waveguide (x-axis) is still intact and therefore its momentum along this axis is conserved.

The second category will be the modes which are propagating and are localized in the waveguide; therefore they are bounded and form a discrete set of frequencies. In conclusion the dispersion relation of the waveguide will be a mix of continuous extended bulk modes and a discrete set of localized modes

Our first step is to look for the bulk modes which are the photonic crystal modes which have k_x conserved or constant. These modes are characterized by a pair of parameters frequency ω and propagating vector k_x. A mode with ω and k_x is a bulk mode if there exists a ky such that $\omega = \omega(kx, ky)$ is photonic crystal mode. In other words we need to find the projection of the band diagram along the kx.

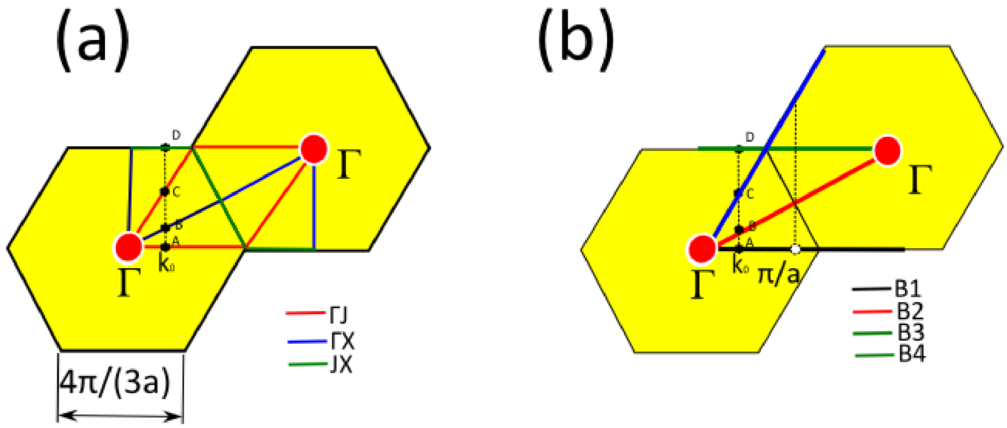

Figure 6.24 The projection of the band diagram of the photonic cyrstal slab as a function of Kx. For a given Ko the frequency changes continuously from the frequencies values determined by its intersection with the bands along the high symmetric direction in the irreducible zone

The band projection along kx is the function $\omega = \omega(k_x)$. For constructing these projection we first consider the point $k_x = k_0$ in the first Brillouin zone as shown in Figure 6.24; the modes with a constant value of the k_x are along the dotted line in Figure 6.24(a). We know that the dispersion relation $\omega = \omega(k_x, k_y)$ is only discontinuous at the zone boundary, i.e. $\omega = \omega(k_0, k_y)$ varies continuously from A to B while covering the frequency interval $\omega(A) = \omega_{\Gamma J}(\overrightarrow{\Gamma A}) = \omega_{\Gamma J}(k_0)$ to $\omega(B) = \omega_{\Gamma X}(\overrightarrow{\Gamma B}) = \omega_{\Gamma X}\left(\frac{2k_0}{\sqrt{3}}\right)$; There is also a continuous range of frequencies from the point B to C which are the frequencies from $\omega(B) = \omega_{\Gamma X}\left(\frac{2k_0}{\sqrt{3}}\right)$ to $\omega(C) =$

$\omega_{\Gamma J}(\overrightarrow{\Gamma C}) = \omega_{\Gamma J}(2k_0)$; and finally also there are a continuous range of frequencies from point C to D which are the frequencies from $\omega(C) = \omega_{\Gamma J}(2k_0)$ to $\omega(B) = \omega_{XJ}(k_0)$; where $\omega_{\Gamma J}(k)$ is the band function along the ΓJ orientation, $\omega_{\Gamma X}(k)$ the band function along the ΓX orientation and $\omega_{XJ}(k)$ the band function along the XJ orientation in the first Brillouin zone. We can define the following "projection" functions in the interval $0 \le k \le \pi/a$ as:

$$b1(k) = \omega_{\Gamma J}(k)$$

$$b2(k) = \omega_{\Gamma X}\left(\frac{k}{\cos(30°)}\right) = \omega_{\Gamma X}\left(\frac{2k}{\sqrt{3}}\right)$$

$$b3(k) = \begin{cases} \omega_{XJ}(k) & 0 \le k \le \dfrac{2\pi}{3a} \\ \omega_{\Gamma J}\left(\dfrac{4\pi}{3a} - k\right) & \dfrac{2\pi}{3a} \le k \le \dfrac{\pi}{a} \end{cases}$$

$$b4(k) = \begin{cases} \omega_{\Gamma J}\left(\dfrac{k}{\cos(60°)}\right) = \omega_{\Gamma J}(2k) & 0 \le k \le \dfrac{2\pi}{3a} \\ \omega_{XJ}\left(\dfrac{8\pi}{3a} - 2k\right) & \dfrac{2\pi}{3a} \le k \le \dfrac{\pi}{a} \end{cases} \tag{6.1}$$

We notice that if we consider k values larger that π/a the bands just flip their order as they fold back into the Brillouin zone, providing the same range in frequencies. The First Brillouin zone is symmetric so we only need to define the projection function in the interval $0 \le k \le \pi/a$.

In our case we are only dealing with modes that are symmetric along the direction of propagation so we only consider band which are symmetric (see bands 1 3 and 5 in Figure 6.8). The gap in this particular case is delimited by band 1 and 3 so only these two bands need to be considered. The projected bands function b1 to b4 define in equation 6.1 are plotted in Figure 6.25.

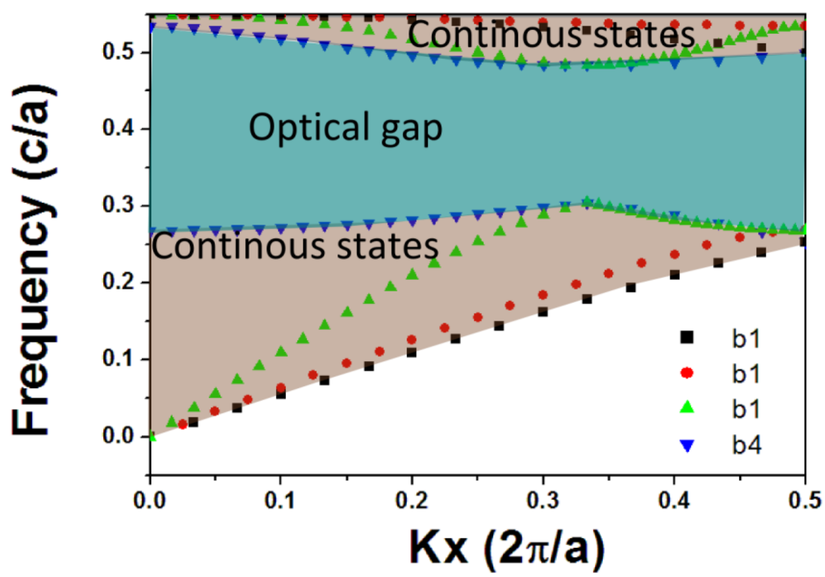

Figure 6.25 The projected band diagram over k_x. Here b1 to b4 are the projected function defined in equation 6.1. For a give k_x we have that the frequency changes continuously in k space from two consecutive intersections of the line with constant value k_x and the zone boundary.

Now that the extended bulk modes are obtained we are only left with the modes which are bounded to the waveguide; to calculate the bounded modes we used FDTD. These modes are obtained by exciting the waveguide with a pulse localized at arbitrary points inside the waveguide as shown in Figure 6.26. For a given value of k_x we set the boundaries which are consistent with the Bloch function $e^{-ik_x x}$. And we let the system evolve in time. We monitor the field at various arbitraries points inside the waveguide region and waveguide modes appear as resonant frequencies of the cell structure.

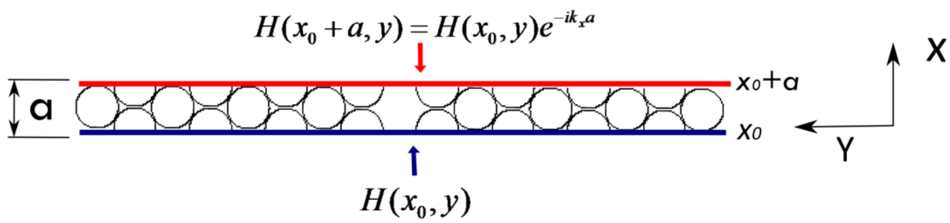

Figure 6.26 The unit cell employed in the calculations of the waveguide modes; the cell is excited by a broad pulse in an arbitrary point in the cell, the fields inside are left to evolve subject to the boundary condition set by the Bloch function, the resulting resonant frequencies are the eigenvalues for the particular Bloch function employed.

In Figure 6.27 we show the localized modes for the waveguide, unsurprisingly being localized they lie in the region of the photonic gap. For the two dimensional structure that we are considering here there are 4 waveguide bands. The higher frequency bands are pulled from the continuous states down into the optical gap. The second higher frequency band is nearly flat. This particular band will have a very slow group velocity. An interesting feature is also observed here: there is an anticrossing between the two higher frequency bands; these bands in a bulk dielectric will cross each other but in the photonic waveguide the discrete translation symmetry produces a strong coupling between these two bands which produces this anticrossing.

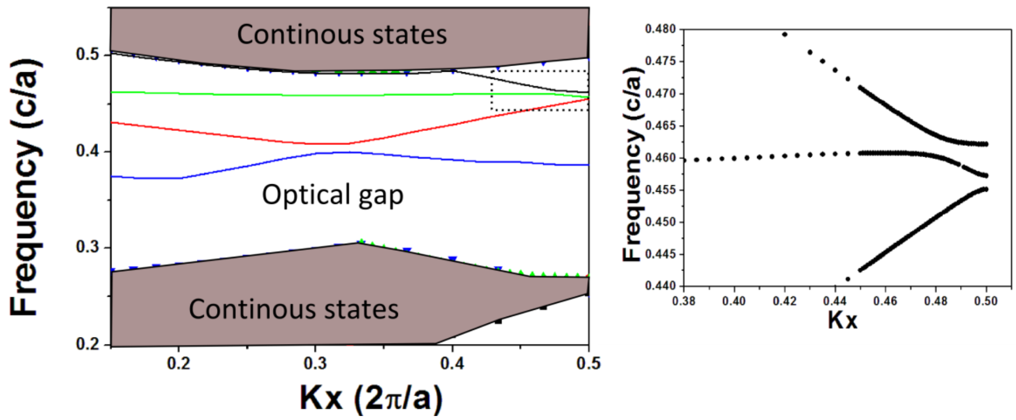

Figure 6.27 Band diagram for the two dimensional triangular photonic crystal. The gray areas are continuous bulk modes while the solid lines are the localized modes of the waveguide. A more detailed look at the zone boundary of the three upper frequency bands reveals an anticrossing between the two higher waveguide bands.

The waveguide band structure in now known. We have now calculated the resonant modes of the photonic crystal cavity for a two dimensional crystal. The idea is that the coupling among the waveguide and the cavity will be similar in the two dimensional case as in the three dimensional photonic crystal slab; also from the measurement of the photonic crystal gap we have that the two dimensional model is a good first approximation of the properties of three dimensional structure.

Figure 6.28 shows the field profile and the resonant frequencies for two modes which are very close to those found in the experiment.

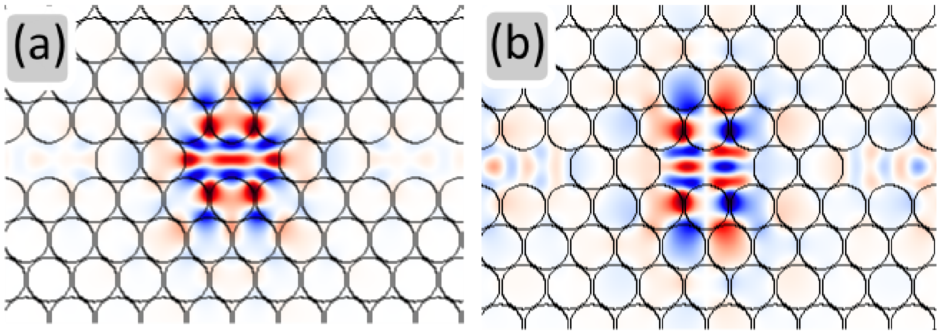

Figure 6.28 The Ez field profile for two resonant modes of the two dimensional photonic crystal cavities. (a) The resonant frequencies is located at 0.4527 (c/a) and (b) the resonant frequency is located at 0.4601 (c/a).

The modes in Figure 6.28 have the same field configuration as modes (a) and (e) in Figure 6.22 found in the three dimensional photonic crystal slab.

To qualitatively describe the coupling between the modes in Figure 6.28 we plot the resonant frequency of the cavity in the waveguide band diagram. We examine the Ez field profile in a few selected points in the waveguides. The points marked in the dispersion relation as C and F show the field of the waveguide at the coupling frequency. We see the field profile in C has a three nodes in y direction and a single node in the x direction which matches very well the field configuration corresponding to the modes shown in Figure 6.28(b). The mode profile for the waveguide at point F, and in general the band that contains F, has a single node while the field corresponding to the mode in Figure 6.28(a) has three nodes; therefore the coupling is negligible.

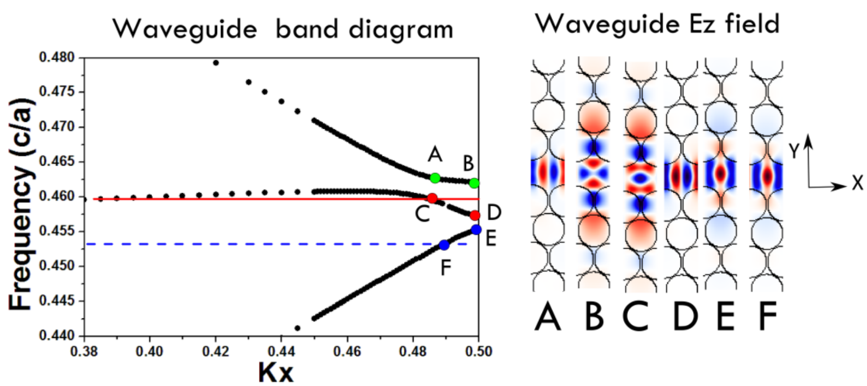

Figure 6.29 Band diagram of the waveguide showing the coupling point between the waveguide and the cavity. For the marked points in the band diagram we show the field configuration. Here the dotted (blue) line corresponds to the lower frequency mode shown in figure 6.28(a). The solid (red) line corresponds to the higher frequency cavity mode shown in figure 6.28(b).

2. Three dimension cavity modes

By studying the simpler two dimensional case we can explain more easily the coupling the three dimensional photonic crystal slab. The waveguide band diagram for the three dimension photonic crystal wave guide as shown in Figure 6.30 is constructed in the same way as in the two dimensional case.

The situation for the three dimensional case has a few more complications. The first is that there is a light cone and, within this region, the modes leaks out of the slab. Being in the light cone means that that the wave vector is complex and therefore exponentially decays as it propagates. If a particular cavity mode couples to one of these nodes it will have a very small transmittance through the filter as it will be exponential attenuated. In the frequency region near the resonant modes of the cavity we have four band instead the three that appear in the two dimensional case[5].

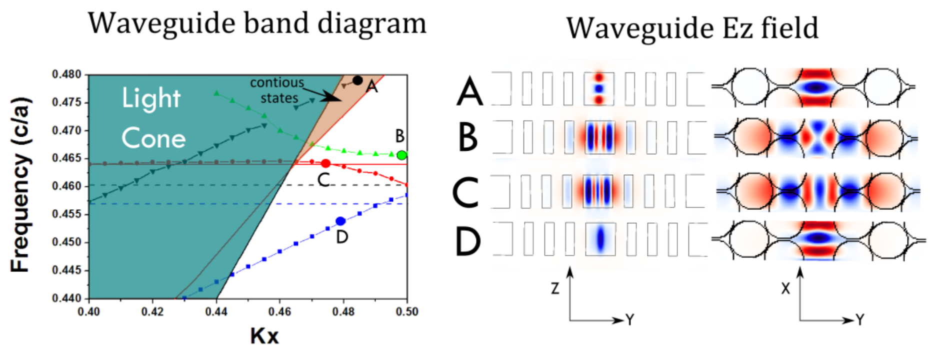

Figure 6.30 Band diagram of the photonic crystal waveguide showing the coupling point between the waveguide and the cavity. For the marked point the band diagram we show the field configuration in the plane of the waveguide and also the field across the thickness of the slab.

From the four waveguide bands that appear in Figure 6.30 three bands can be associated directly to the two dimensional bands and they are the ones whose Ez field has a single node in the z direction. The extra waveguide band is located in the light cone and in the continuous states it has three nodes. By examining the field we have that it is just a harmonic of the waveguide band that contains the point D in Figure 6.30. Using the same argument that for the two dimensional case we can discard the cavity mode corresponding to Figure 6.22(a) due to it having three nodes while the waveguide to which it could couple only has one node. The cavity corresponding to Figure 6.22(a) on the other hand can only strongly couple to the

[5] In the two dimensional case, four bands appear but only three are in the vicinity of the cavity resonances as is shown in Figure 6.29.

extra band with three nodes and is on the light cone therefore the coupling to this particular mode will not show up in the transmittance spectrum.

After discarding two modes in Figure 6.22 we have that only one mode is able to properly couple to the waveguide. This mode which corresponds to Figure 6.22(e)-(f) is a cavity resonance mode appearing in the transmittance. Its frequency position is at 1.0319 (0.9951) THz for the 135(140) μm with a quality factor Q=1630. We have that by employing temporal coupled mode theory (Appendix C) the ratio of the resonant frequency divided by the width of the resonant peak is the quality factor of the cavity. We have that the Q factors found in the experiment are 1190 with a resonant frequency of 0.9824 THz for the 140 μm sample and Q=1540 with resonant frequency at 1.0209 for 135 μm sample. The departure from the perfect Lorentzian line for the 135 μm sample could be explained as a result of the coupling in the nearly flat region of the waveguide while the cavity in the 140 μm sample is located a slightly smaller dimensionless frequency 0.4584 (c/a) compared to 0.4594 (c/a) for the 135 μm and therefore in the linear region of the waveguide.

The discrepancy for frequency resonance between the experiment and the theory is 10 GHz or 1% explained by an error in the FDTD or by small differences in the parameters of the structure being simulated.

7 High-Q photonic crystal cavity for 0.24 THz electron spin resonance.

In this chapter we move our attention to the sub THz regime where an intense work has been done on characterizing complex system by using Electron Spin Resonance (ESR) at 8.5 Tesla. ESR is a powerful technique in which a high Q low volume cavity will enhance the sensitivity of the system, and therefore a motivation for exploring the possibility of integrating a terahertz photonic crystal in a well establish experimental technique.

The strategy we use for constructing a photonic crystal cavity at 0.24 THz follows the trend from the previous chapter where an L3 cavity with a TE polarization shows a cavity resonance as high as 1020 [41].

Using the property of scalability of photonic crystals for working at 0.24 THz we only need to scale our samples properly. For a frequency of operation at 0.24 THz we are required to construct our samples using a lattice constant of a=335 μm in a 190 μm thick wafer. The fabrication process is explained in chapter 3 and the complete recipe is reported in appendix D.

We characterize our sample using a transmission experiment and scattering. For the transmission experiment we use the setup shown in Figure 7.1. The THz source is manufactured by Virginia diodes Inc. It consists of a frequency synthesizer that covers the range from 14 to 16 GHz. It is then followed by four frequency doublers multiplying the signal by 16 times to cover the range from 0.225 to 0.255 THz in steps as small 16Hz. It has frequency dependent power ranging from 10 to 30mWwith the power around 240GHz approximately 20mW. The source launches a Gaussian beam which at 240GHz has beam waist diameter of 5.6 mm.

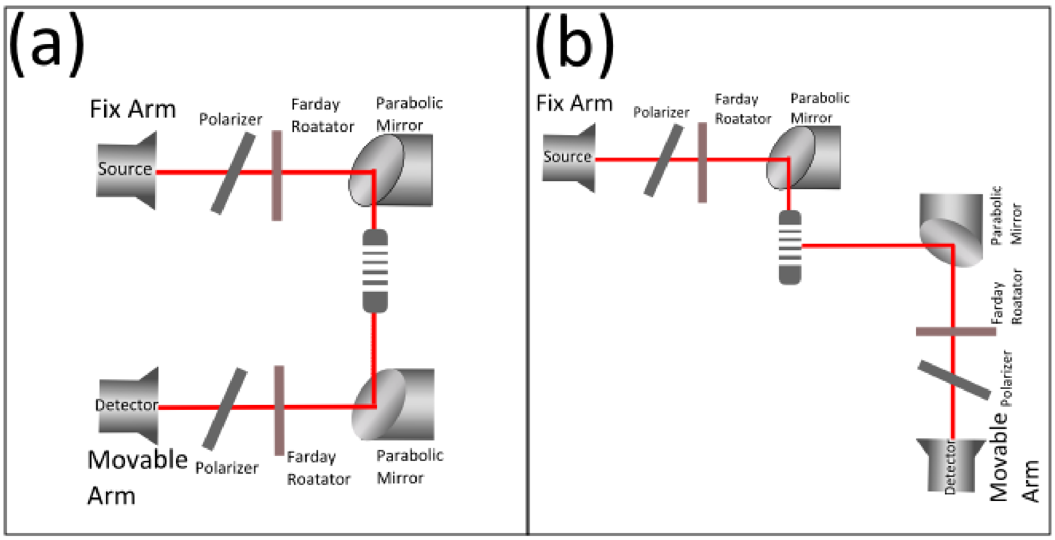

Figure 7.1 Experimental setup. (a) Transmission configuration. (b) Scattering configuration.

The source is mounted into a setup designed by Tomas Keating, Inc.; The source is mounted on a 45 degree plate and it passed first through a wire grid polarizer which is polarized also at 45 degree to match the polarization of the source. The beam then passed through a 45 degree Faraday rotator to eliminate standing waves. The beam emerges at the end with vertical polarization with respect to the optical table. An off-axis parabolic mirror focuses the beam into a sample. Here any reflection that comes from the sample will be rotated an additional 45 degrees and will be cross polarized to the first wire grid and be taken out of the system eliminating standing waves between the sample and the source.

A similar strategy is used for the detection. But this time the detection part of the setup is mounted on a movable arm that can rotate 90 degrees. It consists on an off-axis parabolic mirror which collects the light and then it goes to a wire grid polarizer with axis perpendicular to the table. Then it goes to a 45 degree Faraday rotator and is then detected with a Schottky diode which is polarization selective. This configuration eliminated the standing waves formed either from the source to the sample and from the sample to the detector. The configuration could be used in two schemes: a direct transmission with the configuration shown in Figure 7.1(a) or by measuring the scattering as shown in Figure 7.1(b).

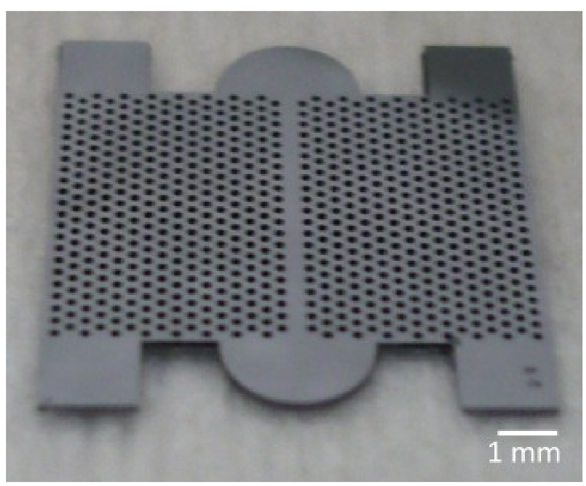

Figure 7.2 Photonic crystal waveguide

Our first measurement was the characterization of a waveguide as shown in Figure 7.2 . The waveguide is a linear defect along the TJ directions in the triangular lattice. The dimension of the sample are 9 mm by 14 mm. The samples have an immersion lenses for increasing the coupling from and into free space.

The spectrum of the photonic crystal waveguide is shown in Figure 7.3; we used as a reference the source spectrum in free space. The spectrum shows a sharp transmittance edge at 237 GHz. The waveguide has a sharp transmittance edge and also a dip in the transmittance at 242.5 GHz.

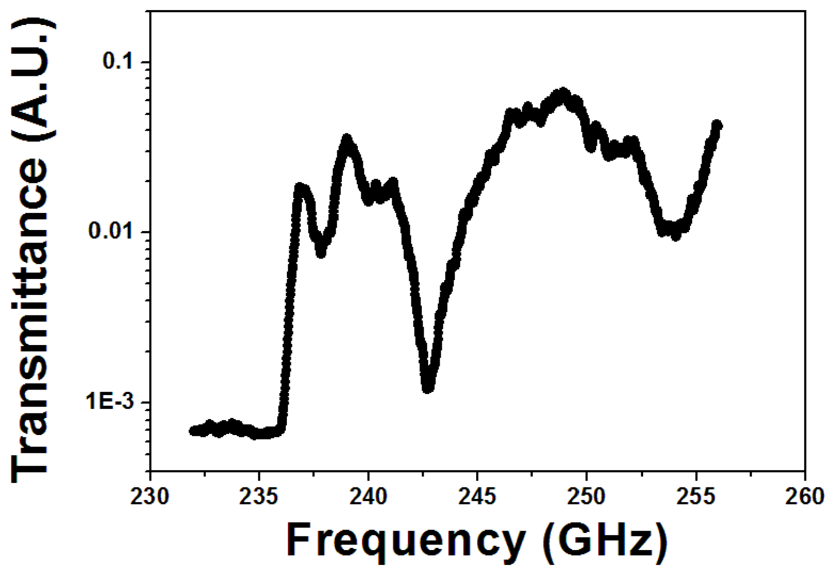

Figure 7.3 Photonic crystal waveguide transmittance. The transmittance is normalized using the spectrum of the source. At sharp transmittance turn on is visible at 236 GHz while a dip in the transmittance is located at 242.5 GHz.

Once we now have a photonic crystal waveguide working in the desire frequency range we proceed to construct a photonic crystal cavity. The sample design relies on the L3 cavity, which is a cavity formed by removing three holes in the ΓJ orientation in a triangular lattice. The L3 cavity was inserted into a photonic crystal waveguide forming a structure known as Lorentzian filter. This structure is the same type that one used in the two previous chapters. We have several samples that we can divide in two main sets: The first set consists of three samples where we change the number of holes that form the barriers which define the cavity in the waveguide from two to four holes. The second set of samples consists of cavities with barriers consisting of three holes where the hole closest to the cavity in the waveguide is shifted outward enlarging the cavity as shown in Figure 7.4. The shifting of the inner hole tunes the quality factor of the cavity. In particular Figure 7.5 shows a sample with three holes as a barrier for the photonic crystal cavity. The dimensions for both sets of samples are the same that were used for the waveguide, 9 mm by 14 mm. We also included a pair of immersion lenses in each sample, enhancing the in/out coupling from free space into the device.

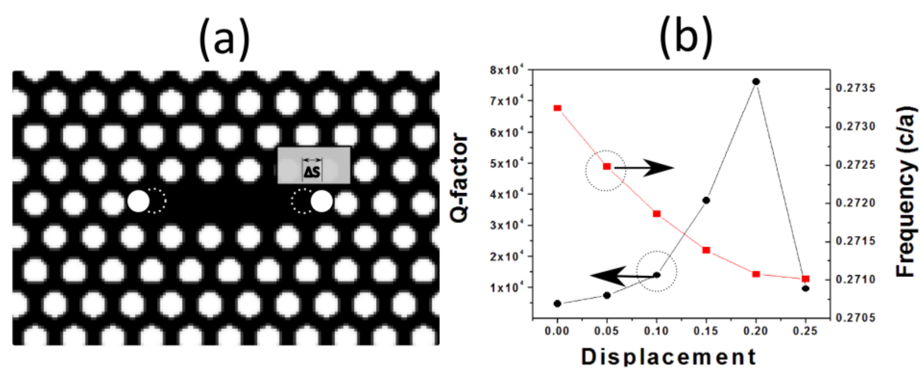

Figure 7.4 The cavity quality factor of an isolated cavity (not coupled to any waveguide) can be tuned by displacing the nearest hole to cavity outwards (a). The Q factor changes as a function of displacement in (b), also a small change in frequency is induced by the effective index of the cavity mode.

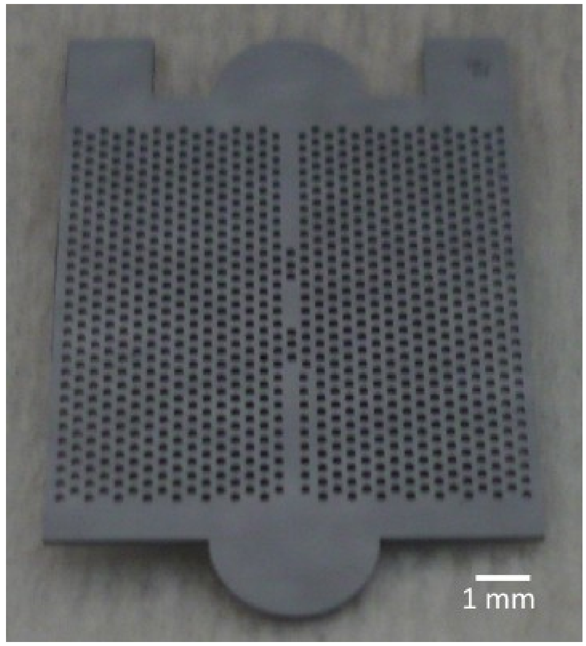

Figure 7.5 Photonic crystal Le cavity inserted into the waveguide. Here three holes delimit the cavity in the waveguide forming a narrow band Lorentzian filter

The effective quality factor, i.e. the ratio of total energy stored to the energy lost per cycle, in a photonic crystal could be written as:

$$\frac{1}{Q} = \frac{1}{Q_{in}} + \frac{1}{Q_r} + \frac{1}{Q_{abs}} + \frac{1}{Q_{fab}} \tag{7.1}$$

Here every term is associated with a different loss mechanism, Q_{in} is the in plane loss associated with the two dimensional photonic crystal, Q_r is the radiative loss to free space (also in the literature it is called Q_V or vertical loss), Q_{abs} is the material absorption and finally Q_{fab} is the loss associated with surface roughness and in general any deviation from the desired structure as a product of the fabrication process. This last loss is negligible at terahertz frequencies due to the size of the samples; however Q_{abs} is the limiting factor at room temperature. At 240 GHz the material loss is produced by free carrier absorption.

The in plane loss Q_{in} could be made very large by increasing the length of the crystal surrounding the cavity. In the case of our samples which are in the Lorentzian filter scheme the in plane loss is dominated by the waveguide coupling.

The radiative or vertical loss could be minimized by carefully choosing the design of the cavity. One way to increase Q_r (i.e. decrease the radiative loss) was first suggested by S. Noda et al [25]. They correctly addressed that by reducing the abrupt discontinuity of the field inside the cavity i.e. by letting them penetrate inside the dielectric mirror we are "gently confining" the fields, and so they do not suddenly vanish at the interface and the leaky component are minimized.

The key to having a very effective mirror is periodicity. Therefore if we want to make the mirror a little less reflective we only need to change the periodicity. There are several ways to change the periodicity however the simplest way is just to move the holes that are delimiting the cavity as shown in Figure 7.4.

Figure 7.4 shows the calculated quality factor and frequency for a cavity with a thickness a=0.6 and hole radius r=0.30 for an index of refraction n=3.42 with a lattice constant a=335 μm correspond to our samples. It is important to notice that the highest quality is located around Δs=0.15a. We also notice a very small resonant frequency shift to a lower frequency from Δs=0 to Δs=0.25. As we increase the size of the cavity the effective index of refraction of the cavity in also increased, pushing the mode to a lower frequency until it is large enough to be more energetically favored for it to have an extra node.

To understand the effect of the holes displacements consider the field profile corresponding to the resonant mode of cavity. Figure 7.6 (a) shown the Ey field component and Figure 7.6(b) the Fourier components of the Ey field for the unmodified cavity $\Delta s=0.00$. We clearly see that the modes are delocalized in the Fourier space mostly confined in the X point, this modes extends weakly into the leaky region. Being relatively small this cavity has an intrinsically high Q value. Figure 7.6 (c) and Figure 7.6(d) shows the Ey field and its two dimensional Fourier transform, again the mode is mostly confined in the X point in the reciprocal space but now as a comparison with Figure 7.6(b) the leaky components are negligible and therefore it has a higher Q value.

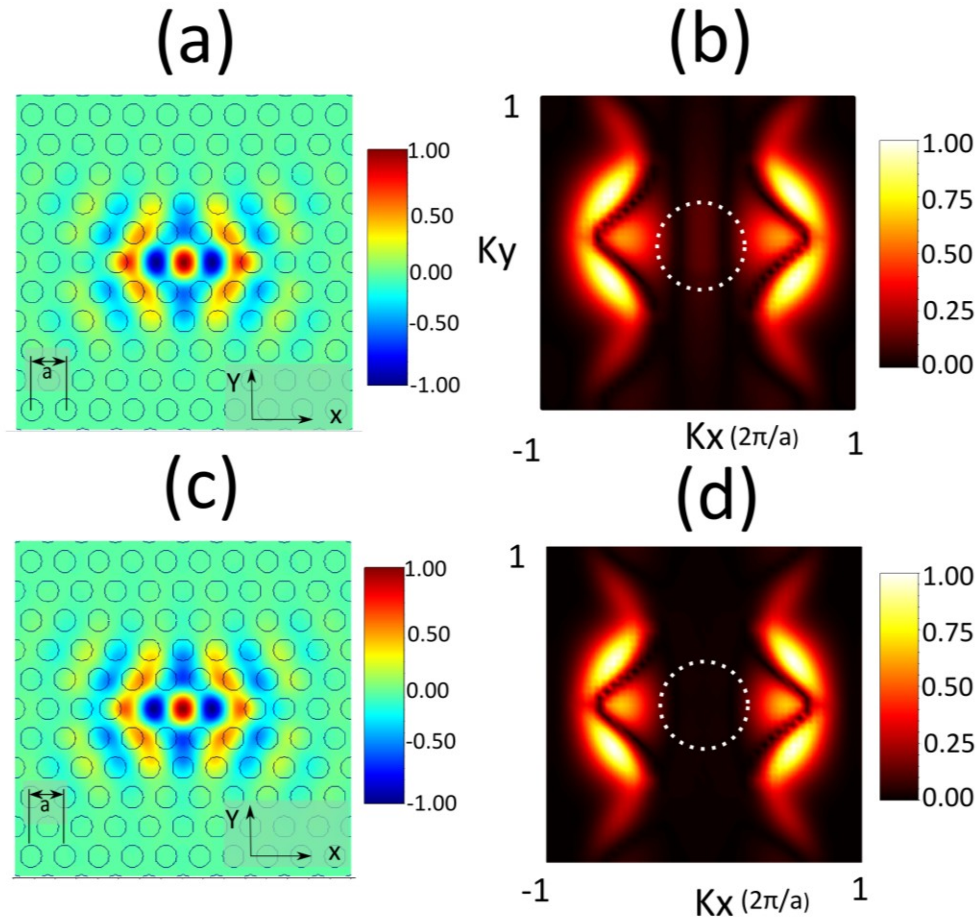

Figure 7.6 The cavity field for bare L3 cavity for the simple cavity (not displaced) and for the tuned cavity. (a) The Ey field profile for the simple L3 cavity. (b) The Fourier transform of the Ey field shows field component in the leaky zone marked by the circle. (c) Field component of the tuned L3 cavity. (d) The Fourier transform for the tuned cavity shows a significant decrease in the leaky component of the cavity with respect to the original L3 cavity and therefore a higher Q value.

A. Photonic crystal resonance as a function of the length of the barrier in a Lorentzian filter

Our first set of samples looks to increase the quality factor by increasing the in plane quality factor which for the Lorentzian filter is dominated by the waveguide coupling Q_ω . We increase Q_ω by adding more holes to form the barrier that set the boundaries of the cavity inside the waveguide. We expect that as we increase the number of holes the quality factor should also increase.

Figure 7.7(a) corresponds to a filter in which there are two holes delimiting the cavity inside the waveguide. The spectrum shown a prominent peak located at 243.77 GHz which is associate with a cavity resonance. We clearly observe the edge of the gap located at 231 GHz and also we have small transmittance from 238 to 240 GHz which is associated with the continuous states of the bulk photonic crystal. In Figure 7.7(b) we show a close up into the resonance located at 243.77 GHz the resonance could be fitted using a Lorentzian line. The quality factor associate with the resonance line is Q=1313.

In Figure 7.7(c) we show the transmittance for the L3 cavity but this time the cavity is delimited inside the waveguide by three holes. We observe in the transmittance a resonant peak located at 243.36 GHz associate with a cavity resonance, there is also a prominent peak at 252 GHz which correspond to a higher frequency mode of the L3 cavity.

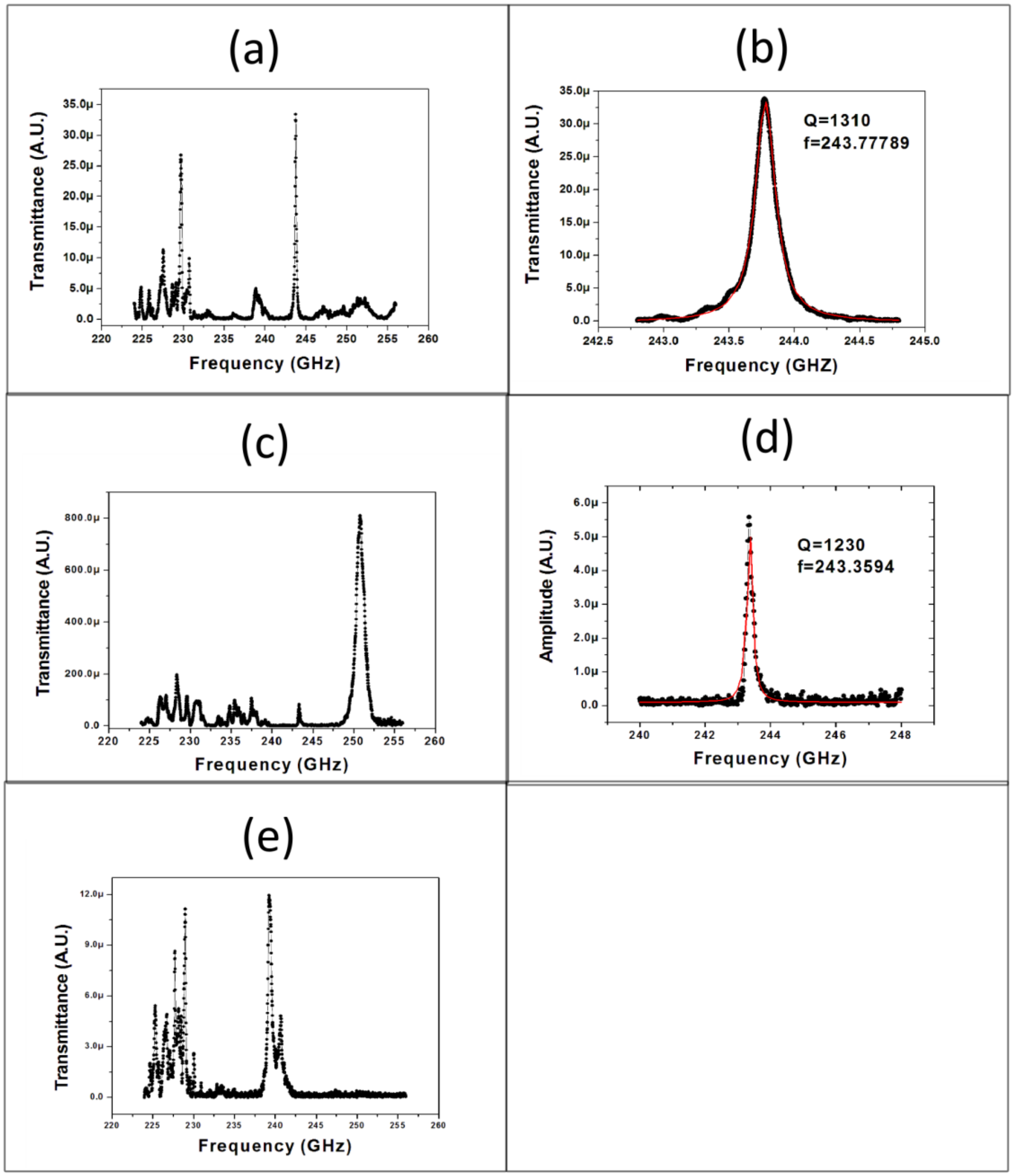

Figure 7.7 Transmittance through the filter for samples with two, three and four hole barriers. For the sample with two and three holes a sharp resonance at a frequency corresponding to a cavity mode is found. For the sample with four holes no frequency was found that could be associated with a resonance. (a) and (b) correspond to two hole barriers. (c) and (f) the transmittance for three hole barriers. (e) Transmittance for the sample with a four hole barrier.

This higher frequency mode corresponds to the cavity mode in which the Ey field is antisymmetric with respect to the y axis. This particular high frequency cavity mode has the inconvenience that its quality factor is considerably lower. The resonant cavity mode located at 243.36 GHz is fitted using a Lorentzian line with a Q=1230 as seen in Figure 7.7(d).

Finally in Figure 7.7(e) we show the transmittance corresponding to a filter in which the L3 cavity is defined inside the waveguide by four holes at each side. The spectrum shows the transmittance edge of the photonic crystal and also a small transmittance at 238 to 240 GHz corresponding to the bulk modes in the photonic crystal. There is no signal above this frequency which is consistent if we recall that the coupling from the waveguide into the cavity decreases rapidly with the separation as shown in Figure 7.8, which is also reported in the literature [43].

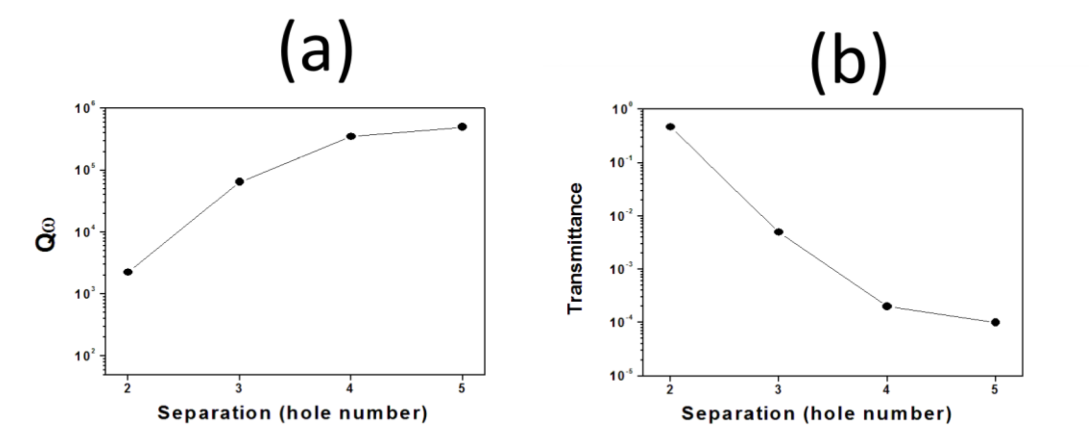

Figure 7.8 (a) In plane quality factor as a function of the number of holes. (b) Transmittance as a function of the number holes in the barrier.

Figure 7.8 shows Q_ω as function of the number of holes and also the calculated transmittance assuming no material absorption. We have that the transmittance decreases dramatically from two to three holes and is very small for four holes which agrees with the relative magnitude of transmittance as shown in Figure 7.7 (b) and (c). We were expecting that the quality factor would increase; however, we clearly see that it does not in the experiment. This particular issue is treated in more detail in the next section.

B. Photonic crystal resonance as a function of the hole displacement in the barrier for a Lorentzian filter

In section A we analyze the effect of the length of the barrier in the cavity resonance. In the present section we will consider the effect of the hole displacement in the frequency and quality factor of the cavity.

The set of samples that we are considering here are an L3 cavity with a three hole barrier as shown in Figure 7.5 in which the inner hole in the barrier as shown in Figure 7.4 is displace from its original position. The dependence of the resonant frequency and the quality factor as a function of the hole displacement for a three hole barrier is shown in Figure 7.9.

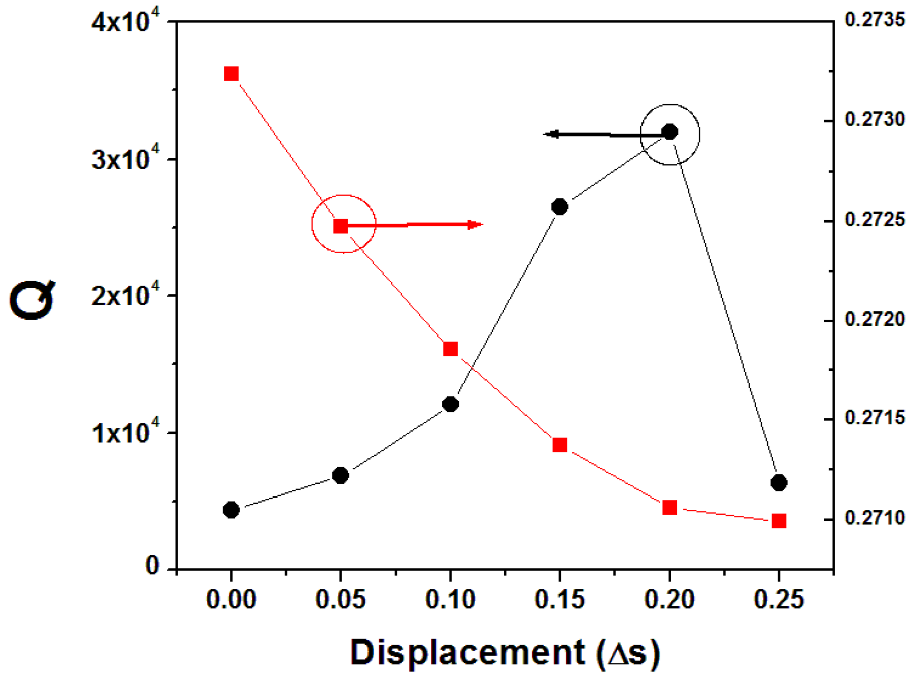

Figure 7.9 Quality factor and resonant frequency for the L3 cavity with a three hole barrier inside a photonic crystal waveguide.

The experimental results for the 6 different samples are shown in Figure 7.10 and in Figure 7.11 we show the detail of the peak in the transmittance that we associate with the resonant mode of the cavity.

As we see in these measurements we have that the quality factor degrades as we make the theoretical values of the cavity higher. This apparent discrepancy may be solved if we consider the effects if non linear waveguide dispersion on coupling with the cavity.

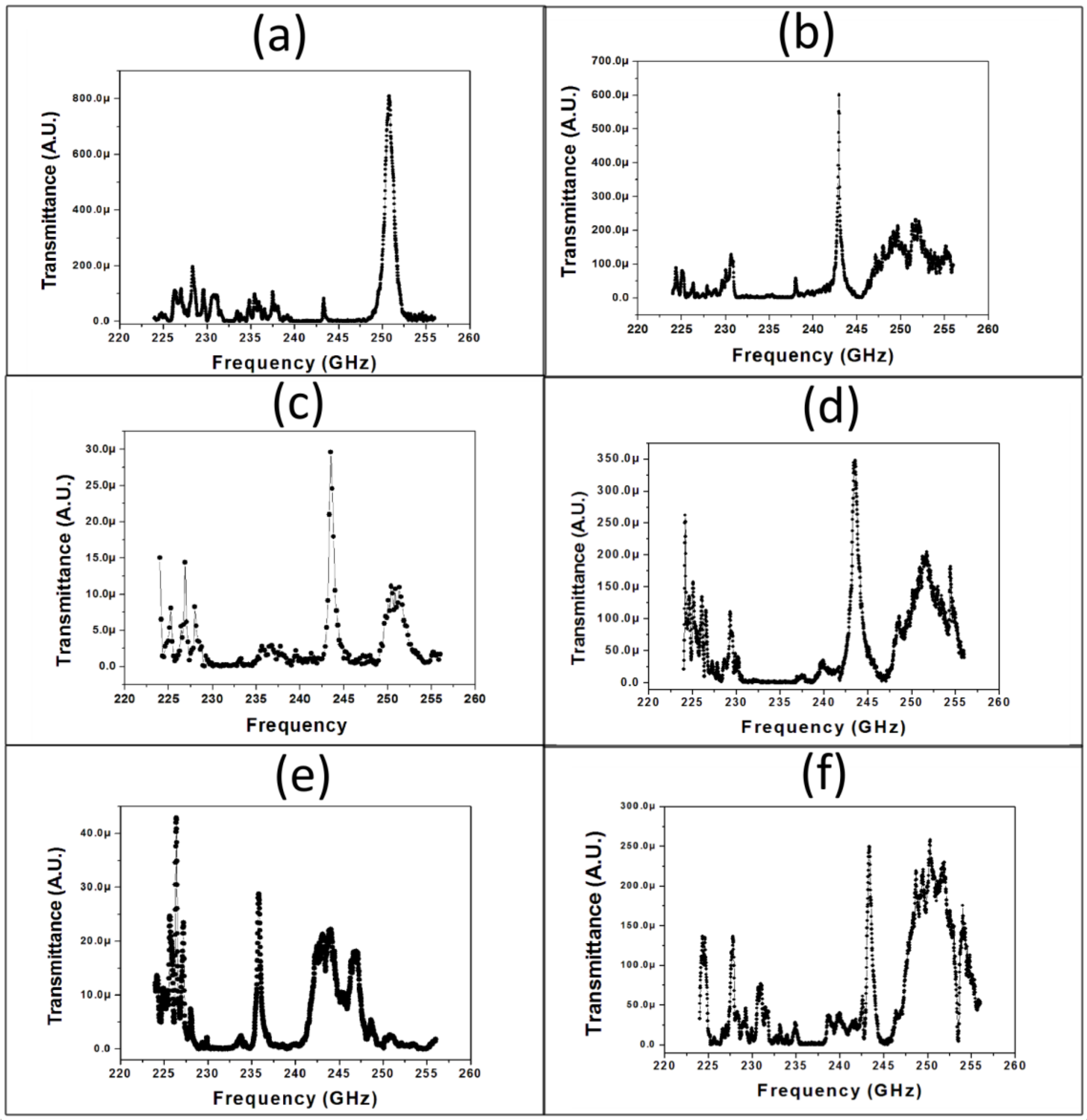

Figure 7.10 Transmittance through the filter for different displacement of the inner hole of the cavity. (a) for Δs=0.00, (b) for Δs=0.05, (c) for Δs=0.10, (d) for Δs=0.15, (e) for Δs=0.20 and (f) for Δs=0.25.

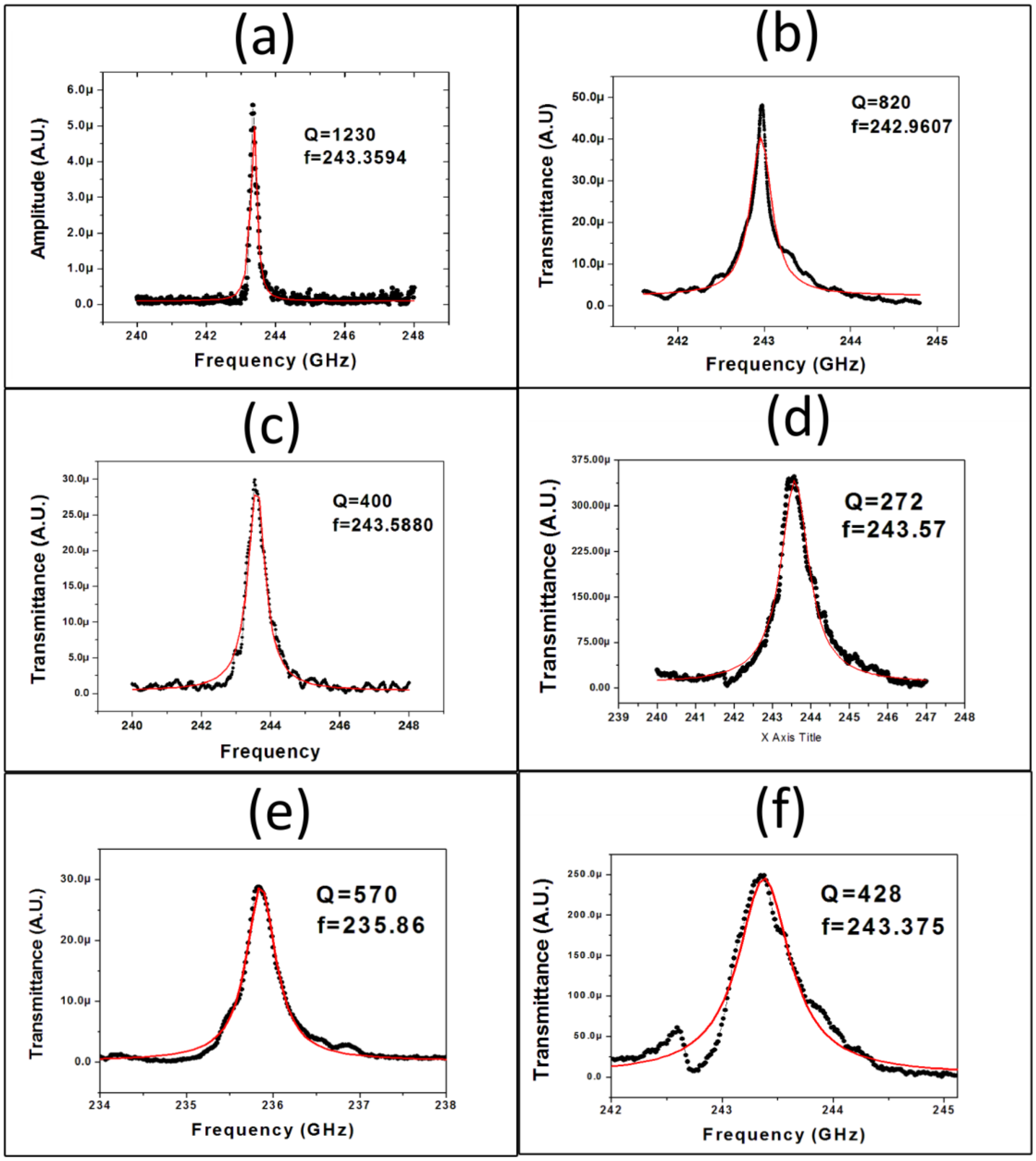

Figure 7.11 Lorentzian fit for the resonant peak found in the transmittance as a function of inner hole displacement. (a) for Δs=0.00, (b) for Δs=0.05, (c) for Δs=0.10, (d) for Δs=0.15, (e) for Δs=0.20 and (f) for Δs=0.25.

To understand the effect of the non-linear regime of the waveguide we shown in Figure 7.12(a) the waveguide dispersion. Comparing to the cavity resonance in Figure 7.9 we have that they are very close to the flat region of the waveguide. The importance of being close to the flat region is that the coupling from the waveguide into the cavity is roughly dependent of the inverse of the group velocity. The group velocity is shown in Figure 7.12(b) although the calculation is more complicated [44] we can extract a important piece of information from here, that the coupling is very large for k vectors close to the zone boundary.

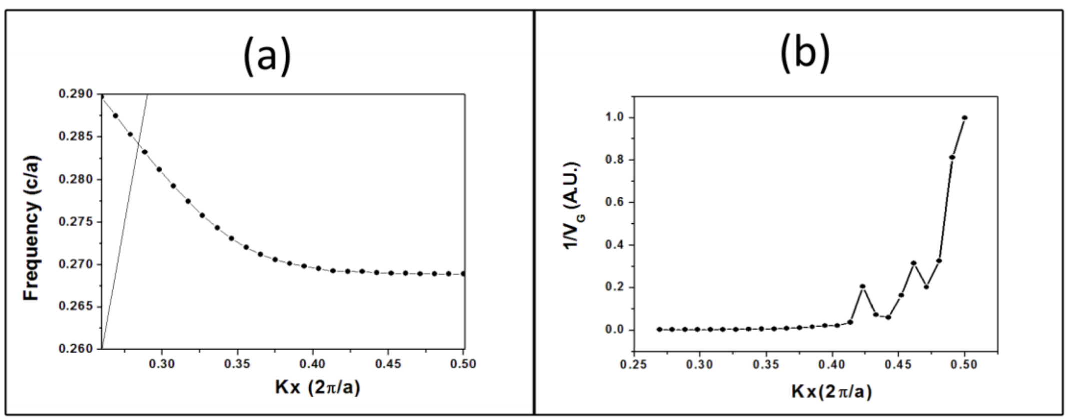

Figure 7.12 (a) Waveguide dispersion. (b) The coupling waveguide-cavity at first approximation is proportional to inverse of the group velocity.

This is essential to explain the results from the transmittance. In the linear regime of the waveguide the coupling factor is directly a factor multiplied by the group velocity and therefore a constant. The response is a simple Lorentzian line. However as shown in Figure 7.6(d), for a high Q cavity most of the components are near the zone boundary and therefore the coupling at the points is higher. As a consequence the Q factor is no longer the center frequency divided by the full width at half maxima of the transmittance. In particular, the coupling for the higher quality factor with its components in k space more confined at the zone boundary will be stronger. As we can see the magnitude in the transmittance for the sample with $\Delta s=0.15$ is the highest of all, which also correspond to a resonance with the larger frequency width, a larger transmittance means a larger in plane coupling. Also in the transmittance there is a small kink below the resonant peak, which is nothing else than the effect that as the group velocity goes to zero, i.e. the density of state increases abruptly as we approach to the zone boundary. This higher density of states allows the fields to be evanescently couple from the input waveguide into the output waveguide and gives us a good reference as to how far the resonant frequency is with respect to the edge of waveguide.

In conclusion the cavity has a larger quality factor than the one that can be inferred from the measurement.

We also did a scattering measurement, but also as we see in Figure 7.6(d) a high quality cavity means that there is almost no component near the Γ point in the Brillouin zone, which means that the radiation into free space will be nearly parallel to the surface of the sample. Having in our setup a finite numerical aperture we expect that the measurement of the scattering produced by the cavity will be very small, as indeed we were only able to measure the scattering from two samples which are shown in Figure 7.13.

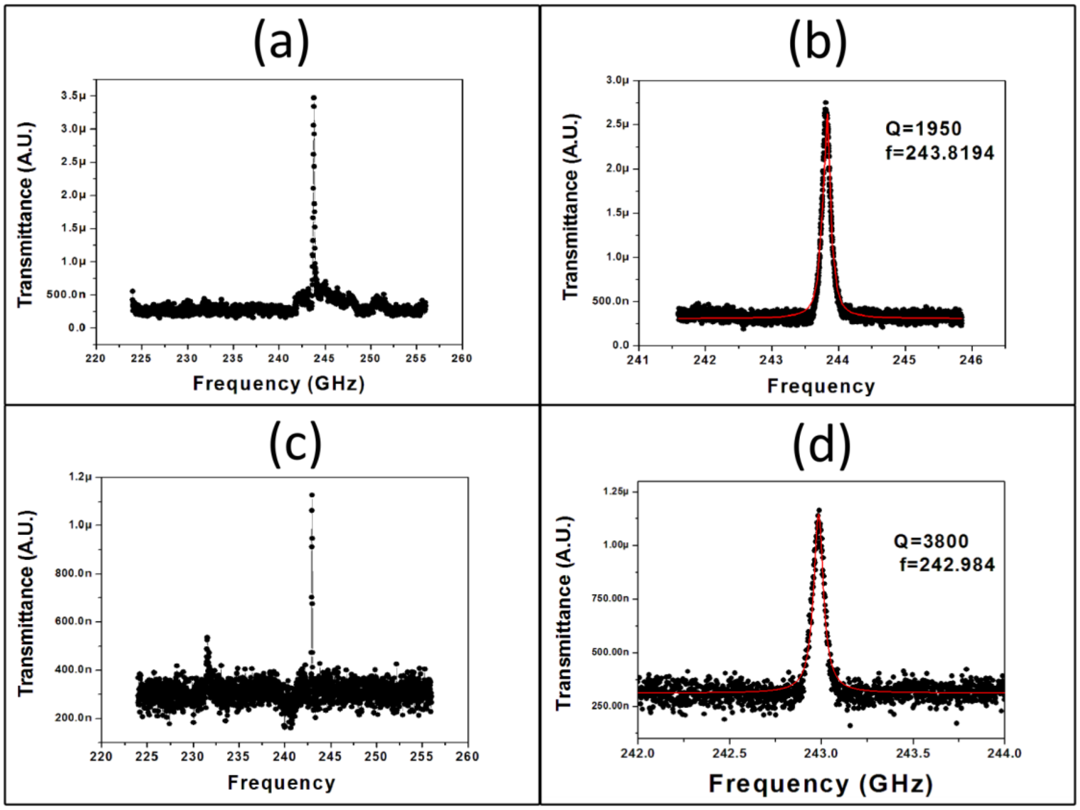

Figure 7.13 (a) Full frequency range measurement of the light scattering by the cavity for the sample with a two hole barrier. (b) Lorentzian fit for the cavity resonance found for a two hole barrier. (c) Full frequency scan for the sample with a three hole barrier and Δs=0.05. (d) Lorentzian fit for the cavity resonance found for a three hole barrier and Δs=0.05.

We have that the shapes of the scattering out of the plane for the two samples that we were able to measure are very symmetric and they are fit very well using a Lorentzian line shape. We have that the values measured are considerably higher than the ones obtained for the same sample in the transmission mode; also the frequency is very slightly (less that 1/1000) shifted to higher frequency. The essential difference with respect to the transmission mode is that while in transmission there is a frequency cutoff in the transmittance. This cutoff is inexistent for the radiation into free space and therefore the Q factor is directly the center frequency dived by width of the Lorentzian line.

Thus we have that the sample with a three hole barrier with $\Delta s=0.05$ has a quality factor of 3800. This is the highest measured for a photonic crystal cavity at Terahertz frequencies, and is the highest quality factor measured at room temperature\. The predicted quality factor for this is 6850 so that sets an estimated loss of 1/3800-1/6850=117 μrad which is consistent with the values reported in literature [45].

C. Photonic crystal resonances in the channel drop configuration.

An alternative cavity-waveguide coupling scheme to the Lorentzian filter is the channel drop configuration [25,46]. A cavity is located adjacent to the waveguide and the evanescent field is coupled to the cavity as shown in Figure 7.14. The flux through the waveguide shows a drop in its transmittance produce by the coupling to the cavity, the magnitude of the drop is given by $(Q/Q_r)^2$ where Q_r is the radiative loss and Q is the total quality factor of the cavity. The limitations present in the Lorentzian filter, for which the transmittance becomes increasingly small as the quality factor of the cavity is increased, are not present for the channel drop coupling, since the in-plane quality factor Q_ω could be always be made comparable to Q_r and therefore Q and Q_r are comparable.

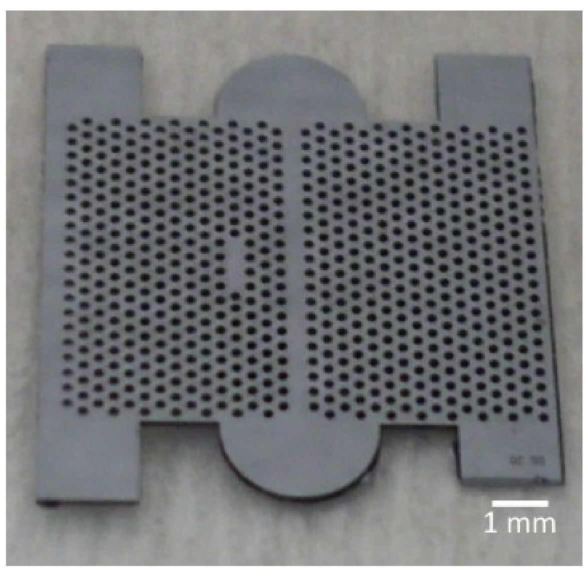

Figure 7.14 Photonic crystal cavity in the channel drop configuration

We constructed two set of samples in the channel drop configuration. The cavity was located two and three rows of holes from the waveguide. Figure 7.14 shows a sample with three rows separation from the waveguide. For each separation distance from the waveguide we fabricated six samples displacing the nearest hole in the cavity as shown in Figure 7.4(a). The total size of the sample is 10X10 mm, with 3mm diameter immersion lenses to enhance the coupling between the sample and free space.

The typical spectrum of a channel drop transmittance is shown in Figure 7.15. The spectrum here was not normalized due to that the width of the drop is expected to be very small since the transmittance does not change abruptly.

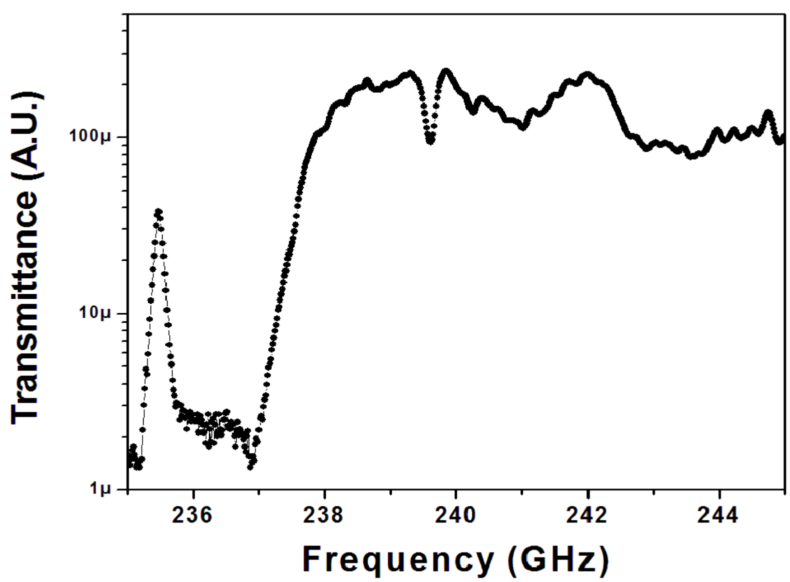

Figure 7.15 Typical transmittance for a Channel drop L3 cavity. A clear drop in the transmittance is visible in the vicinity of 240 GHz.

The spectrum shows a clear turn on in the transmittance of the waveguide, with a clear drop located in the vicinity of 240 GHz. The frequency width of the drop is around 0.2 GHz. A detailed zoom of the transmittance is shown in Figure 7.16. Here due to that the transmittance does not changes abruptly and the frequency width of the drop is small, we can consider the reference transmittance to be a linear function. By reference transmittance we mean the transmittance considering that the cavity is decoupled from the waveguide. The ratio for the transmittance value in the deepest point in the transmittance to the reference line is a measure of the coupling strength of the cavity – waveguide system. From appendix C, we have that for the channel drop scheme the magnitude of the drop is given by $T_1/T_0 = (Q/Q_r)^2$. Here T_1 is the transmittance value in the deepest point in the drop; T_0 is the value of the reference line at the frequency corresponding to the deepest point in the drop, *Q* the quality factor of the waveguide and *Qr* the radiative loss.

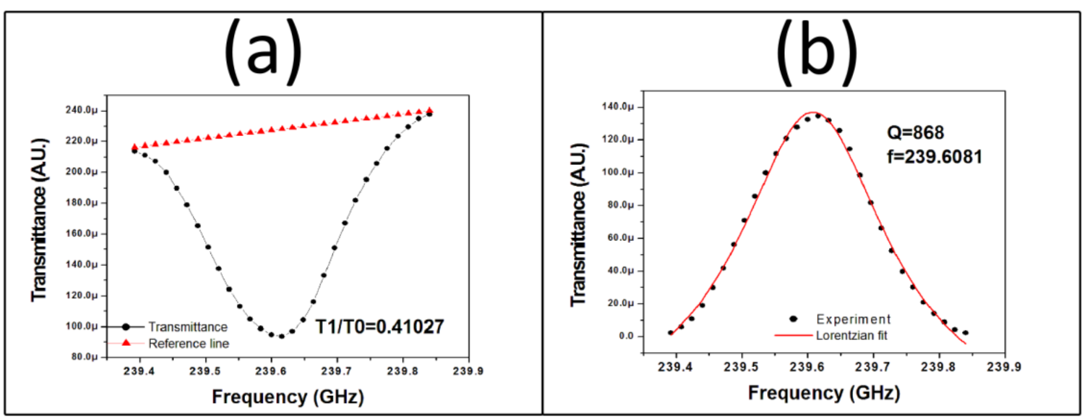

Figure 7.16 (a) A detailed zoom into the drop zone of the transmittance, the reference line is the estimated transmittance if the cavity was decoupled from the waveguide. The ratio of the transmittance with respect to the base line is a measure of the coupling strength of the waveguide –cavity system. (b) Lorentzian fit of the transmittance drop obtained by subtracting the drop signal from the reference line.

The drop into the waveguide is obtained by subtracting the drop signal from the reference line in the transmittance as shown if Figure 7.16(a). The drop signal is then fitted using a Lorentzian line and with the quality factor Q of the cavity given by $Q=\omega_0/\Gamma$ where Γ is the width at half maxima. This process is repeated for two set of samples.

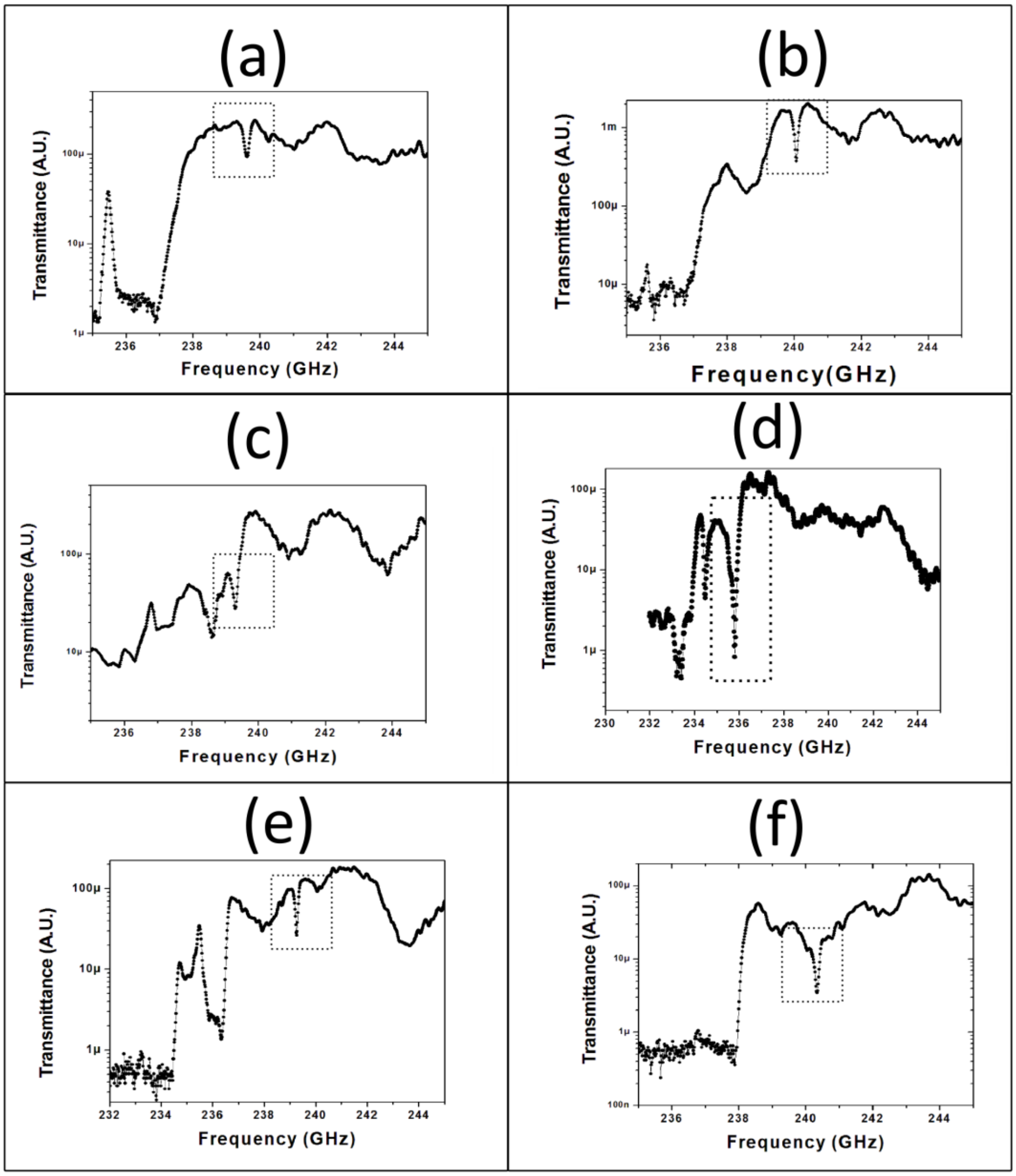

Figure 7.17 Transmittance of cavity waveguide coupled using the channel drop configuration as a function of the inner hole displacement, the zone marks the position of the drop. (a) for Δs=0.00, (b) for Δs=0.05, (c) for Δs=0.10, (d) for Δs=0.15, (e) for Δs=0.20 and (f) for Δs=0.25.

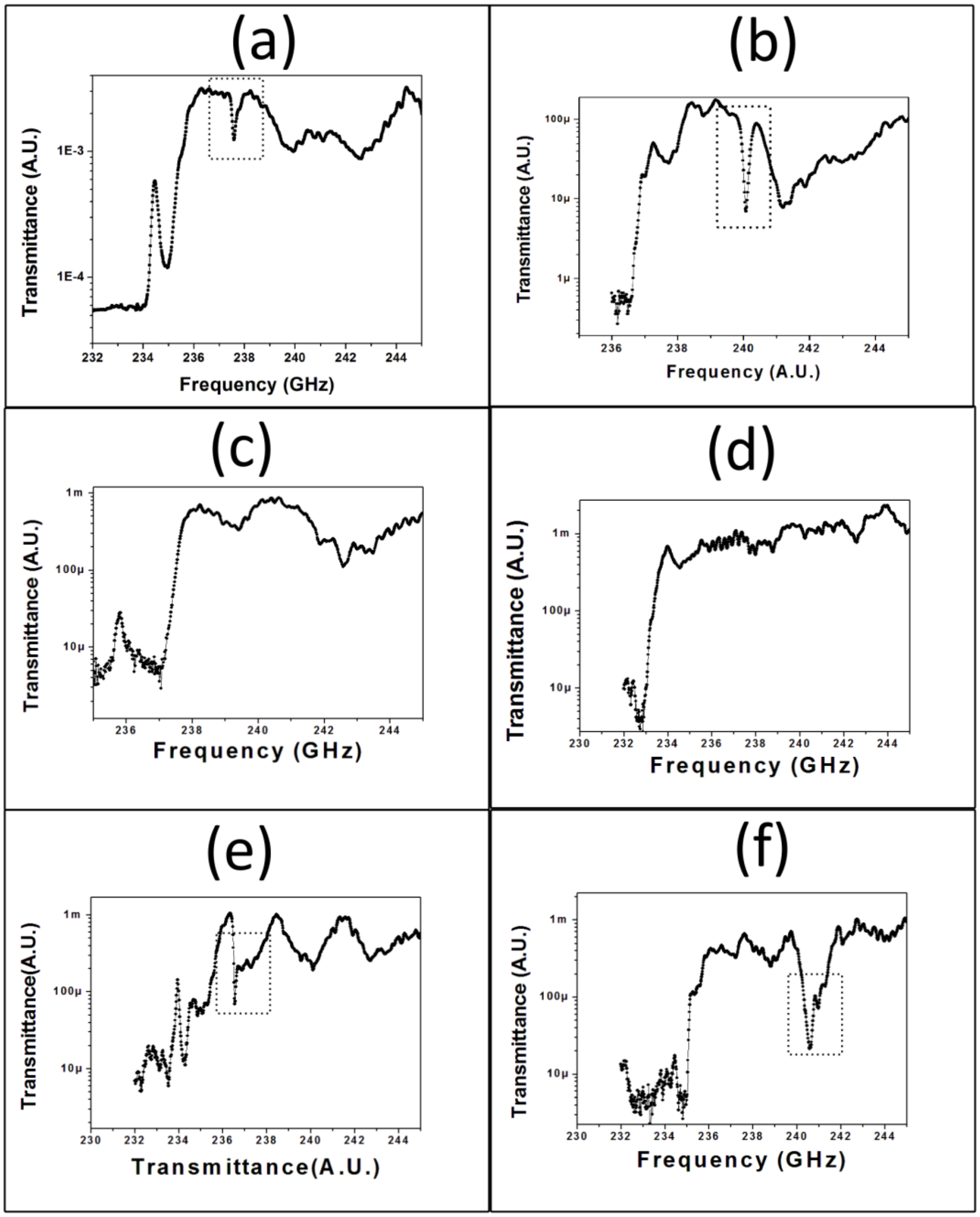

Figure 7.18 Transmittance of cavity waveguide coupled using the channel drop configuration as a function of the inner hole displacement. (a) for Δs=0.00, (b) for Δs=0.05, (c) for Δs=0.10, (d) for Δs=0.15, (e) for Δs=0.20 and (f) for Δs=0.25.

The transmittance spectrum for channel drop samples with two and three row separation as a function of the displacement of the nearest hole to the cavity are shown in Figure 7.17 and Figure 7.18, The detailed characteristics of the transmittances are reported in table 7.1.

Δs	f_c (GHz)	Δf (GHz)	T_1/T_0	Q	Q_r
			Two hole separation		
0.00	239.608	0.2760	0.4103	868	1355
0.05	240.067	0.2121	0.2201	1132	2412
0.10	239.318	0.2030	0.3463	1179	2003
0.15	235.808	0.1601	0.0920	1473	4856
0.20	239.270	0.1849	0.2373	1294	2656
0.25	240.334	0.2562	0.2205	938	1997
			Three hole separation		
0.00	240.1027	0.3745	0.0705	641	2414
0.05	240.0605	0.2111	0.2619	1137	2428
0.10	N/O	N/O	N/O	N/O	N/O
0.15	N/O	N/O	N/O	N/O	N/O
0.20	236.528	0.1536	0.1250	1539	4355
0.25	240.623	0.29568	0.2664	813	1575

Table 7.1 Experimental values for the cavity - waveguide coupled system in the channel drop scheme. Here for sample with three holes and displacement Δs=0.10 and Δs=0.15 not clear drop is observed.

For the set of samples with two holes separation between the cavity and the waveguide we observe a change in the quality factor of the cavity coupled to the cavity and in the radiative quality factor, the trend is more clearly seen in Figure 7.19.

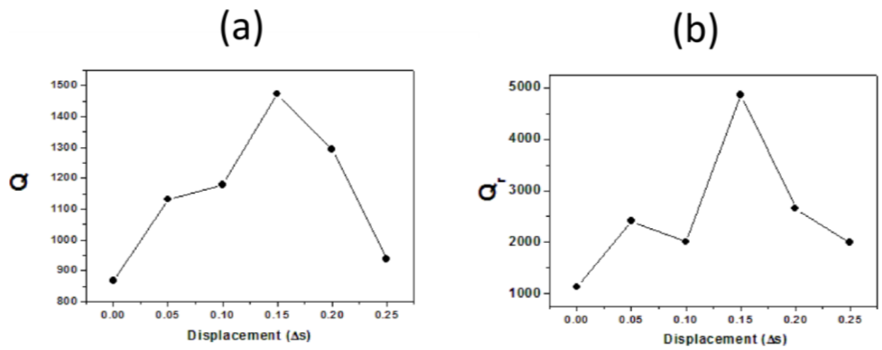

Figure 7.19 (a) Total quality factor of the L3 cavity in the channel drop configuration as function of the inner hole. (b) Radiative quality factor as a function of the displacement derived from the quality factor Q and the magnitude of the drop.

As we expected Figure 7.19(a) shows the quality factor of the structure should increase with the displacement as it has a maximum between Δs=0.15 and Δs=0.20, while the radiative quality factor also shows a peak for Δs=0.15 Figure 7.19(b).

For the set of samples with three rows separation we notice that we're able to observe a drop for all the samples except for two samples with three hole separation and displacement Δs=0.10 and Δs=0.15. However the measured drops reveals the same trend as I begin to increased from Δs=0.00 to Δs=0.10 and decreased from Δs=0.20 to Δs=0.25.

To complement the transmittance measurement we also realized scattering measurements. Again due that a high Q cavity has a radiation distribution nearly parallel to the surface of the sample we were only able to measure few samples. The measured samples are reported in Figure 7.20.

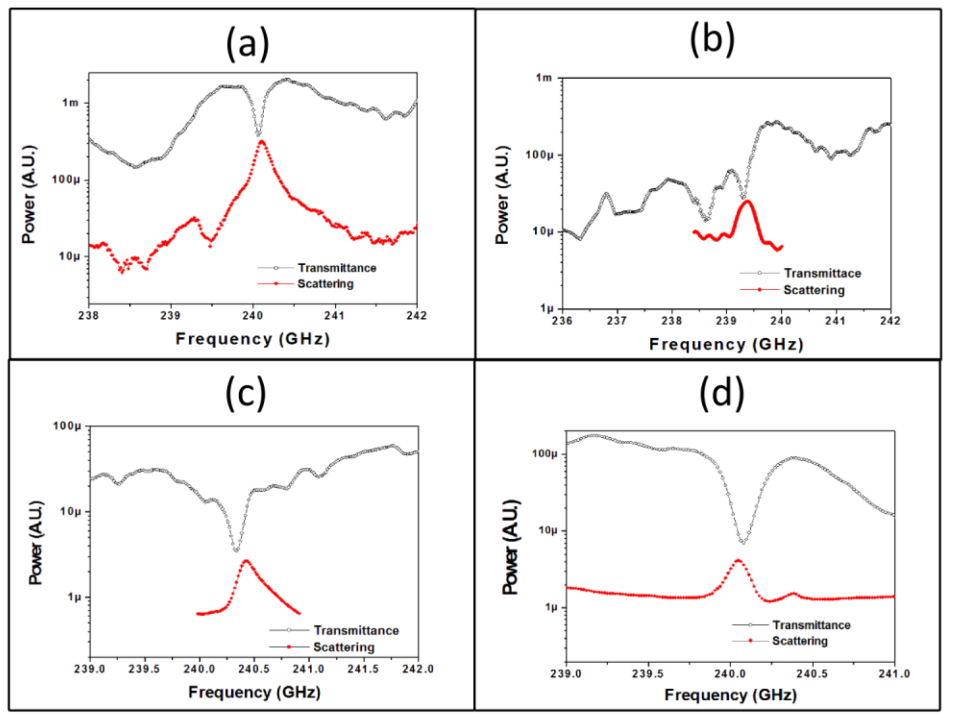

Figure 7.20 Transmittance and scattering measurements for the samples that we we're able to measure a scattering signal.(a) Two rows separation Δs=0.05. (b) Two rows separation Δs=0.10. Two rows separation Δs=0.25. Three rows separation Δs=0.05.

Figure 7.20 shows the scattering and the transmittance for the samples that we were able to obtain a scattering signal from. We observe that the scattering signal peaks where the transmittance has a drop as expected. The frequencies is slightly higher in the scattering as it was also observed for the Lorentzian filter. This is produced by the effect of the cavity resonance is very close to the non-linear regime of the waveguide. The detailed spectrum near the peak in the scattering is shown in Figure 7.21 .

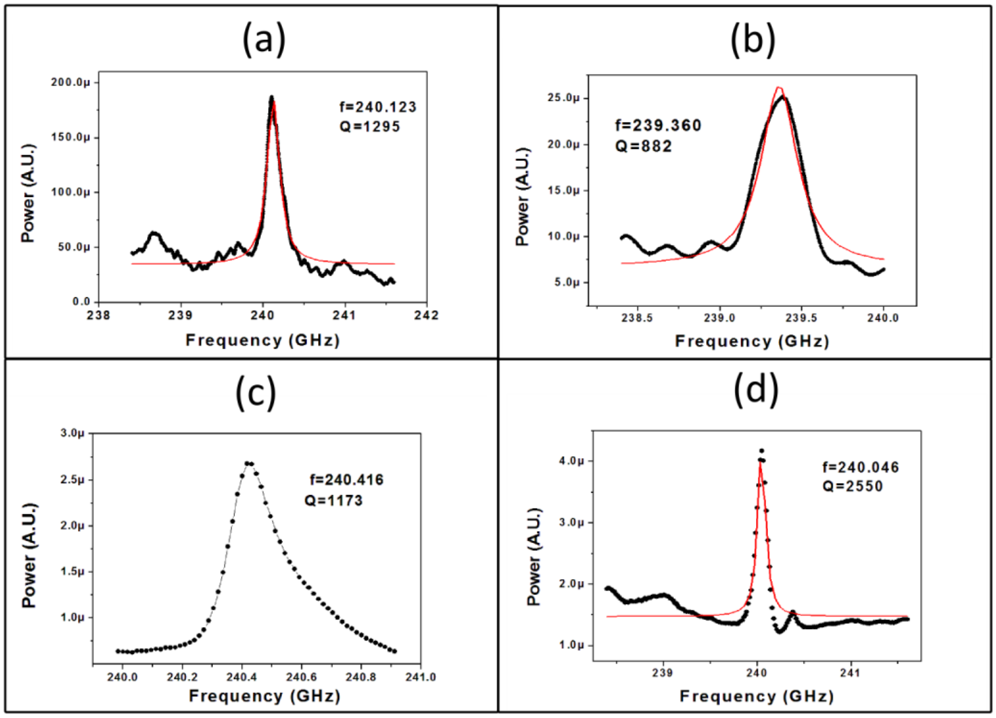

Figure 7.21 Scattering peak and quality factor associated with the width of the scattering peak for each sample where scattering signal was observed. (a) Two rows separation Δs=0.05. (b) Two rows separation Δs=0.10. Two rows separation Δs=0.25. Three rows separation Δs=0.05.

Figure 7.21 shows a very symmetric shape for the scattering in (a) and (d) corresponding to Δs=0.05 for two and three rows. And the highest quality factor in the channel drop is 2550. The non-symmetric shape in the scattering in (c) is produced by the coupling in the non-linear regime and the shape of spectrum is consisted with the estimated transmittance shape in this regime as is reported in literature [44]

D. Summary for the 240 GHz cavities.

We have constructed and measured high Q cavities at 240 GHz. By tuning the L3 cavity it is possible to reach Q values as high as Q=3800 for the Lorentzian filter coupling scheme as is measured with the scattering into free space by the cavity. However the Lorentzian scheme is not well suited for the search for even higher Q because the measurement depends of the amount of light coupled into the cavity and because in-plane coupling decrease more rapidly than the total loss of the cavity, the transmittance decreases very rapidly and therefore is very hard to measure.

The channel drop is more suited for measuring high Q cavity because, to have and significant drop, we need to balance the coupling from the waveguide to the radiative loss. For a given radiative loss we can always equal or at least have the same order of magnitude loss by changing the distance between the cavity and the waveguide.

We have that the quality factor calculated from the width of the transmittance in both the Lorentzian filter and the channel drop could lead to errors if the cavity resonance is very close to the flat region of the waveguide dispersion relation.

8 Conclusions

The experimental results reported in chapter 4 to 7 shows that indeed we succeeded in constructing a high Q cavity that operates at Terahertz frequencies. At 1 THz we constructed and measured a photonic crystal cavity as high as Q=1020, which compared with the metallic waveguide photonic crystal cavity with a Q≈100 provides a sharper resonance. We believe that the quality factor could reach higher Q and at room temperature will be limited by the free carrier absorption.

A cavity with a Q=1020 will enable the strong coupling between shallow donors in GaAs, therefore the next step has to be in the direction of fabricating the cavity using GaAs instead of silicon. The processing of GaAs is slightly more difficult that for silicon but it's been already proven that high quality photonic crystal could be constructed using reactive ion etching.

Also at 1 THz we constructed a transversal magnetic cavity intended to be coupled to a quantum post with Q as high as 1560. The quality factor of the cavity can be improved by carefully tuning the design of the cavity.

In the 240 GHz regime we also were able to obtain encouraging results by constructing a cavity with quality factor near 4000, which is still below the value needed for it to have a strong coupling to a spin ensemble; however, the measurement was done at room temperature where the quality factor is severely restricted by free carrier absorption, an inconvenience not present at low temperature. Precisely, low temperatures are needed for it to be coupled to an ensemble of spins because only a low temperature could the spins be properly polarized. The cavity with a Q=4000 is however very promising for spin resonance and we were looking to integrate this into the UCSB 240 ESR system.

The future path of work is work into reducing the insertion loss of the structure, and also the waveguide needs to be modified in order to couple the cavity to the linear dispersion of the waveguide. As we have shown in chapter 7 the cavities we used are very close to the edge of the transmittance. To work in the linear dispersion region the holes next to the waveguide need to be made smaller in order to increase the effective index of the waveguide and therefore push to lower frequencies the dispersion of the waveguide.

Photonic crystal structures are useful and very easy to integrate into more complex devices and they are now one more tool available to the THz community and science at large.

Appendix A. Eigen Value problem Maxwell equations.

In this appendix we will present the Maxwell equations for a lossless non dispersive media as an eigenvalue problem.

The set of Maxwell equations without sources are:

$$\nabla \cdot B = 0\,; \quad \nabla \times E + \frac{\partial B}{\partial t} = 0$$
$$\nabla \cdot D = 0\,; \quad \nabla \times H - \frac{\partial D}{\partial t} = 0 \tag{A.1}$$

If we consider that the displacement field ***(D)*** and induction field ***(B)*** are linear function of the electric field *E* and magnetic field *H*. That the media is a non-magnetic and the solutions for the fields are harmonic, i.e.:

$$D(r,t) = \varepsilon_0 \varepsilon(r) E(r,t); \;\; B(r,t) = \mu(r) H(r,t)$$
$$\mu(r) = \mu_0 \tag{A.2}$$
$$E(r,t) = E(r) e^{-i\omega t}; \;\; H(r,t) = H(r) e^{-i\omega t}$$

We have that the set of Maxwell's equations for the filed can be simplifies as:

$$\nabla \times E - i\mu_0 H = 0$$
$$\nabla \times H + i\omega\varepsilon_0 \varepsilon(r) E = 0 \tag{A.3}$$

From here its follows that:

$$E = \frac{i}{\omega \varepsilon_0 \varepsilon(r)} \nabla \times H$$
$$\nabla \times \left[\frac{1}{\varepsilon(r)} \nabla \times H\right] - \left(\frac{\omega}{c}\right)^2 H = 0 \tag{A.4}$$

Here we have that $c = 1/\sqrt{\mu_0 \varepsilon_0}$. The equation for the magnetic field H, could be formulated as a eigenvalue by defining an operator Ω as:

$$\Omega H = \nabla \times \left[\frac{1}{\varepsilon(r)} \nabla \times \mathrm{H}\right] \tag{A.5}$$

is an hermitic vector field operator. With the above definition for Ω we have the equation for H can be written as:

$$\Omega H - \left(\frac{\omega}{c}\right)^2 H = 0 \tag{A.6}$$

Equation A.6 is denominated "Mater equation"; The solution of the master equation that satisfies the transversality condition given by the divergence equation in A.1 are the normal modes of systems.

In order to probe that Ω is a hermitic operator we first need a definition of the inner product of two vector fields. We can use the canonical definition of inner product for a vectorial space.

$$\langle A, B \rangle \stackrel{\text{def}}{=} \int d^3r\, A^*(r) \cdot B(r) \tag{A.7}$$

Here A(r) and B(r) are three dimensional vector field and " * " denotes the complex conjugate and " . " is the normal dot product for two vectors. In order to prove that Ω is a Herminitan operator we need to prove that:

$$\langle A, \Omega B \rangle = \langle \Omega A, B \rangle \tag{A.8}$$

To verify this condition we only need to integrate by part twice:

$$\langle A, \Omega B \rangle = \int d^3r A^*(r) \cdot \nabla \times \left(\frac{1}{\varepsilon(r)} \nabla \times B(r)\right) \tag{A.9}$$

$$=\int d^3r\left(\nabla \times A(r)\right)^* \cdot \frac{1}{\varepsilon(r)} \nabla \times B(r)$$

$$= \int d^3r\left[\nabla \times \left(\frac{1}{\varepsilon(\mathrm{r})} \nabla \times A(r)\right)\right]^* \cdot B(r)$$

$$= \langle \Omega A, B \rangle$$

Here we neglect the surface terms of the integral because either the fields vanish at the boundaries or they are periodical. In either case the surface integral vanishes at the boundaries.

Because Ω is a Hermitian operator, it lets us reformulate Maxwell's equations for a lossless, non dispersive, non magnetic, linear media in the absence of sources, into an eigenvalue problem for the magnetic field ***H***. The different modes obtained are orthogonal and they form a basis from which a general solution for the Maxwell equations can be constructed.

The present eigenvalue formulation is based on the magnetic field and not in the electric field, however once the solution for the magnetic field are known, the electric field can be calculated using (A.4).

Appendix B. Bloch Theorem.

In this appendix we will present the photonic crystal concept. First we define the translation operation in the crystal; and show the translation commutes by the operator Ω defined in the master equation for the magnetic field H. We show that the common solutions are indeed Bloch functions. Finally the concepts of band diagram and reduce zone applied to photonic crystal are explain.

A crystal is a periodic structure. As any periodic structure it will repeated itself, the length at which the structure is repeated is called lattice constant. For a three dimensional crystal there are three independent orientation and therefore three different repetition lengths. Let $\mathbf{a_1}$, $\mathbf{a_2}$ and $\mathbf{a_3}$ be three vector along each independent orientation and be they magnitude the lattice constant along each orientation.

Lets know define the discrete translation operator as:

$$T_R A(r) = A(r+R) \tag{B.1}$$

Where $\mathbf{R}= l\mathbf{a_1} + p\mathbf{a_2} + q\mathbf{a_3}$, here l,p and are q integers; the eigenvalues of the translation operator are $e^{-ik\cdot R}$ with k in a vector in the reciprocal lattice space.

From the concept of a crystal in which two points in the crystal are separated by any integer linear combination of the lattice vectors are equivalent is natural to consider that any operator that represents a physical quantity should be the same, i.e. the operator representing a physics quantities must commute with the translation operator.

In the language of operators if two operators commute it is possible to find a common representation for both operators. In particular we are interested in the operator defined by the master equation Ω; from its definition we know that because $\varepsilon(r)$ is periodic the operator Ω will commute with the translation operator. To actually prove that the translation operator T_R commutes with the operator Ω we apply it over an arbitrary field *H(r)*.

$$T_R \Omega H(r) = T_R \left[\nabla \times \frac{1}{\varepsilon(r)} \nabla \times\right] H(r) = T_R \left[\nabla \times \left(\frac{1}{\varepsilon(r)} \nabla \times H(r)\right)\right]$$

$$= \left[\nabla_{\mathrm{R}} \times \left(\frac{1}{\varepsilon(r+R)} \nabla_{\mathrm{R}} \times H(r+R)\right)\right]$$

$$= \left[\nabla \times \left(\frac{1}{\varepsilon(r)} \nabla \times H(r+R)\right)\right] = \left[\nabla \times \frac{1}{\varepsilon(r)} \nabla \times\right] H(r+R)$$

$$= \Omega T_R H(r)$$

Since Ω and T_R commute there hast to be a common set of eigenfuncions. Suppose that *H(r)* is a common eigenfunction. The condition for *H(r)* to be an eingenfunction of T_R is:

$$T_R H(r) = H(r+R) = e^{-ikR} H(r)$$

We can define a function $u(r) = e^{-ikr} H(r)$; and the easily prove that $u(r)$ is a periodic function in R.

$$u(r+R) = e^{-ik(r+R)} H(r+R) = e^{-ikR} \left(e^{-ikr} H(r)\right) = e^{-ikR} u(r)$$

With the periodicity of $u(r)$ we can write a final form for the Bloch theorem as:

$$H_k(r) = e^{ikr}u(r) \tag{B.2}$$

Here we are explicitly setting the k dependence in *H*. The solutions to the operator Ω are planes waves modulated by a periodic function of the crystal; equation B.2 is the Bloch theorem and its function are called Bloch waves.

Will be use the form of the Bloch function and substitute it inside the master equation A.6.

$$\Omega H_k(r) = \left(\frac{\omega(k)}{c}\right)^2 H_k(r)$$

Inserting the expression B.2 for H_k , and the definition of Ω we have that:

$$\left[\nabla \times \frac{1}{\varepsilon(r)} \nabla \times\right] e^{ik\cdot r}u(r) = \left(\frac{\omega(k)}{c}\right)^2 e^{ik\cdot r}u(r)$$

By Applying the vector operations on the left side of the equation and by factoring the exponential in both sides we have that the periodic function *u(r)* satisfies:

$$\left[(ik + \nabla) \times \frac{1}{\varepsilon(r)} (ik + \nabla) \times\right] u(r) = \left(\frac{\omega(k)}{c}\right)^2 u(r)$$

Now defining the Hermitian operator Ω_k as:

$$\Omega_k(r) = \left[(ik + \nabla) \times \frac{1}{\varepsilon(r)} (ik + \nabla) \times\right] \tag{B.3}$$

The master equation for the periodic function *u(r)* is:

$$\Omega_k(r)u(r) = \left(\frac{\omega(k)}{c}\right)^2 u(r) \tag{B.4}$$

By using the relation B.2, we find that the solutions of B.4 are the modes profile, provided that they satisfy the tranversality condition inherited from A.2:

$$\nabla \cdot H_k = 0$$

This condition could be written in terms of $u(r)$ as:

$$(ik + \nabla)u(r) = 0 \tag{B.5}$$

A. *Reduced Zone scheme*

The functional form of the Bloch functions defined in B.2 does not put any condition on *k*, however the periodicity of the function *u(r)* allows the restriction of the range of the *k* vector to the first Brillouin zone.

Considering an arbitrary value of *k,* it is always possible to find a reciprocal lattice vector G and a k' vector in the first Brillouin zone such that:

$$k = k^{'} + G \tag{B.6}$$

The Bloch function $H_k(r)$ associate with *k* satisfies the following equations:

$$H_k(r) = e^{ikr} u(r)$$

$$\Omega_k(r)u(r) = \left(\frac{\omega(k)}{c}\right)^2 u(r)$$

Now let's "fold" the *k* vector into the first Brilloin zone by using B.6:

$$H_k(r) = e^{ikr} u(r) = e^{i(k^{'}+G)r} u(r) = e^{ik'r}\left(e^{iGr} u(r)\right) = e^{ik'r} u'(r)$$

Where the function $u^{'}(r)$ defined as $u^{'}(r) \equiv e^{iGr} u(r)$ is a periodic function of the lattice. This property follows from:

$$u^{'}(r+R) = e^{iG(r+R)} u(r+R) = e^{iGr} u(r) = u^{'}(r)$$

Let's apply the operator $\Omega_{k'}$ over $u^{'}(r)$ using relation B.6 and the definition of $u^{'}(r)$.

$$\Omega_{k'} u' = \Omega_{k-G} e^{iGr} u = [i(k-G) + \nabla] \times \left\{ \frac{1}{\varepsilon} [i(k-G) + \nabla] \times e^{iGr} u \right\}$$

$$= [i(k-G) + \nabla] \times \left\{ \frac{1}{\varepsilon} \left[i(k-G) \times e^{iGr} u + \nabla \times e^{iGr} u \right] \right\}$$

$$= [i(k-G) + \nabla] \times \left\{ \frac{1}{\varepsilon} \left[i(k-G) \times e^{iGr} u + e^{iGr} (iG + \nabla) \times u \right] \right\}$$

$$= [i(k-G) + \nabla] \times e^{iGr} \left\{ \frac{1}{\varepsilon} [(ik + \nabla) \times u] \right\}$$

$$= i(k-G) \times e^{iGr} \left\{ \frac{1}{\varepsilon} [(ik + \nabla) \times u] \right\} + \nabla \times e^{iGr} \left\{ \frac{1}{\varepsilon} [(ik + \nabla) \times u] \right\}$$

$$= i(k-G) \times e^{iGr} \left\{ \frac{1}{\varepsilon} [(ik + \nabla) \times u] \right\} + i e^{iGr} G \times \left\{ \frac{1}{\varepsilon} [(ik + \nabla) \times u] \right\}$$

$$+ e^{iGr} \nabla \times \left\{ \frac{1}{\varepsilon} [(ik + \nabla) \times u] \right\} = e^{iGr} (ik + \nabla) \times \left\{ \frac{1}{\varepsilon} [(ik + \nabla) \times u] \right\}$$

$$= e^{iGr} \Omega_k u = e^{iGr} \left(\frac{\omega(k)}{c} \right)^2 u = \left(\frac{\omega(k' + G)}{c} \right)^2 u'$$

From here we have that:

$$\Omega_{k'} u'(r) = \left(\frac{\omega(k' + G)}{c} \right)^2 u'(r) \qquad \text{(B.7)}$$

i.e. $u'(r)$ is solution of $\Omega_{k'}$. From equations B.6 and B.7 we conclude that for any arbitrary *k* vector exist a *k'* in the first Brillouin zone such that the solution to Ω_k is also solution of $\Omega_{k'}$. In conclusion the master equation B.4 only needs to be solved inside the First Brillouin zone.

Equation B.7 also shows that there are a discrete number of eigenvalues for the operator Ω_k, by ordering the eigenvalues we can introduce *n* as an index to distinguish between different modes for the same *k* value, therefore we can write the frequencies solution as ω_{nk}. The operator Ω_k is a function of k and inside the first Brillouin zone k can be varied continuously, therefore we can expect that ω_{nk} also to change continuous as a function of k.

It Is convenient to express the continuous variation of ω_{nk} as a function of k explicitly as $\omega_{nk} = \omega_n(k)$. The set of functions $\omega_n(k)$ is called a band structure.

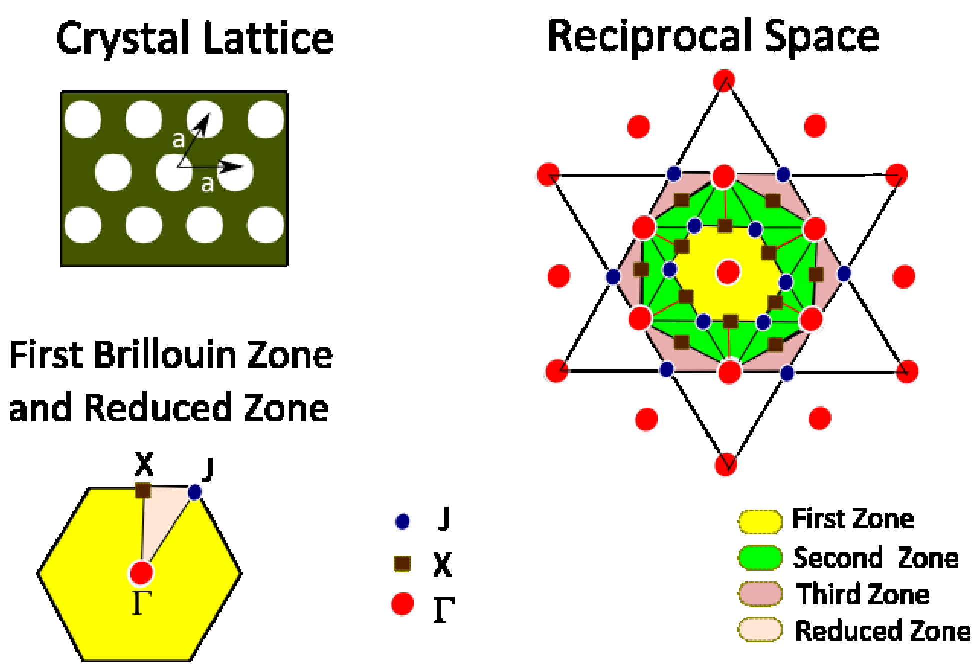

Figure B.1 The triangular lattice of holes; The reciprocal space with the first three zones highlighted. The high symmetry points are shown and the detail of the first Brillouin zone with its irreducible zone.

Figure B.1 shows the reciprocal space for the triangular lattice; the different Brillouin zones and the high symmetric point are shown in the reciprocal space. The underlying hexagonal symmetry is evident and it suggests that by rotating by 60 degrees and using plane symmetries the calculation space could be further shrink to only consider the irreducible zone. The irreducible zone is the smallest set of *k* vector with which rotations, reflections and inversions can reproduce the entire first Brillouin zone and therefore the entire reciprocal space.

In this appendix we have found that photonic crystal modes are subject to the proper symmetries of the crystal. The modes turns out to be Bloch functions which are plane waves modulated by a periodic function of the lattice. A general solution for the system is formed by a superposition of the Bloch modes, associated which each Bloch function there is a *k* vector, which by the sole use of the translation symmetries we only need to employ first Brillouin zone. Furthermore the use of rotations and reflection reduces the problem to only solve for *k* vectors in the irreducible zone.

Appendix C. Mode Couple Theory.

Couple mode theory is an approximation theory used to describe the interaction in a complex system that can be broken down into simpler idealized components. The solution to the overall systems is then expanded using the solutions or modes for each component. The amplitudes of each modes will depend on the particular set of rules obeyed by the overall systems, these rules will determine the couplings among each component in the system.

A. Lorentzian Filter

We will apply couple mode theory to our particular case of a complex system with a cavity and one or more waveguides. The localized modes for the cavity and the propagating modes for the waveguide will be the components of the overall system. The set of rules that the complex systems obeys are very general: Weak coupling, energy conservation, time reversal invariance, time invariance and linearity. The essential rule is weak coupling while the other four could be relaxed as we will see.

We will first apply these ideas to the simple case of a filter. The filter consists of an input waveguide through which the light is injected into the cavity, the cavity, and the output waveguide that carries the filtered signal (C.1).

In figure C.1 we have A proportional to the amplitude of the electromagnetic field of the cavity mode, in general it is a complex quantity and is chose such that the square of its magnitude ($|A|^2$) is the energy stored in the cavity. $S_{1,2}\pm$ are the complex quantities proportional to the propagating field in the waveguides such that $|S_{1,2\pm}|^2$ are the energies fluxes. Here $\tau_{1,2}$ are the coupling factors between the cavity and the waveguides.

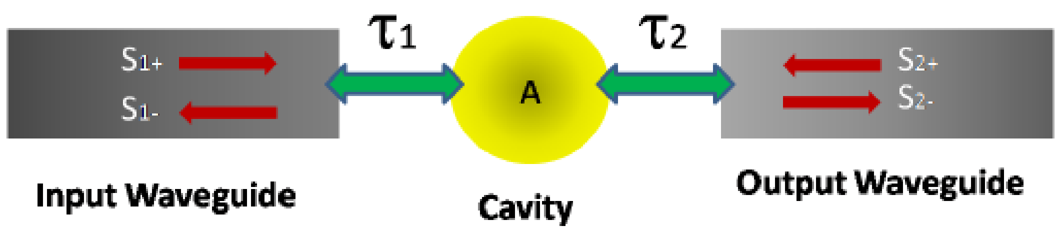

Figure C.1 The Lorentzian filter system. The filter could break down into an input and output waveguide coupled trough a cavity. Mode couple theory solves the relation between the different scattering parameter and the coupling factor of the waveguides to the cavity.

The temporal mode coupling theory equation for the field A in the cavity, with a first order approximation, can be written as:

$$\frac{dA}{dt} = -i\omega_0 A - \frac{A}{\tau_1} - \frac{A}{\tau_2} + \alpha_1 S_{1+} + \alpha_2 S_{2+} \quad \text{(C.1)}$$

$$S_{1,2-} = \beta_{1,2} S_{1,2+} + \gamma_{1,2} A \quad \text{(C.2)}$$

Here ω_0 is the frequency mode of the cavity, $\alpha_{1,2}$ are the coupling factors from the waveguide that is going into the cavity, $\beta_{1,2}$ are the reflection coefficients produced by the cavity and $\gamma_{1,2}$ the coupling factor from the cavity into the waveguide. All these quantities are not independents of each other.

To derive the relation among different couplings we first consider that there is not incident flux going towards the cavity, i.e. $S_{1,2+}=0$. The equation for the field A in the cavity and the fluxes $S_{1,2-}$ are given by:

$$\frac{dA}{dt} = -i\omega_0 A - \frac{A}{\tau_1} - \frac{A}{\tau_2} \tag{C.3}$$

$$S_{1-} = \gamma_1 A \tag{C.4}$$

$$S_{2-} = \gamma_2 A \tag{C.5}$$

From C.3 it is straightforward to derive that:

$$\frac{dA^*A}{dt} = -2\left[\frac{1}{\tau_1} + \frac{1}{\tau_2}\right] A^*A$$

Here A^* is the complex conjugate of the field amplitude in the cavity. The quality factor is defined as 2π times the ratio of the time-average energy stored in the cavity to the energy loss per cycle[ref jackson]. As a result the quality factor is given by:

$$\frac{1}{Q} = \frac{2}{\omega_0}\left[\frac{1}{\tau_1} + \frac{1}{\tau_2}\right] \tag{C.6}$$

Now consider the case where the right waveguide in figure C.1 is decoupled from the cavity, i.e. $1/\tau_2 = \gamma_2 = 0$. Applying energy conservation we have that the energy lost by the cavity is the energy of the flux moving out through the left waveguide. So we have that:

$$\frac{2}{\tau_1}A^*A = |\gamma_1|^2 A^*A$$

We can chose an arbitrary phase for the reflection coefficient, such that the reflection coefficient real. Under this condition the coupling coefficient from the cavity into the waveguide is $\gamma_1 = \sqrt{2/\tau_1}$. Using a similar argument for the case in which the left waveguide is decoupled from the cavity we have that $\gamma_2 = \sqrt{2/\tau_2}$. These coefficients are correct to the first order even when both waveguides are coupled. The second order corrections are negligibly small due to the nature of the coefficients which are already small quantities.

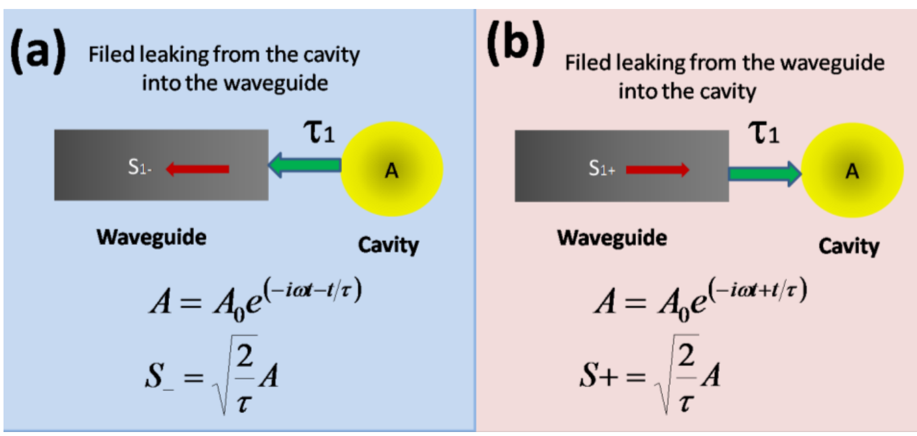

Figure C.2 Time reversal symmetry for the solution of the coupled system cavity-waveguide.

We have found that for the coupled cavity-waveguide system with no input flux of power, the field inside the cavity leaks into the waveguide and the field inside the cavity decays as $e^{(-i\omega t - t/\tau)}$. We also found that the flux is related to the field amplitude inside the cavity as $S_{1-} = \sqrt{2/\tau_1}\,A$ with as $\gamma_1 = \sqrt{2/\tau_1}$ as shown in figure C.2(a). If we apply the time reversal symmetry we find that for a flux coupling from the waveguide into the cavity the field inside the cavity grows as $e^{(-i\omega t + t/\tau)}$ and the field inside the cavity is related with the flux as $S_{1+} = \sqrt{2/\tau_1}\, A$ as shown in figure C.2(b).

For this solution there is not output fluxes $S_{1,2-} = 0$ and when this conditions are inserted into equations C.1 and C.2 (here we decouple the right waveguide) we find that:

$$\frac{dA}{dt} = -i\omega_0 A - \frac{A}{\tau_1} + \alpha_1 S_{1+} \tag{C.7}$$

$$0 = \beta_1 S_{1+} + \gamma_1 A \tag{C.8}$$

From equation C.8 with the solution from the time reversal we have that:

$$S_{1+} = -\frac{\gamma_1}{\beta_1} A = -\frac{\sqrt{\frac{2}{\tau_1}}}{\beta_1} A = \sqrt{\frac{2}{\tau_1}} A$$

From the last equation we immediately find that $\beta = -1$. Inserting the $S_{1+} = \sqrt{2/\tau_1}\, A$ into C.7 we have:

$$\frac{dA}{dt} = -i\omega_0 A - \frac{A}{\tau_1} + \alpha_1 \sqrt{\frac{2}{\tau_1}} A$$

After some simple math we have that the change in energy of the cavity is given by:

$$\frac{dA^* A}{dt} = -\frac{2A^* A}{\tau_1} + 2\alpha_1 \sqrt{\frac{2}{\tau_1}} A^* A$$

Energy conservation requires that this increase in the energy in the cavity to be equal to the energy of the flux; we arrive to the following condition:

$$-\frac{2A^*A}{\tau_1} + 2\alpha_1\sqrt{\frac{2}{\tau_1}}A^*A = \frac{2}{\tau_1}A^*A$$

From the last equation we found that $\alpha = \sqrt{\frac{2}{\tau_1}}$; We can realize the same analysis for the second waveguide and we will arrive to a similar results. Using the values found for the different couplings we arrive to the mode coupling equations:

$$\frac{dA}{dt} = -i\omega_0 A - \frac{A}{\tau_1} - \frac{A}{\tau_2} + \sqrt{\frac{2}{\tau_1}}S_{1+} + \sqrt{\frac{2}{\tau_1}}S_{2+} \tag{C.9}$$

$$S_{1,2-} = -S_{1,2+} + \sqrt{\frac{2}{\tau_{1,2}}}A \tag{C.10}$$

Let now analyze how the frequency filtering works. In a filter's normal operation we have an incident signal that travels through the waveguide and then interacts with the cavity. The signal could be formed by a single frequency wave or it could have some frequency bandwidth. In either case only the frequencies component that lies in a certain frequency width around a cavity resonant mode are able to couple into the cavity; the remaining frequency components will be strongly reflected. The signal appearing in the output waveguide will therefore be filtered by showing only frequencies that were able to couple into the cavity. The amplitude of the transmission for each frequency component (frequency response) of the filter depends on the filter structure. We will show that for the Lorentzian filter shown in figure C.1 the frequency response is precisely a Lorentzian centered on the cavity resonant and the width of the Lorentzian will correspond to the inverse of quality factor of the cavity multiply by its resonant frequency.

We start with the couple mode theory equations C.9 and C.10 and considering that for normal filter operation there is no input energy from the output (left waveguide in figure C.1) waveguide, i.e $S_{2+} = 0$, and field amplitude inside the cavity are harmonics, i.e. $A(t,\omega) = Ae^{-i\omega t}$, under these conditions we have that the couple mode equations are:

$$-i\omega A = -i\omega_0 A - \frac{A}{\tau_1} - \frac{A}{\tau_2} + \sqrt{\frac{2}{\tau_1}} S_{1+} \tag{C.11}$$

$$S_{1-} = -S_{1+} + \sqrt{\frac{2}{\tau_1}} A \tag{C.12}$$

$$S_{2-} = \sqrt{\frac{2}{\tau_2}} A \tag{C.13}$$

From equation C.11 we have that:

$$S_{1+} = \sqrt{\frac{\tau_1}{2}} \left[i(\omega_0 - \omega) + \frac{1}{\tau_1} + \frac{1}{\tau_2} \right] A$$

From the above equation the transmission coefficient is simple given by:

$$T(\omega) = \left| \frac{S_{2-}}{S_{1+}} \right|^2 = \left| \frac{\sqrt{\frac{2}{\tau_2}}}{\sqrt{\frac{\tau_1}{2}} \left[i(\omega_0 - \omega) + \frac{1}{\tau_1} + \frac{1}{\tau_2} \right]} \right|^2 = \frac{\frac{4}{\tau_1 \tau_2}}{(\omega_0 - \omega)^2 + \left(\frac{1}{\tau_1} + \frac{1}{\tau_2} \right)^2}$$

Now using the definition for the quality factor C.6 the transmittance for a symmetric case ($\tau = \tau_1 = \tau_2$) can be rewritten as:

$$T(\omega) = \frac{\frac{1}{4Q^2}}{\left(\frac{\omega_0 - \omega}{\omega_0}\right)^2 + \frac{1}{4Q^2}} \tag{C.14}$$

This is a Lorentzian line center at the resonant frequency of the cavity. At resonance we have that:

$$T(\omega_0) = 1$$

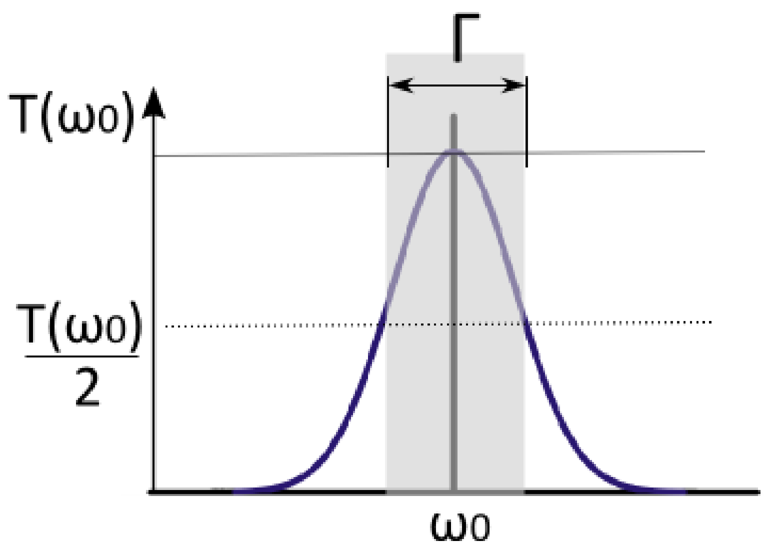

Figure C.3 Illustration of the full width at half maxima for a transmittance curve. The quality factor is given by the $Q = \omega_0/\Gamma$; where Γ is the full width at half maxima of the transmittance curve and ω_0 is the frequency resonant of the cavity in this case the frequency corresponding to the peak in the transmittance.

The frequency width of the peak in the transmittance also includes important information regarding the quality factor. The full width at half maxima (Γ) for the transmittance (as illustrated in figure C.3) is defined as the frequency width of the curve take at half the maximal value in the transmittance. At half maxima we require that both terms in the denominator in equation C.9 to be equal. i.e.:

$$\frac{\Gamma}{\omega_0} = \frac{1}{Q}$$

Which turns out to be what we expected that the width of the Lorentzian is the inverse quality factor of the cavity times the resonant frequency. For the special symmetric case in which the coupling to both waveguides are equal we have that the transmittance at resonance is 100%.

The reflection coefficient is given by:

$$R(\omega) = \left|\frac{S_{1-}}{S_{1+}}\right|^2 = \left|\frac{-\sqrt{\frac{\tau_1}{2}}\left[i(\omega_0 - \omega) + \frac{1}{\tau_1} + \frac{1}{\tau_2}\right] + \sqrt{\frac{2}{\tau_2}}}{\sqrt{\frac{\tau_1}{2}}\left[i(\omega_0 - \omega) + \frac{1}{\tau_1} + \frac{1}{\tau_2}\right]}\right|^2$$

$$= \left|\frac{\left[i(\omega_0 - \omega) + \frac{1}{\tau_1} + \frac{1}{\tau_2}\right] - \sqrt{\frac{1}{\tau_2\tau_2}}}{\left[i(\omega_0 - \omega) + \frac{1}{\tau_1} + \frac{1}{\tau_2}\right]}\right|^2 = \frac{(\omega_0 - \omega)^2 + \left(\frac{1}{\tau_1} - \frac{1}{\tau_2}\right)^2}{(\omega_0 - \omega)^2 + \left(\frac{1}{\tau_1} + \frac{1}{\tau_2}\right)^2}$$

Again for the symmetric case the reflection simplifies to:

$$R(\omega) = \frac{\left(\frac{\omega_0 - \omega}{\omega_0}\right)^2}{\left(\frac{\omega_0 - \omega}{\omega_0}\right)^2 + \frac{1}{4Q^2}}$$

With the result that the reflection vanishes at resonance. In conclusion for a Lorentzian filter without losses the transmittance is a Lorentzian function whose frequency width is the inverse of the quality factor times the resonant frequency of the cavity and whose transmittance at resonance is 100%

B. Lorentzian Filter with losses

In a more realistic situation we have a Lorentzian filter which has external losses such as radiative cavity losses and material absorption. We will focus on the former effect due that radiative loss is intrinsic to the design of the cavity. Material losses in principle are small[6] and in can be incorporate to the calculation using the same formalism.

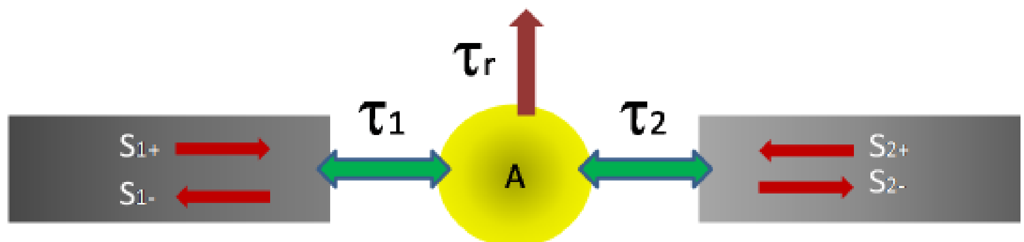

Figure C.4 The Lorentzian filter with losses. The radiative loss is considered as an extra decay mechanism for the radiation confined inside the cavity. In absence of any other decay mechanism the quality factor of the cavity is given $Q = \frac{\omega_0 \tau_r}{2}$ this factor is also called Q-radiative or Q_r.

The schematics for a Lorentzian filter with loses is shown in figure C.4. The coupled equations are simply modified from the Lorentzian filter without loss by adding an extra channel for decay. For normal filtering operation we consider that there is no input flux from the right, i.e. $S_{2+} = 0$. Under these conditions and assuming harmonic fields the coupled equations are:

[6] This is not true for Terahertz photonic crystal at room temperature due to residual carrier absorption. However, this loss can be minimized by cooling down the samples.

$$-i\omega = -i\omega_0 A - \frac{A}{\tau_1} - \frac{A}{\tau_2} - \frac{A}{\tau_r} + \sqrt{\frac{2}{\tau_1}} S_{1+} \tag{C.15}$$

$$S_{1-} = -S_{1+} + \sqrt{\frac{2}{\tau_1}} A \tag{C.16}$$

$$S_{2-} = \sqrt{\frac{2}{\tau_2}} A \tag{C.17}$$

The extra term in equation C.15 $1/\tau_r$ is the radiative loss of the cavity and it represents the field decay in the absence of all the other dissipation mechanisms. The above equations are solved for the *S* parameter as a function of the field in the cavity as follows:

$$S_{1+} = \sqrt{\frac{\tau_1}{2}} \left[i(\omega_0 - \omega) + \left(\frac{1}{\tau_1} + \frac{1}{\tau_2} + \frac{1}{\tau_r} \right) \right] A$$

$$S_{2-} = \sqrt{\frac{2}{\tau_2}} A$$

From here we have the transmission and reflection coefficients given by:

$$T(\omega) = \left| \frac{S_{2-}}{S_{1+}} \right|^2 = \frac{\frac{4}{\tau_1 \tau_2}}{(\omega_0 - \omega)^2 + \left(\frac{1}{\tau_1} + \frac{1}{\tau_2} + \frac{1}{\tau_r} \right)^2}$$

$$R(\omega) = \left| \frac{S_{1-}}{S_{1+}} \right|^2 = \frac{(\omega_0 - \omega)^2 + \left(-\frac{1}{\tau_1} + \frac{1}{\tau_2} + \frac{1}{\tau_r} \right)^2}{(\omega_0 - \omega)^2 + \left(\frac{1}{\tau_1} + \frac{1}{\tau_2} + \frac{1}{\tau_r} \right)^2}$$

For a symmetric system we have that $\tau_\omega = \tau_1 = \tau_2$ and defining Q_T, Q_ω and Q_r as:

$$\frac{1}{Q_r} = \frac{2}{\omega_0 \tau_r}$$

$$\frac{1}{Q_\omega} = \frac{4}{\omega_0 \tau_\omega}$$

$$\frac{1}{Q_T} = \frac{1}{Q_\omega} + \frac{1}{Q_r} = \frac{4}{\omega_0 \tau_\omega} + \frac{2}{\omega_0 \tau_r}$$

Here we have that Q_T is the quality factor of the cavity embedded in the waveguide; for the coupled equation C.15 with not fluxes $S_{1,2+} = 0$ the field decays with a decay constant given by:

$$\frac{1}{\tau} = \frac{2}{\omega_0}\left[\frac{2}{\tau_\omega} + \frac{1}{\tau_r}\right]$$

With the definitions of the partial quality factor the transmittance can be rewritten as:

$$T(\omega) = \frac{\frac{1}{4Q_\omega^2}}{\left(\frac{\omega_0 - \omega}{\omega_0}\right)^2 + \frac{1}{4Q_T^2}} \tag{C.18}$$

$$R(\omega) = \frac{\left(\frac{\omega_0 - \omega}{\omega_0}\right)^2 + \frac{1}{4Q_r^2}}{\left(\frac{\omega_0 - \omega}{\omega_0}\right)^2 + \frac{1}{4Q_T^2}} \tag{C.19}$$

We have that *T(ω)* for the Lorentzian filter with loss is also a Lorentzian line and, we have that at resonance the transmittance is:

$$T(\omega_0) = \frac{Q_T^2}{Q_\omega^2}$$

The transmittance is not longer 100%. The full width at half maxima Γ requires that the both terms in denominator in equation C.18 to be equal. Under this condition we have that:

$$\frac{\Gamma}{\omega_0} = \frac{1}{Q_T}$$

In conclusion we have that for a Lorentzian filter with losses the transmittance is a Lorentzian line with a full width give by equation C.18 and transmittance at resonance given by Eqn. C.18.

C. Channel drop configuration

The channel drop configuration for waveguide-cavity system in one where the cavity is located next to the waveguide. Light traveling through the waveguide is evanescently coupled into the cavity; the transmittance there will be a "drop" in the signal with respect to a reference in which there is only a waveguide and no cavity. From the drop of the signal and the width of the drop is possible to obtain the total quality factor and the radiative quality factor of the cavity. The configuration for this coupling scheme is shown in figure C.5.

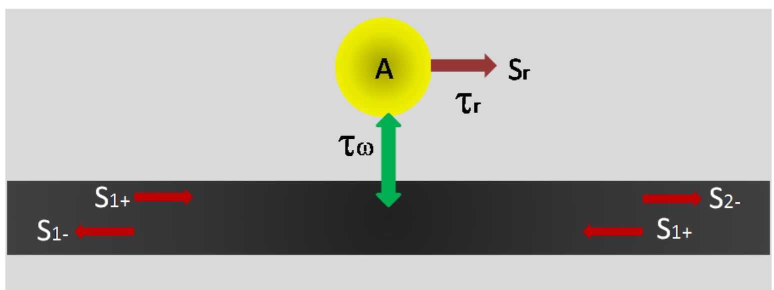

Figure C.5 Channel drop configuration

For simplification here we consider that the system is symmetric and the observation planes for the S parameter are located at the same distance from the cavity. The first order coupled equations for the systems are the following.

$$\frac{dA}{dt} = -i\omega_0 A - \frac{A}{\tau_\omega} - \frac{A}{\tau_r} + \alpha_1 S_{1+} + \alpha_2 S_{2+} \tag{C.20}$$

$$S_{1,2-} = \beta_{1,2} S_{2,1+} - \gamma_{1,2} A \tag{C.21}$$

$$S_r = \kappa A \tag{C.22}$$

By symmetry we have that $\beta=\beta_1=\beta_2$, $\alpha=\alpha_1=\alpha_2$ and $\gamma=\gamma_1=\gamma_2$. Considering weak coupling we have that α,γ, and $1/\tau_\omega$ are small.

Our objective is to calculate the coupling factors α, β, and γ. To do this we first consider a cavity that is decoupled from the waveguide. Thus we have that $1/\tau_\omega=\alpha=\gamma=0$.

The coupled equation simplifies to:

$$\frac{dA}{dt} = -i\omega_0 A - \frac{A}{\tau_r} \tag{C.23}$$

$$S_{1,2-} = \beta_{1,2} S_{2,1+} \tag{C.24}$$

$$S_r = \kappa A \tag{C.25}$$

The energy conservation for systems require that energy leaking from the cavity to be equal to the flux escaping from the cavity, i.e. it requires that:

$$-\frac{dA^*A}{dt} = \frac{2A^*A}{\tau_r} = |\kappa|^2 A^*A = |S_r|^2$$

The above equation is obtained by multiplying equation C.14 by A^* and adding the complex conjugated of the result. From here we derive that:

$$\kappa = \sqrt{\frac{2}{\tau_r}} \tag{C.26}$$

Also we have that the energy traveling to the waveguide is conserved therefore we have that:

$$\beta = -1 \tag{C.27}$$

Now lets consider that the coupling is weak and there is not input flux, i.e. $S_{1,2+} = 0$. The energy present in the cavity will decay into the waveguide and also radiated out of the slab as shown in figure C.6(a).

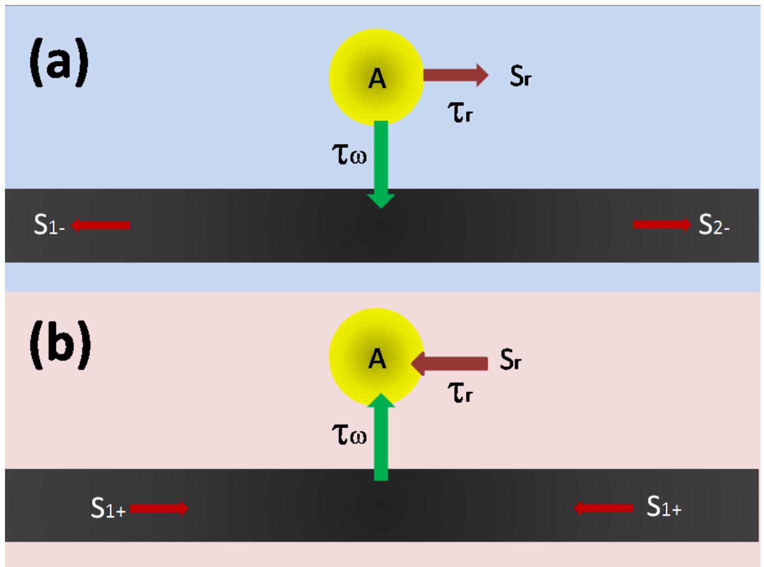

Figure C.6 (a) Cavity decaying into the waveguide and frees space (b) Time reversal solution, here the power in the cavity is increasing by in coupling radiation.

Here we have that the mode a couple equations reduce to:

$$\frac{dA}{dt} = -i\omega_0 A - \frac{A}{\tau_\omega} - \frac{A}{\tau_r} \quad \text{(C.28)}$$

$$S_{1,2-} = -\gamma A \quad \text{(C.29)}$$

$$S_r = \kappa \sqrt{\frac{2}{\tau_r}} A \quad \text{(C.30)}$$

Energy conservation requires that the energy lost by the cavity to be equal to the flux leaking into the waveguide plus the energy leaking out of the slab. Thus energy conservation requires:

$$-\frac{dA^*A}{dt} = 2\left(\frac{1}{\tau_\omega} + \frac{1}{\tau_r}\right)A^*A = 2|\gamma|^2A^*A + \frac{2}{\tau_r}A^*A$$

From here we have that the coupling from the cavity into the waveguide is given by:

$$\gamma = \sqrt{\frac{1}{\tau_\omega}} \tag{C.31}$$

Finally lets use the time reversal symmetry as shown in figure C.6 (b). In this case the direction of the flux is inverted i.e. $S_{1,2-} = 0$, while the flux S_r is now revered; it's energy is coupling from the exterior into the cavity. The corresponding time reversal equations are:

$$-\frac{dA}{dt} = i\omega_0 A - \frac{A}{\tau_\omega} - \frac{A}{\tau_r} - \alpha S_{1+} - \alpha S_{2+} \tag{C.32}$$

$$0 = -S_{2,1+} - \sqrt{\frac{1}{\tau_\omega}}A \tag{C.33}$$

$$-S_r = \sqrt{\frac{2}{\tau_r}}A \tag{C.34}$$

Energy conservation requires that the energy increase in the cavity to be equal to the energy coming from the fluxes. However, since the fluxes S_{1+} and S_{2+} traveling through the waveguide are equal in magnitude by symmetry and traveling in opposed direction, these two fluxes cancel each other and, the net flux in then just given by S_r, from energy conservation we can derive that:

$$\frac{dA^*A}{dt} = \left[2\left(\frac{1}{\tau_\omega} + \frac{1}{\tau_r}\right) - 2\alpha\sqrt{\frac{1}{\tau_\omega}}\right] A^*A = \frac{2}{\tau_r} A^*A$$

From here we have that the coupling into the cavity is given by:

$$\alpha = \sqrt{\frac{1}{\tau_\omega}} \tag{C.35}$$

Finally the couple mode theory for the channel drop is given by:

$$\frac{dA}{dt} = -i\omega_0 A - \frac{A}{\tau_\omega} - \frac{A}{\tau_r} + \sqrt{\frac{2}{\tau_\omega}} S_{1+} + \sqrt{\frac{2}{\tau_\omega}} S_{2+} \tag{C.36}$$

$$S_{1,2-} = S_{2,1+} - \sqrt{\frac{2}{\tau_\omega}} A \tag{C.37}$$

$$S_r = \sqrt{\frac{2}{\tau_r}} A \tag{C.38}$$

Now lets show how the filtering actually work. Consider figure C.5, for the normal filtering operation we have that there is no input from the right, i.e $S_{2+} = 0$. Considering a harmonic field in the cavity the couple mode equation C.26 and C.27 reduce to:

$$-i\omega = -i\omega_0 A - \frac{A}{\tau_\omega} - \frac{A}{\tau_r} + \sqrt{\frac{1}{\tau_\omega}} S_{1+} \tag{C.39}$$

$$S_{1-} = -\sqrt{\frac{1}{\tau_\omega}} A \tag{C.40}$$

$$S_{2-} = S_{1+} - \sqrt{\frac{1}{\tau_\omega}} A \tag{C.41}$$

This system is easily solved, for S_{1-}, S_{2-} and S_{1+} as a function of A.

$$S_{1+} = \sqrt{\tau_\omega}\left[i(\omega - \omega_0) + \left(\frac{1}{\tau_r} + \frac{1}{\tau_\omega}\right)\right] A$$

$$S_{1-} = -\sqrt{\frac{1}{\tau_\omega}} A$$

$$S_{2-} = \sqrt{\tau_\omega}\left[i(\omega - \omega_0) + \frac{1}{\tau_r}\right] A$$

From here the transmittance and reflection coefficient can be written as:

$$T(\omega) = \left|\frac{S_{2-}}{S_{1+}}\right|^2 = \frac{(\omega - \omega_0)^2 + \frac{1}{\tau_r{}^2}}{(\omega - \omega_0)^2 + \left(\frac{1}{\tau_r} + \frac{1}{\tau_\omega}\right)^2} \tag{C.42}$$

$$R(\omega) = \left|\frac{S_{2-}}{S_{1+}}\right|^2 = \frac{\frac{1}{\tau_\omega{}^2}}{(\omega - \omega_0)^2 + \left(\frac{1}{\tau_r} + \frac{1}{\tau_\omega}\right)^2} \tag{C.43}$$

We can define the quality factors as the following:

$$\frac{1}{Q_r} = \frac{2}{\omega_0 \tau_r}$$

$$\frac{1}{Q_\omega} = \frac{2}{\omega_0 \tau_\omega}$$

$$\frac{1}{Q_T} = \frac{1}{Q_r} + \frac{1}{Q_\omega} = \frac{2}{\omega_0 \tau_r} + \frac{2}{\omega_0 \tau_\omega}$$

The transmission and reflection coefficients can be rewritten as:

$$T(\omega) = \left|\frac{S_{2-}}{S_{1+}}\right|^2 = \frac{\left(\frac{\omega - \omega_0}{\omega_0}\right)^2 + \frac{1}{4{Q_r}^2}}{\left(\frac{\omega - \omega_0}{\omega_0}\right)^2 + \frac{1}{4Q_T^2}} \tag{C.44}$$

$$R(\omega) = \left|\frac{S_{2-}}{S_{1+}}\right|^2 = \frac{\frac{1}{4{Q_\omega}^2}}{\left(\frac{\omega - \omega_0}{\omega_0}\right)^2 + \frac{1}{4Q_T^2}} \tag{C.45}$$

The transmittance given by equation C.44 corresponds to a Lorentzian drop with respect to a reference line as shown in figure C.7.

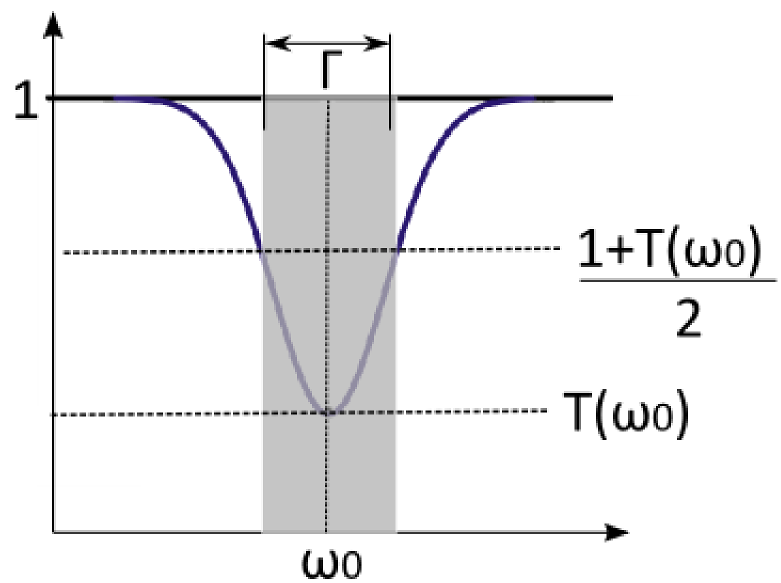

Figure C.7 Channel drop transmittance spectrum.

We have that the Q of the cavity is obtained from the full width at half maxima of the drop by $Q_T = \omega_0/\Gamma$, and that at resonance we have that:

$$T(\omega_0) = \left(\frac{Q_T}{Q_r}\right)^2$$

The magnitude of the drop depends on the total Q_T factor of the cavity and Q_r the radiative quality factor. To have a significant drop we require both to be in same order of magnitude. This is easily obtained even for very high Q_T since Q_ω could be increase faster than Q_r by just increasing the distance between the waveguide and the cavity. These represent an advantage over the Lorentzian filter since the magnitude of peak in the transmittance involves the ratio of Q_T and Q_ω in which the waveguide coupling decrease more quickly that the radiative loss and therefore yields a very low transmittance. In principle the channel drop scheme could be used to measure very high Q cavities up to the point that material loss became important.

Appendix D. Fabrication recipes.

The fabrication process consists of a single lithography step following a reactive ion etching. The photoresist used in the lithography is changed for the different samples according to the thickness and the corresponding etching time.

A. Carrier wafer coating

This process is for the preparation of the carrier wafer used during the etching process, for this purpose we use a silicon wafer with a thickness of around 500 μm. For the wafer coating we use the Plasma Enhance Chemical Vapor Deposition (PECVD) Plasma-Therm model 790 system. This system uses a capacitively-coupled RF plasma source produced between two parallel aluminum plates. The typical deposition rate is 400 A/min. at 300 mT pressure for a 250°C deposition.

[1] Wafer cleaning and drying takes two minutes in an ultra sound bath of Acetone, Isopropanol and Methanol and DI water. Followed with N2 dry and 5 minutes on the 110 C hot plate.

[2] PECVD clean and coating of the chamber takes 10 minutes at 250°C.

[3] PECVD deposition of 2 or 6 microns depending of the thickness of the samples to construct.

B. *Handling wafer preparation*

For the construction of samples with a thickness of 50 μm, due to the fragility, we used a handling wafer. For the thicker samples this step is omitted.

[1] We used a piece of silicon large enough for the samples and coated it following the procedure for the carrier wafer. This piece of coated silicon will be the handle wafer.

[2] We clean and dry for two minutes in a ultra sound bath of Acetone, Isopropanol and Methanol and DI water. Followed with N2 dry and 5 minutes in the 110 C hot plate.

[3] Spin photoresist Az4110 on the handling wafer at 4k rpm for 30 seconds.

[4] Put the sample onto the handle wafer and apply uniform pressure on the sample; I used a rectangular glass slide and a small weight (an empty small bottle, two or three ounces in volume, used to storage small quantities of photoresist).

[5] Bake for about 5 to 10 minutes on the 95°C hot plate will help the sample stick to the handling wafer.

C. *Lithography process*

In this part of the process we use the handling wafer for the 50 μm thick samples or just the wafer for the thicker samples. The specific process for each of the three samples sets are:

1. TE photonic crystal samples 1 THz

[1] Cleaning and drying for two minutes in a ultra sound bath of Acetone, Isopropanol and Methanol and DI water. Followed with N2 dry and 5 minutes in the 110 C hot plate.

[2] Spining the AZ4210 photoresist at 4k rpm for 30 seconds.

[3] Baking at 95°C for 60 seconds.

[4] Edge removal[7].

[5] Expose for 15 seconds.

[6] Develop in Az400K diluted 1:4 for 70 seconds or until inspected under the microscope that the features are clearly defined using a yellow light filter.

2. TM photonic crystals sample 1 THz

[1] Cleaning and drying for two minutes in an ultra sound bath of Acetone, Isopropanol and Methanol and DI water. Followed with N2 dry and 5 minutes in the 110 C hot plate.

[2] Due to the thickness of photoresist used for this set of samples we need to promote adherence; so we spin the HDMS at 3500 rpm for 30 seconds prior to the photoresist.

[3] Spin-on SPR220-7.0 resist at 3500 rpm for 45.

[7] Edge removal is a optional step but in general leads to better results due to a better contact between the sample and the photomask.

[4] Bake at 115°C for 120 seconds.

[5] Edge removal.

[6] Expose for 60 seconds.

[7] Wait for 5 minutes to complete the reaction.

[8] Develop MF701 for 70 seconds or until inspected under the microscope the features are clearly defined using a yellow light.

3. TE photonic samples 240 GHz

[1] Cleaning and drying for two minutes in a ultra sound bath of Acetone, Isopropanol and Methanol and DI water. Followed with N2 dry and 5 minutes in the 110 C hot plate.

[2] Spin AZ4330 photoresist at 4k rpm for 30 seconds.

[3] Bake at 95°C for 60 seconds.

[4] Edge removal.

[5] Expose for 20 seconds.

[6] Develop in Az400K diluted 1:4 for 90 seconds or until inspected under the microscope the features are clearly defined using a yellow light.

D. Etching process

The etching was done using a Silicon Deep Reactive Ion Etching system (SiRIE) Plasma-Therm 770 SLR. The system has an Inductively Coupled Plasma (ICP) coil which also is coupled to an independent radio frequency supply (used to control the generated plasma). This system is dedicated to deep etching in silicon and is specially suited for the fabrication for Micro Electric Mechanical systems (MEMs). In our case our samples has a range of thickness from 50 μm to 380 μm and this systems produces high aspect ratio structures. The etching process consists of two steps: First, a polymer deposition for passivation using C4F8 in which there is no substrate bias, Second, is an etching cycle using a SF6 / Ar mixture with a substrate bias.

We use Si02 coated silicon wafers as carrier wafers and photoresist patterned samples. The etch rate of silicon and Si2 is 200:1 while the etch rate ratio of the silicon photoresist is 80:1. The etch rate is highly dependent on the exposed silicon; large open areas etches slower than small open area. Also high aspect ratio features also etch slower than more open areas.

The first step of the process is a chamber clean out using a dedicated batch process called season process. I usually use this step due to the recommendation of the person in charge of the etcher. This process is recommended if the machine has not been use in a couple of days. However it is recommended for consistency to have the chamber in the same condition every time samples are processed. It is common that more than one etch step is required however the cleaning only has to be done once at the beginning and not between each etch process. The season process is made with a blank silicon wafer.

Once the sample is ready for the etch process, it is mounted on the carrier wafer which is coated with Si02, the sample can be glued to the carrier either using a thin layer of photoresist or using Santovac. For convenience we used a few drop of Santovac while applying pressure on the sample. Here it is important to make sure that all excess oil is removed so that the wafer doesn't get stuck to the robot arm or inside the camber.

The time in the camber was calculated according to the thickness of the slab using the nominal etch rate of 2 μm per minute. The 50 μm samples spend in the chamber around 25 minutes. It could take up to several hours for the 380 μm samples at the nominal etch rate (~190 minutes). Its recommend to divide this time in several etch steps so the sample does not stay more than one hour inside the chamber. An estimate of the etch rate could be done by estimating the depth of the etch using a optical microscope because the etch rate in general is different from that of the nominal rate. In our case, most of the samples had a slower etch rate.

E. Unmount of the wafers

This is the simplest but no less important part of the process. It is not uncommon to break the sample at this the very last part of the process.

To remove the samples from the carrier wafer use Acetone and let it stays until it can be easily slid out of the wafer. For the case of the thin wafer that was glued to a handling wafer, an overnight bath in Acetone is needed. Cover the container with Aluminum foil to avoid evaporation.

F. Edge removal

After the spinning step an excess of photoresist may accumulate on the edge of the samples. This can produce make the sample stick to the photomask or just not have a proper contact with the photomask, so is recommended to remove the edges. Here we have two techniques that are commonly practiced:

Razor Blade

[1] Use a razor blade to scrape off resist from edges of the sample before baking.

[2] Soft-bake resist as described in the particular recipe.

Overexpose and overdevelop

[1] Expose the sample 1 mm from its edge for 3 times the normal exposure time. Use aluminum foil or any other material to block or absorb the UV light. Develop using the corresponding developer for at least twice the recommended time.

[2] Rinse with DI water and dry the sample with nitrogen.

[3] Inspect with the microscope using yellow light to verify the edge are removed. If need it redo the process

Appendix E. Thin sample thickness measurement.

We estimate the thickness of the slab by measuring FTIR transmission normal to the sample. We did this with either directly on sample in a region where there was no photonic crystal structure or with a part of the wafer that was not processed. The FTIR transmittance experiments were done in the near mid-infrared with a KBr (Potassium Bromide) beam splitter using a DTGS (Deuterated Triglycine Sulfate) detector.

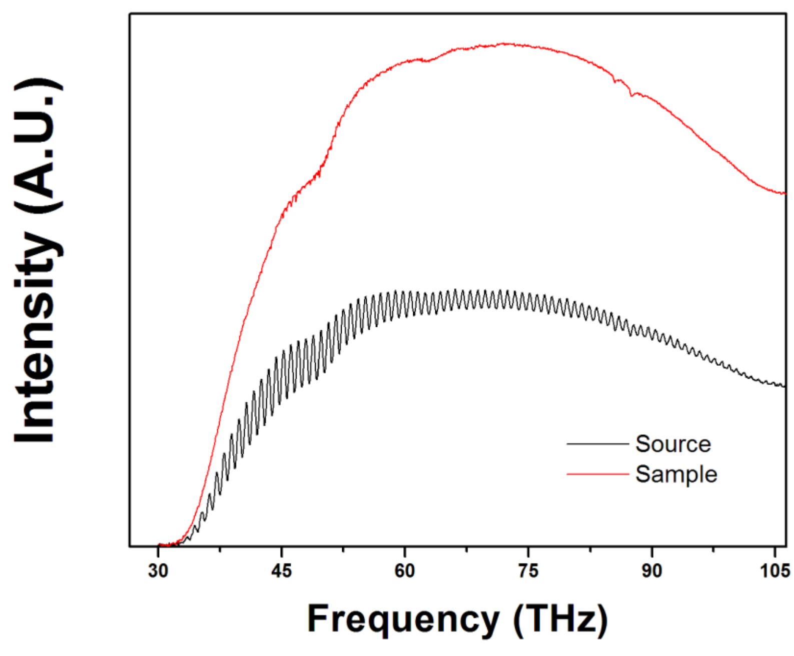

Figure E.1 The Fabry-Pérot interference is shown in the transmission normal to the wafer. The interference patters is a product of the finite thickness of the slab.

A typical transmission is shown in Figure E.1 where clearly resolved Fabry-Perot interferences fringes are observed when they are compared with the spectrum of the source. From the period of oscillation the thickness of the sample could be estimated.

A. Photonic crystal slab samples

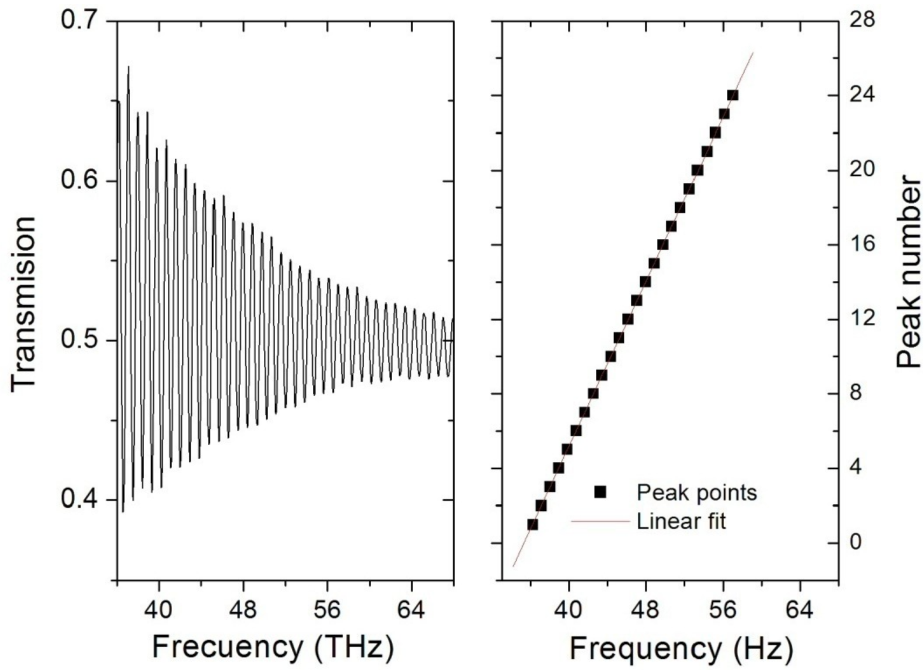

Figure E.2 Normalized FTIR transmittance normal to the slab. (b) Linear fit of the peak in the transmittance, the calculated slop δ=0.9043 THz which corresponds a slab thickness of t=48.56 μm.

Figure E.2 (a) shows the normalized transmittance for the photonic crystal slab used in chapter 4. In this transmittance we used as a reference the source spectrum scaled by an arbitrary unit. The peak on the oscillation is linearly fit as shown in Figure E.2(b). The thickness of the slab is computed from the slope of the lines using the formula $t = c/2n\delta$; here n=3.416 is the index of refraction of Silicon in the 1 THz region [47] and δ=0.9043 is the period of the oscillation (inverse of slop of the line in Figure E.2 (b)). With these values we found the thickness is $t = 48.56 \pm 0.03\ \mu m$.

B. High Q photonic crystal samples

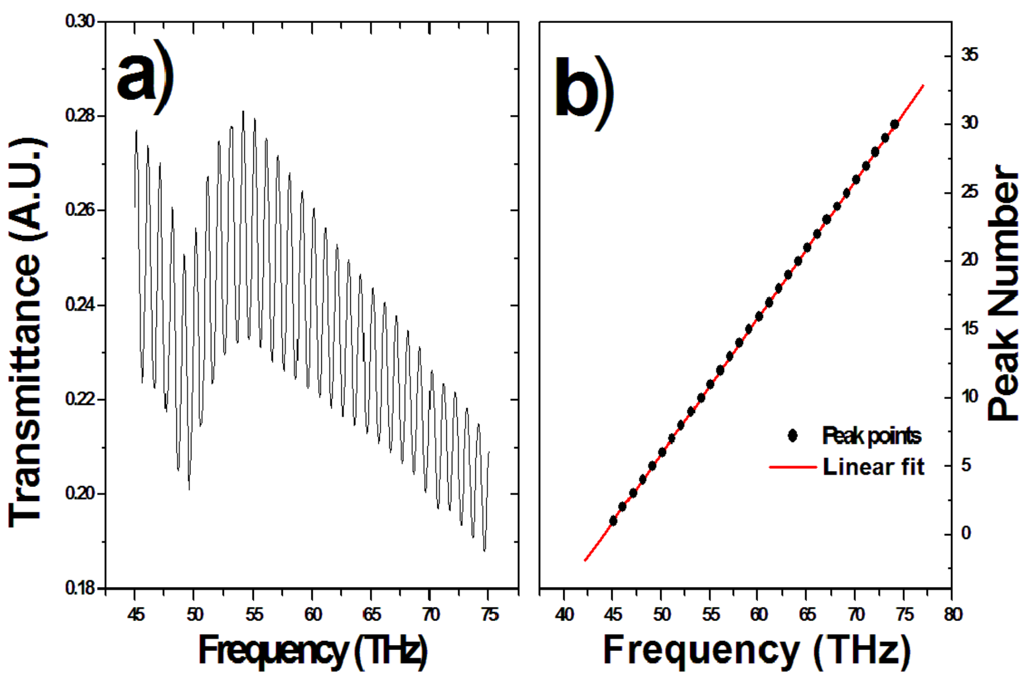

Figure E.3 (a) Normalized FTIR transmittance normal to the slab. (b) Linear fit of the peak in the transmittance, the calculated slop δ=0.9043 THz which correspond a slab thickness of t=48.56 μm.

For the High Q photonic crystal cavity the transmittance perpendicular to the slab in shown in Figure E.3(a), where clearly resolved Fabry-Perot oscillation are observed. From the fit of the peak position as a function of the frequency in Figure

E.3(b), we found that the Fabry-Perot oscillations have a frequency period of $\Delta f = 0.9999 \pm 0.0004$ THz. The corresponding thickness from the fit is $t = 43.83 \pm 0.02$. The thickness measurement was done in a single point measure in the center of the wafer with a beam size of several millimeters. The flatness across the wafer is specified by the manufacturer to be 2 μm so we estimate the thickness of the wafer to be $t = 44 \pm 2$ μm.

Appendix F. MPB and MEEP files.

In the present appendix we show the files used for the simulation in thesis. In each file we explain briefly the parameter that can be override by a command line. There are several parameter that are common to all the structures, these parameters are:

[1] ***r*** is the hole radius, for TE we used r=0.30 for TM we used r=0.465

[2] ***thick*** is the thickness of the slab; we used the dimensionless experimental thickness, typically for TE t=0.6 and for TM t=2.80.

[3] ***eps*** is the value for the dielectric constant for silicon t=11.68.

[4] ***resolution*** is the number of point per unit cell, default value 32 for pc band calculations, a value of 20 for TE cavity resonances and transmittance for TE photonic crystal; and 32 for TM cavity and transmittance for TM photonic crystals.

A. MPB : band diagram of a Photonic crystal

Here we present the code used for calculating the band diagram structure for a photonic crystal.

1. Specific parameters:

[1] ***num-bands*** number of bands to calculate

[2] ***k-interp*** number of point between two high symmetric used in the band diagram, the default value is 14.

[3] ***point*** optional parameter if only one point in the Brillouin Zone is desired.

2. CTL file

band.ctl ---

```
; Triangular lattice of air holes in dielectric
; the parameter used for this simulations are

; first, define the lattice vectors and k-points for a triangular lattice:
(define-param sz 10)
(set! geometry-lattice (make lattice (size 1 1 sz)
                         (basis1 (/ (sqrt 3) 2) 0.5)
                         (basis2 (/ (sqrt 3) 2) -0.5)))
(define-param kz 0) ; use non-zero kz to consider vertical propagation
(set! k-points (list (vector3 0 0 kz)          ; Gamma
                     (vector3 0 0.5 kz)        ; M
                     (vector3 (/ -3) (/ 3) kz) ; K
                    (vector3 0 0 kz) ))

; For simulating the whole diagram Gamma-M-K-Gamma
; use the paramenter k-interp and interpolates between
; the high symmetric point

(define-param k-interp 14)
(set! k-points (interpolate k-interp k-points))


; For runnin at specific point not the whole diagram
; uncomment the following two expressions (and comment the two above)

(define-param point (vector 3 0 0 0))
(set! k-points (list point))


; Here we define the geometry:

(define-param eps 11.68) ; the dielectric constant of the background
(define-param r 0.30) ; the hole radius
(define-param thick 0.6); the thickness of the slab


(set! geometry (append
(list  (make block (size infinity infinity thick) (center 0 0 0)(material (make
dielectric (epsilon eps) ))) )
(list (make cylinder (center 0) (material air)
                     (radius r) (height infinity)))))

; here are the resolution and number of bands for the simulation
(set-param! resolution 32)
(set-param! num-bands 16)


; here we select to run the te and tm bands if only one is desire
; comment the the other one.
```

```
(if (= kz 0)
    (begin
      (run-te)
      (run-tm))
    (run)) ; if kz != 0 there are no purely te and tm bands
```

End band.ctl --

3. Examples

[1] For calculating the band structure of a photonic crystal slab with a hole radius r=0.30 and thickness 0.575.

mpb r=*0.30* thick=*0.575 band.ctl* > band.out

[2] For calculating the band structure of a photonic crystal slab with a hole radius r=0.465 and thickness 2.81.

mpb r=*0.465* thick=*2.81 band.ctl* > band.out

B. MEEP: Waveguide dispersion relation

Here we present the code used for calculating the waveguide band diagram structure for a photonic crystal. The strategy used to calculate the waveguide dispersion, is to employ a pulse inside the optical gap of the photonic crystal structure, and look for the resonances for the waveguide structure employing the boundary conditions set by the Bloch function associate for each k vector from Γ to the zone boundary.

1. Specific parameter

[1] ***fcen*** is the center frequency used for calculating the waveguide modes.

[2] ***df*** is the frequency width used for the excitation pulse.

[3] ***k-inter*** is the number of point to calculate the waveguide dispersion relation from the Γ point to the boundary zone.

[4] ***point*** useful for running at a single reciprocal point.

2. CTL file

wgband.ctl --

```
; Some parameters to describe the geometry:
(reset-meep);
(define-param eps 11.682) ; dielectric constant of silicon
(define-param r 0.3) ; radius of holes

; The cell dimensions
(define-param sy (* 10 (sqrt 3)))
(define-param dpml 1) ; PML thickness
(define-param sx 1) ; size of cell in x direction
(define-param sz 5)
(define-param thick 0.575)
(define-param av false)
(set! eps-averaging? false)
(set! geometry-lattice (make lattice (size sx sy sz)))
(set-param! resolution 20)

; parameter of the excitation pulse
(define-param fcen 0.27) ; pulse center frequency
(define-param df 0.1)  ; pulse width (in frequency)

; array used for containing the photonic crystal
(define pc (list ))

; pc geometry

;### center hole
(do ((j  -4 (+ j 1))) (( > j 4))
              (set! pc (append pc (list (make cylinder (center 0 (* j (sqrt 3)))(material air)
(radius r) (height thick) ) )) ))
;### side holes
(do ((j -4 (+ j 1))) ((> j 3))
(do ((i -1 (+ i 1))) ((> i 0 ))
       (set! pc (append pc (list (make cylinder (center (+ i 0.5) (+ (/ (sqrt 3) 2) (* j (sqrt
3))))(material air) (radius r) (height thick) ) )) )))

;### covering the center hole
(set! pc (append pc (list (make cylinder (center 0 0 0)(material (make dielectric (epsilon eps)))
(radius r) (height thick) ) )) )


(set! geometry (append
                     (list (make block (center 0 0) (size infinity infinity thick) (material
(make dielectric (epsilon eps)))))
                     pc ))

(set! pml-layers
              (list  (make pml (direction Z) (thickness dpml))
                     (make pml (direction Y) (thickness  dpml))))


; for TM band diagram use Ez instead of Hz
(set! sources (list
                     (make source
                 (src (make gaussian-src (frequency fcen) (fwidth df)))
                 (component Hz)
                 (center 0.123 0 0)
```

```
                (size 0 0 thick))))

(set! symmetries
      (list
       (make mirror-sym (direction Y) (phase -1))
       (make mirror-sym (direction Z) (phase 1))))

; use a output directory
(use-output-directory)

;For calculating the dispersion relation from the gamma point to the Brillouin edge
(define-param k-interp 24); iterpolation
(run-k-points 600 (interpolate k-interp (list (vector3 0 0 0) (vector3 0.5 0 0))))


; if only point is requiere commend the two above expression and uncoomment
; the next three commands, also change Hz by Ez for TM polarization
;(define-param point 0) ;Brillouin boundary
;(set-param! k-point (vector3 point 0 0))
;(run-sources+ 600 (harminv Hz (vector3 0.1234 0 0) fcen df)))
```

End wgband.ctl ---

3. Examples

[1] For calculating the waveguide band structure of a photonic crystal slab with a hole radius r=0.30 and thickness 0.575; the waveguide dispersion is located inside the gap near 0.27 (c/a).

meep r=*0.30* thick=*0.575 fcen=0.27 df=0.2 wgband.ctl* > wgband.out

[2] For calculating the waveguide band structure of a photonic crystal slab with a hole radius r=0.465 and thickness 2.81; the waveguide dispersion in locateded inside the gap near 0.46 (c/a)

mpb r=*0.465* thick=*2.81 fcen=0.46 df=0.2 wgband.ctl* > wgband.out

C. MEEP: Transmittance through the photonic crystal

Here we present the code used for calculating the transmittance through the photonic crystal structure. We used several simulation using pulse with frequency with a moderate frequency width instead doing a single simulation using a very broad frequency single pulse.

user@pc: ~$ meep r=*r0* thick=*t* eps=*value* resolution=*value hds=disp* l3cav.ctl > l3cav.out

1. Specific parameters

[1] ***fcen*** is the center frequency used for calculating the waveguide modes.

[2] ***df*** is the frequency width used for the excitation pulse.

[3] ***nfreq*** is the number of frequencies used for calculating the transmittance.

2. CTL files

trans.ctl --

```
; Some parameters to describe the geometry:
(reset-meep);
(define-param eps 11.68) ; dielectric constant of waveguide
(define-param r 0.30) ; radius of holes

; The cell dimensions
(define-param sy (* 1 (sqrt 3))) ;
(define-param dpml 1) ; PML thickness
(define-param sx 30) ; size of cell in x direction
(define-param sz 5)
(define-param thick 0.6)
(define-param av false)
(set! eps-averaging? av)
(set! geometry-lattice (make lattice (size sx sy sz)))
(set-param! resolution 20)

;parameters of excitation pulse
(define-param fcen 0.27) ; pulse center frequency
(define-param df 0.1)  ; pulse width (in frequency)
(define-param nfreq 1000) ; number of frequencies at which to compute flux

; extra parameter of the structure
(define-param nx 22) ; number of holes in the gamma-j orientation
(define pc (list )) ; array used in the photonic crystal

; geometry of the photonic crystal
; ### center hole
(do ((i (* -1 (/ nx 2)) (+ i 1))) ((> i (/ nx 2 )))
       (set! pc (append pc (list (make cylinder (center i 0 0)(material air) (radius r) (height
thick) ) )) ))

;### side holes
(do ((i (* -1 (/ nx 2)) (+ i 1))) ((> i (- (/ nx 2 ) 1)))
(set! pc (append pc (list (make cylinder (center (+ i 0.5) (* -0.5 (sqrt 3)))(material air)
(radius r) (height thick) ) )) )
(set! pc (append pc (list (make cylinder (center (+ i 0.5) (* 0.5 (sqrt 3)))(material air)
(radius r) (height thick) ) )) ))
```

```
(set! geometry (append
                     (list (make block (center 0 0) (size infinity infinity thick) (material
(make dielectric (epsilon eps)))))
                     pc            ))

(set! pml-layers
              (list  (make pml (direction X) (thickness dpml))
                     (make pml (direction Z) (thickness dpml))))


; used Ez if for TM photonic crystal
(set! sources (list
                     (make source
                 (src (make gaussian-src (frequency fcen) (fwidth df)))
                 (component Hz)
                 (center -13 0 0)
                 (size 0 sy thick))))

(set! symmetries
      (list
       (make mirror-sym (direction Y) (phase -1))
       (make mirror-sym (direction Z) (phase 1))))

(define trans ; transmitted flux
        (add-flux fcen df nfreq
                  (make flux-region
                    (center 13 0) (size 0 sy thick)  )))

(use-output-directory)

(run-until 1000 )
(display-fluxes trans) ; print out the flux spectrum
```

End trans.ctl --

3. Examples

[1] For calculating the transmittance trough the photonic crystal. For the TE pc with a hole radius r=0.30 and thickness 0.575; the transmittance between 0.20(c/a) to 0.3(c/a) is calculate using the following command.

meep r=*0.30* thick=*0.575 fcen=0.25 df=0.2 trans.ctl* > trans.out

[2] For a TM photonic crystal slab with a hole radius r=0.465 and thickness 2.81; the transmittance between 0.4(c/a) to 0.5 (c/a) is calculated using the following command.

meep r=*0.465* thick=*2.81 fcen=0.45 df=0.2 trans.ctl* > trans.out

D. MEEP: L3 Cavity resonance

Here we present the code used for calculating the resonant modes of the L3 cavity. The calculation can also include the material loss if desired. It also possible to calculate the resonant mode for cavity in which the inner hole in the ΓJ orientation next to the cavity is displaced from its original lattice position, this displacement tunes the quality factor of the cavity.

1. Specific parameters

[1] ***fcen*** is the center frequency used for calculating the waveguide modes.

[2] ***df*** is the frequency width used for the excitation pulse.

[3] ***hds*** is the hole displacement from its original position, positive values increase the size of the cavity.

[4] ***loss*** is the material loss that could be include in the calculation.

2. CTL file

l3cav.ctl---

```
; Some parameters to describe the geometry:
(reset-meep);
(define-param eps 11.68) ; dielectric constant of waveguide
(define-param r 0.30) ; radius of holes

; The cell dimensions
(define-param sy (* 11 (sqrt 3))) ; size of cell in y direction about 5 mm with a=80mu
(define-param dpml 1) ; PML thickness
(define-param sx 25) ; size of cell in x direction
(define-param sz 5)
(define-param thick 0.6)
(define-param av false)
(set! eps-averaging? av)
(define-param hds 0) ; hole displacement
(set! geometry-lattice (make lattice (size sx (+ sy 2) sz)))

(set-param! resolution 20)

; pulse excitation parameters
(define-param fcen 0.27) ; pulse center frequency
(define-param df 0.1)  ; pulse width (in frequency)
```

```
; extra parameter used in the structure
(define-param nx 22); number of holes in the gamma-j orientation
(define pc (list )); array used for the pc structure

; In case of calculating the q factor with losses
(define-param loss 0)
(define-param fc fcen); center frequency for the loss (use the same value for fcen)

; geometry of the cavity

;### center holes in the strcutre
(do ((j  -5 (+ j 1))) (( > j 5))
(do ((i (* -1 (/ nx 2)) (+ i 1))) ((> i (/ nx 2 )))
              (set! pc (append pc (list (make cylinder (center i (* j (sqrt 3)))(material air)
(radius r) (height thick) ) )) )))

;### holes displaced in the unit cell
(do ((j -5 (+ j 1))) ((> j 4))
(do ((i (* -1 (/ nx 2)) (+ i 1))) ((> i (- (/ nx 2 ) 1)))
              (set! pc (append pc (list (make cylinder (center (+ i 0.5) (+ (/ (sqrt 3) 2) (* j
(sqrt 3))))(material air) (radius r) (height thick) ) )) )))

;### covering the holes in the center of the structure
(do ((i -2 (+ i 1))) ((> i 2 ))
       (set! pc (append pc (list (make cylinder (center i 0)(material (make medium (epsilon eps)
(D-conductivity (* 2 pi fc loss)))) (radius r) (height thick) ) )) ))

;### making the holed displaced from the orginal positions
(set! pc (append pc (list (make cylinder (center (- 0 2 hds)  0 0) (material air) (radius r)
(height thick) ) )) )
(set! pc (append pc (list (make cylinder (center (+ 2 hds)  0 0) (material air) (radius r)
(height thick) ) )) )


(set! geometry (append
                     (list (make block (center 0 0) (size infinity infinity thick) (material
(make medium (epsilon eps)  (D-conductivity (* 2 pi fc loss)) ))))
                     pc ))

(set! pml-layers
              (list  (make pml (direction X) (thickness dpml))
                     (make pml (direction Z) (thickness dpml))
                     (make pml (direction Y) (thickness  dpml))))


(set! sources (list
               (make source
                 (src (make gaussian-src (frequency fcen) (fwidth df)))
                 (component Hz)
                 (center 0.5 0 0)
                 (size 0 0 0))
              (make source
                 (src (make gaussian-src (frequency fcen) (fwidth df)))
                 (component Hz)
                 (center -0.5 0 0)
                 (size 0 0 0) (amplitude -1))
))

(set! symmetries
      (list
          (make mirror-sym (direction X) (phase 1))
           (make mirror-sym (direction Y) (phase -1))
              (make mirror-sym (direction Z) (phase 1))))

(use-output-directory)

(run-sources+ 1000
(after-sources
(harminv Hz (vector3 0.5 0 0) fcen df)
(harminv Hz (vector3 0.5 0.2 0.2) fcen df)))
```

End l3cav.ctl--

3. Examples

[1] For calculating the cavity resonance of the L3 cavity with a hole radius r=0.30 and thickness 0.6.

meep r=*0.30* thick=*0.6 fcen=0.27 df=0.2 l3cav.ctl > l3cav.out*

[2] For calculating the L3 cavity with a hole radius *r=0.3*, thickness 0.575, with loss 0.001 and the near hole displace by 0.05 *a*.

meep r=0.30 thick=0.575 fcen=0.27 df=0.2 hds=0.05 loss=0.001 l3cav.ctl > a.out

E. MEEP: L3 Lorentzian filter

Here we present the code used for calculating the resonant modes of the L3 cavity inserted into a photonic crystal waveguide to form a Lorentzian filter. Material loss could be included and also the displacement of the inner hole delimiting the cavity inside the waveguide.

1. Specific parameters

[1] ***fcen*** is the center frequency used for calculating the waveguide modes.

[2] ***df*** is the frequency width used for the excitation pulse.

[3] ***hds*** is the hole displacement from its original position, positive values increase the size of the cavity.

[4] ***loss*** is the material loss that could be include in the calculation.

2. CTL file

l3filter.ctl ---

```
; Some parameters to describe the geometry:
(reset-meep);
(define-param eps 11.68) ; dielectric constant of waveguide
(define-param r 0.30) ; radius of holes

; The cell dimensions
(define-param sy (* 11 (sqrt 3))) ; size of cell in y direction about 5 mm with a=80mu
(define-param dpml 1) ; PML thickness
(define-param sx 25) ; size of cell in x direction
(define-param sz 5)
(define-param thick 0.6)
(define-param av false)
(set! eps-averaging? av)
(define-param hds 0) ; hole displacement
(set! geometry-lattice (make lattice (size sx (+ sy 2) sz)))

(set-param! resolution 20)

; pulse excitation parameters
(define-param fcen 0.27) ; pulse center frequency
(define-param df 0.1)  ; pulse width (in frequency)

; extra parameter used in the structure
(define-param nx 22); number of holes in the gamma-j orientation
(define pc (list )); array used for the pc structure

; In case of calculating the q factor with losses
(define-param loss 0)
(define-param fc fcen); center frequency for the loss (use the same value for fcen)

; geometry of the cavity

(do ((j  -5 (+ j 1))) (( > j 5))
(do ((i (* -1 (/ nx 2)) (+ i 1))) ((> i (/ nx 2 )))
              (set! pc (append pc (list (make cylinder (center i (* j (sqrt 3)))(material air)
(radius r) (height thick) ) )) )))

(do ((j -5 (+ j 1))) ((> j 4))
(do ((i (* -1 (/ nx 2)) (+ i 1))) ((> i (- (/ nx 2 ) 1)))
              (set! pc (append pc (list (make cylinder (center (+ i 0.5) (+ (/ (sqrt 3) 2) (* j
(sqrt 3))))(material air) (radius r) (height thick) ) )) )))

(do ((i (* -1 (/ nx 2)) (+ i 1))) ((> i (/ nx 2 )))
       (set! pc (append pc (list (make cylinder (center i 0)(material (make medium (epsilon eps)
(D-conductivity (* 2 pi fc loss)))) (radius r) (height thick) ) )) ))


(set! pc (append pc (list (make cylinder (center (- 0 2 hds)  0 0) (material air) (radius r) (height thick) ) ))
)
(set! pc (append pc (list (make cylinder (center (+ 2 hds)  0 0) (material air) (radius r) (height thick) ) )) )
(set! pc (append pc (list (make cylinder (center 3 0 0) (material air) (radius r) (height thick) ))) )
(set! pc (append pc (list (make cylinder (center -3 0 0) (material air) (radius r) (height thick) ) )) )
(set! pc (append pc (list (make cylinder (center 4 0 0) (material air) (radius r) (height thick) ) )) )
(set! pc (append pc (list (make cylinder (center -4 0 0) (material air) (radius r) (height thick) ) )) )
; for four hole barrier unncomment the next two holes
;(set! pc (append pc (list (make cylinder (center 5 0 0) (material air) (radius r) (height thick) ) )) )
;(set! pc (append pc (list (make cylinder (center -5 0 0) (material air) (radius r) (height thick) ) )) )
; for five hole barrier unncomment the next two holes
;(set! pc (append pc (list (make cylinder (center 6 0 0) (material air) (radius r) (height thick) ) )) )
;(set! pc (append pc (list (make cylinder (center -6 0 0) (material air) (radius r) (height thick) ) )) )
; for six hole barrier unncomment the next two holes
;(set! pc (append pc (list (make cylinder (center 7 0 0) (material air) (radius r) (height thick) ) )) )
;(set! pc (append pc (list (make cylinder (center -7 0 0) (material air) (radius r) (height thick) ) )) )


(set! geometry (append
                     (list (make block (center 0 0) (size infinity infinity thick) (material
(make medium (epsilon eps)  (D-conductivity (* 2 pi fc loss)) ))))
                    pc ))

(set! pml-layers
```

```
              (list  (make pml (direction X) (thickness dpml))
                     (make pml (direction Z) (thickness dpml))
                     (make pml (direction Y) (thickness  dpml))))


(set! sources (list
              (make source
                 (src (make gaussian-src (frequency fcen) (fwidth df)))
                 (component Hz)
                 (center 0.5 0 0)
                 (size 0 0 0))
              (make source
                 (src (make gaussian-src (frequency fcen) (fwidth df)))
                 (component Hz)
                 (center -0.5 0 0)
                 (size 0 0 0) (amplitude -1))))


(set! symmetries
      (list
          (make mirror-sym (direction X) (phase 1))
           (make mirror-sym (direction Y) (phase -1))
              (make mirror-sym (direction Z) (phase 1))))

(use-output-directory)

(run-sources+ 1000
(after-sources
(harminv Hz (vector3 0.5 0 0) fcen df)
(harminv Hz (vector3 0.5 0.2 0.2) fcen df)))
```

End l3filter.ctl ---

3. Examples

[1] For calculating the cavity resonance of the Lorentzian filter with a hole radius r=0.30 and thickness 0.6.

meep r=*0.30* thick=*0.6 fcen=0.27 df=0.2 l3filter.ctl > l3filter.out*

[2] For calculating the Lorentzian filter with a hole radius *r=0.3*, thickness 0.575, with loss 0.001 and the near hole displace by 0.05 *a*.

meep r=0.30 thick=0.575 fcen=0.27 df=0.2 hds=0.05 loss=0.001 l3filter.ctl > filter.out

F. MEEP: L2 Lorentzian filter

Here we present the code used for calculating the resonant modes of the L2 cavity inserted into a photonic crystal waveguide to form a Lorentzian filter.

1. Specific parameters

[1] ***fcen*** is the center frequency used for calculating the waveguide modes.

[2] ***df*** is the frequency width used for the excitation pulse.

2. CTL file

L2filter.ctl ---

```
; Some parameters to describe the geometry:
(reset-meep);
(define-param eps 11.682) ; dielectric constant of waveguide
(define-param r 0.46) ; radius of holes

; The cell dimensions
(define-param sy (* 10 (sqrt 3)))
(define-param dpml 1) ; PML thickness
(define-param sx 22) ; size of cell in x direction
(define-param sz 6)
(define-param thick 2.72)
(define-param av false)
(set! eps-averaging? av)
(set! geometry-lattice (make lattice (size sx sy sz)))
(set-param! resolution 32)

; excitation pulse parameters
(define-param fcen 0.5) ; pulse center frequency
(define-param df 0.2)  ; pulse width (in frequency)

; extra parameters of the structure
(define pc (list )) ;array for the pc crystal
(define nx 18) ;number of holes along the gamma-j orientation

; L2 cavity geometry

;### center hole in the pc structure
(do ((j  -4 (+ j 1))) (( > j 4))
(do ((i (* -1 (/ nx 2)) (+ i 1))) ((> i (+ 1 (/ nx 2 ))))
              (set! pc (append pc (list (make cylinder (center (- i 0.5) (* j (sqrt 3)))(material
air) (radius r) (height thick) ) )) )))

;### side hole in the pc structure
(do ((j -4 (+ j 1))) ((> j 3))
(do ((i (* -1 (/ nx 2)) (+ i 1))) ((> i (/ nx 2 ) ))
              (set! pc (append pc (list (make cylinder (center i (+ (/ (sqrt 3) 2) (* j (sqrt
3))))(material air) (radius r) (height thick) ) )) )))

;### covering the holes to form the waveguide
(do ((i (* -1 (/ nx 2)) (+ i 1))) ((> i (+ (/ nx 2 ) 1)))
       (set! pc (append pc (list (make cylinder (center (- i 0.5) 0) (material (make dielectric
(epsilon eps))) (radius r) (height thick) ) )) ))

;### holes delimiting the cavity inside the waveguide
(set! pc (append pc (list (make cylinder (center 1.5 0) (material air) (radius r) (height thick) ) )) )
(set! pc (append pc (list (make cylinder (center 2.5 0) (material air) (radius r) (height thick) ) )) )
(set! pc (append pc (list (make cylinder (center -1.5 0) (material air) (radius r) (height thick) ) )) )
(set! pc (append pc (list (make cylinder (center -2.5 0) (material air) (radius r) (height thick) ) )) )


(set! geometry (append
                     (list (make block (center 0 0) (size infinity infinity thick) (material
(make dielectric (epsilon eps)))))
                     pc ))

(set! pml-layers
              (list  (make pml (direction X) (thickness dpml))
```

```
                    (make pml (direction Z) (thickness dpml))
                    (make pml (direction Y) (thickness  dpml))))

(set! sources (list
              (make source
                 (src (make gaussian-src (frequency fcen) (fwidth df)))
                 (component Ez)
                 (center 0.5 0 0)
                (size 0 0 thick))
              (make source
                 (src (make gaussian-src (frequency fcen) (fwidth df)))
                (component Ez)
                 (center -0.5 0 0)
                 (size 0 0 thick) (amplitude -1))))



(set! symmetries
      (list
           (make mirror-sym (direction X) (phase -1))
           (make mirror-sym (direction Y) (phase 1))
              (make mirror-sym (direction Z) (phase -1))))

(use-output-directory)

(run-sources+ 600
(after-sources
(harminv Ez (vector3 0.3 0 0) fcen df)
(harminv Ez (vector3 0.5 0 0) fcen df)
(harminv Ez (vector3  0.25 0.23 0.25) fcen df)))
```

3. Examples

[1] For calculating the cavity resonance of the Lorentzian filter with a hole radius r=0.465 and thickness 2.81.

meep r=*0.465* thick=*0.2.8 fcen=0.46 df=0.1 L2filter.ctl > l2filter.out*

G. MEEP: L3 Channel drop

Here we present the code used for calculating the resonant modes of the L3 cavity located next to the waveguide in the channel drop configuration. The calculation include displacement of the inner hole delimiting the cavity inside the waveguide and the distance from the waveguide

1. Specific parameters

[1] ***fcen*** is the center frequency used for calculating the waveguide modes.

[2] ***df*** is the frequency width used for the excitation pulse.

[3] ***hds*** is the hole displacement from its original position, positive values increase the size of the cavity.

[4] ***lp*** is the distance from the waveguide; the default value is 0.5 corresponding to two line of holes. For three holes the value correspond to *lp=1.0*, for four holes *lp=1.5*.

2. CTL file

cdrop.ctl -----------------------------

```
; Some parameters to describe the geometry:
(reset-meep);
(define-param eps 11.68) ; dielectric constant of waveguide
(define-param r 0.30) ; radius of holes

; The cell dimensions
(define-param sy 22) ; size of cell in y direction about 5 mm with a=80mu
(define-param dpml 1) ; PML thickness
(define-param sx 22) ; size of cell in x direction
(define-param sz 5)
(define-param thick 0.6)
(define-param av false)
(set! eps-averaging? av)
(set! geometry-lattice (make lattice (size sx sy sz)))
(set-param! resolution 20)

; pulse excitation parameters
(define-param fcen 0.27) ; pulse center frequency
(define-param df 0.1)  ; pulse width (in frequency)
(define-param nx 22) ; number of holes along the gamma-j orientation

; extra parameters of the structure
(define pc (list ))
(define-param lp 0.5) ;two lines of holes separation
(define-param hds 0)

; geometry of the crystal

; center hole of the crystal
(do ((j  -6 (+ j 1))) (( > j 6))
(do ((i (* -1 (/ nx 2)) (+ i 1))) ((> i (/ nx 2 )))
            (set! pc (append pc (list (make cylinder (center i (* j (sqrt 3)))(material air)
(radius r) (height thick) ) )) )))

; displaced hole in the crystal
(do ((j 6 (+ j 1))) ((> j 5))
(do ((i (* -1 (/ nx 2)) (+ i 1))) ((> i (- (/ nx 2 ) 1)))
            (set! pc (append pc (list (make cylinder (center (+ i 0.5) (+ (/ (sqrt 3) 2) (* j
(sqrt 3))))(material air) (radius r) (height thick) ) )) )))


; here we cover the holes to form the l3 cavity
(set! pc (append pc (list (make cylinder (center 0  (sqrt 3)) (material (make dielectric (epsilon
eps))) (radius r) (height thick) ) )) )
(set! pc (append pc (list (make cylinder (center -1  (sqrt 3)) (material (make dielectric
(epsilon eps))) (radius r) (height thick) ) )) )
```

```
(set! pc (append pc (list (make cylinder (center 1  (sqrt 3)) (material (make dielectric (epsilon
eps))) (radius r) (height thick) ) )) )
(set! pc (append pc (list (make cylinder (center -2  (sqrt 3)) (material (make dielectric
(epsilon eps))) (radius r) (height thick) ) )) )
(set! pc (append pc (list (make cylinder (center 2  (sqrt 3)) (material (make dielectric (epsilon
eps))) (radius r) (height thick) ) )) )
(set! pc (append pc (list (make cylinder (center (- 0 2 hds)  (sqrt 3)) (material air) (radius r)
(height thick) ) )) )
(set! pc (append pc (list (make cylinder (center (+ 2 hds)  (sqrt 3)) (material air) (radius r)
(height thick) ) )) )

; here we set the waveguide in the channel drop
(set! pc (append pc (list (make block (center 0 (* ( - 0 lp) (sqrt 3)) ) (material (make
dielectric (epsilon eps)))  (size infinity 0.8 thick)   )) ))

(set! geometry (append
                      (list (make block (center 0 0) (size infinity infinity thick) (material
(make dielectric (epsilon eps)))))
                      pc           ))

(set! pml-layers
              (list  (make pml (direction X) (thickness (* 2 dpml)))
                     (make pml (direction Z) (thickness dpml))
                     (make pml (direction Y) (thickness  (* 2 dpml)))))

(set! sources (list
                     (make source
                 (src (make gaussian-src (frequency fcen) (fwidth df)))
                 (component Ey)
                 (center 0 (sqrt 3) 0)
                 (size 0 0 0))))

(set! symmetries
      (list
         (make mirror-sym (direction X) (phase 1))
          ;(make mirror-sym (direction Y) (phase -1))
              (make mirror-sym (direction Z) (phase 1))))

(use-output-directory)

(run-sources+ 600
(after-sources
(harminv Ey (vector3 0 (sqrt 3) 0) fcen df)
(harminv Hz (vector3 1.3 (+ 0.2 (sqrt 3)) 0.2) fcen df)))
```

End cdrop.ctl --

3. Examples

[1] For calculating the cavity resonance of the cannel drop, for a hole radius r=0.30, thickness 0.6 located two lines from the waveguide

meep r=*0.30* thick=*0.6 fcen=0.27 df=0.2 lp=0.5 cdrop.ctl > cdrop.out*

[2] For calculating the cavity resonance of the channel drop, for a hole radius *r=0.3*, thickness 0.575, three lines from the waveguide and the near hole displace by 0.05 *a*.

meep r=0.30 thick=0.575 fcen=0.27 df=0.2 hds=0.05 loss=0.001 l3filter.ctl > filter.out

Appendix G. Sample inventory.

The samples measured in this thesis are the following ones:

A. *Photonic crystal gap 1.4 THz*

Only two samples labeled PC-Jorientation 40-50 cm^{-1}.

B. *TE Photonic crystal waveguide and cavities at 1 THz*

Lattice constant	Waveguide	Lorentzian filter	Comments:
76	L76R30WG	L76R30H2	Published
78	L78R30WG	L78R30H2	Not published
80	L80R30WG	L80R30H2	Published
78	78WG	78H2	Not published

C. *TM Photonic crystal waveguide and cavities at 1 THz*

Lattice constant	Lorentzian filter	Comments:
150	150H2	
145	145H2	Not published
140	150H2	
135	150H2	

D. TE 240 Waveguide and Photonic crystal cavity

1. Direct coupling scheme

Displacement	Label	Comments
0.00	L3H3	
0.05	L3H3S05	
0.10	L3H3S10	
0.15	L3H3S15	
0.20	L3H3S20	
0.25	L3H3S25	
0.00	L3H2	
0.00	L3H4	
N/A	WGR28	Waveguide with r=0.28
N/A	WGR30	Waveguide with r=0.30

2. Channel drop coupling

Displacement	Two hole	Three holes	Comments
0.00	N2DS00	N3DS00	
0.05	N2DS05	N3DS05	
0.10	N2DS10	N3DS10	
0.15	N2DS15	N3DS15	
0.20	N2DS20	N3DS20	
0.25	N2DS25	N3DS25	
N/A	WG		Waveguide

References

[1] L S Rothman et al., "The HITRAN 2008 molecular spectroscopic database," *Journal of Quantitative Spectroscopy and Radiative Transfer*, vol. **110** , no. 9-10, p. 533, (2009).

[2] Jing Xu, Kevin W. Plaxco, and S. James Allen, "Probing the collective vibrational dynamics of a protein in liquid water by terahertz absorption spectroscopy," *Protein Science*, vol. **15** , p. 1175, (2006).

[3] P Boucaud et al., "Saturation of THz-frequency intraband absorption in InAs/GaAs quantum dot molecules," *Applied Physics Letters*, vol. **77** , no. 4, p. 510, (2000).

[4] Andrea G Markelz, Joseph R Knab, Jing Yin Chen, and Yunfen He, "Protein dynamical transition in terahertz dielectric response," *Chemical Physics Letters*, vol. **442** , no. 4-6, p. 413, (2007).

[5] Bin Xu, Qing Hu, and Michael R Melloch, "Electrically pumped tunable terahertz emitter based on intersubband transition," *Applied Physics Letters*, vol. **71** , no. 4, p. 440, (1997).

[6] M Lončar, A Scherer, and Y Qiu, "Photonic crystal laser sources for chemical detection," *Applied Physics Letters*, vol. **82** , p. 4648, jun (2003).

[7] Marco Lončar, Tomoyuki Yoshie, Axel Scherer, Pawan Gogna, and Yueming Qiu, "Low-threshold photonic crystal laser," *Applied Physics Letters*, vol. **81** , no. 15, p. 2680, (2002).

[8] J. He et al., "Growth, Structural, and Optical Properties of Self-Assembled (In,Ga)As Quantum Posts on GaAs," *Nano Letters*, vol. **7** , no. 3, p. 802, (2007).

[9] G. Feher, "Electron Spin Resonance on Donors in Silicon," *Physical Review*, vol. **114** , no. 5, p. 1219, (1959).

[10] A. M. Tyryshkin, S. A. Lyon, A. V. Astashkin, and A. M. Raitsimring, "Electron spin relaxation times of phosphorus donors in silicon," *Physical Review B*, vol. **68** , p. 193207, (2003).

[11] Timothy D Drysdale, Richard J Blaikie, and David R Cumming, "Calculated and measured transmittance of a tunable metallic photonic crystal filter for terahertz frequencies," *Applied Physics Letters*, vol. **83** , no. 26, pp. 5362, (2003).

[12] L Fekete, F Kadlec, H Nemec, and P Ku\vzel, "Fast one-dimensional photonic crystal modulators for the terahertz range," *Opt. Express*, vol. **15** , no. 14, p. 8898, (2007).

[13] Li Jiusheng, "Terahertz modulator using photonic crystals," *OPTICS COMMUNICATIONS*, vol. **269** , no. 1, p. 98, (2007).

[14] Hamza Kurt and D S Citrin, "Photonic crystals for biochemical sensing in the terahertz region," *Applied Physics Letters*, vol. **87** , no. 4, p. 041108, (2005).

[15] Naolci Matsumoto, Takuji Nakagawa, Keisuke Kageyama, Nobuyuki Wada, and Yukio Sakabe, "Terahertz band-pass filter fabricated by multilayer ceramic technology," *JAPANESE JOURNAL OF APPLIED PHYSICS PART 1-REGULAR PAPERS BRIEF COMMUNICATIONS & REVIEW PAPERS*, vol. **45** , no. 9B, p. 7499, SEP (2006).

[16] H Nemec et al., "Highly tunable photonic crystal filter for the terahertz range," *Opt. Lett.*, vol. **30** , no. 5, p 549, (2005).

[17] Lorenzo Sirigu et al., "Terahertz Quantum Cascade Lasers based on two-dimensional photonic crystal resonators," *OPTICS EXPRESS*, vol. **16** , no. 8, p. 5206, APR 14 (2008).

[18] Hui Zhang, Peng Guo, Ping Chen, Shengjiang Chang, and Jinghe Yuan, "Liquid-crystal-filled photonic crystal for terahertz switch and filter," *J. Opt. Soc. Am. B*, vol. **26** , no. 1, p. 101, (2009).

[19] Tomoyuki Yoshie, Jelena Vučković, Axel Scherer, Hao Chen, and Dennis Deppe, "High quality two-dimensional photonic crystal slab cavities," *Applied Physics Letters*, vol. **79** , no. 26, p. 4289, (2001).

[20] Y Akahane, T Asano, B S Song, and S Noda, "Investigation of high-Q channel drop filters using donor-type defects in two-dimensional photonic crystal slabs," *Applied Physics Letters*, vol. **83** , p. 1512, aug (2003).

[21] A L Bingham and D Grischkowsky, "Terahertz two-dimensional high-Q photonic crystal waveguide cavities," *Opt. Lett.*, vol. **33** , no. 4, p. 348, (2008).

[22] Makoto Yamada and Kyohei Sakuda, "Analysis of almost-periodic distributed feedback slab waveguides via a fundamental matrix approach," *Applied Optics*, vol. **26** , no. 16, p. 3474, (1987).

[23] JW Strutt, "On the Maintenance of Vibrations by Forces of Double Frequency, and on the Propagation of Waves Through a Medium Endowed with a Periodic Structure," *Phil. Mag., S.5*, vol. **24** , p. 145, (1887).

[24] Bong-Shik Song, Susumu Noda, Takashi Asano, and Yoshihiro Akahane, "Ultra-high-Q photonic double-heterostructure nanocavityl," *Nature Materials*, vol. **4** , no. 3, p. 207, (2003).

[25] Yoshihiro Akahane, Takashi Asano, Bong-Shik Song, and Susumu Noda, "High-Q photonic nanocavity in a two-dimensional photonic crystal," *Nature*, vol. **425** , no. 8, p. 944, (2003).

[26] Steven G Johnson and J D Joannopoulos, "Block-iterative frequency-domain methods for Maxwell's equations in a planewave basis," *Opt. Express*, vol. **8** , no. 3, p. 173, (2001).

[27] Allen Taflove and Susan C Hagness, *Computational Electrodynamics: The Finite-Difference Time-Domain Method*, 3rd ed.: Artech House, Incorporated, 2005.

[28] N Jukam and M S Sherwin, "Two-dimensional terahertz photonic crystals fabricated by deep reactive ion etching in Si," *Applied Physics Letters*, vol. **83** , p. 21, (2003).

[29] Hongqian Sun et al., "Bragg Reflectors and 2-D Photonic Crystals in the THz Region," *Terahertz for Military and Security Applications III*, (2005).

[30] M S Sherwin, A Imamoglu, and T Montroy, *Phis. Rev. A*, vol. **60** , p. 3508, (1999).

[31] A Imamoglu et al., *Phis. Rev. Lett.*, vol. **83** , p. 4207, (1999).

[32] J Dai, W Zhang, J Zhang, and Daniel Grischkowsky, "Terahertz time-domain spectroscopy characterization of the far-infrared absorption and index of refraction of high-resistivity, float-zone silicon," *JOSA B*, vol. **21** , no. 7, p. 1379, (2004).

[33] Cristo Yee, Nathan Jukam, and Mark Sherwin, "Transmission of single mode ultrathin terahertz photonic crystal slabs," *Applied Physics Letters*, vol. **91** , no. 19, p. 194104, (2007).

[34] Zhongping Jian, Jeremy Pearce, and Daniel M Mittleman, "Defect modes in photonic crystal slabs studied using terahertz time-domainspectroscopy," *Optics Letters*, vol. **29** , no. 17, p. 2067, (2004).

[35] Kelley Rivoire, Andrei Faraon, and Jelena Vuckovic, "Gallium phosphide photonic crystal nanocavities in the visible," *Applied Physics Letters*, vol. **93** , no. 6, p. 063103, (2008).

[36] Sei-ichi Takayama, Hitoshi Kitagawa, Yoshinori Tanaka, Takashi Asano, and Susumu Noda, "Experimental demonstration of complete photonic band gap in two-dimensional photonic crystal slabs," *Applied Physics Letters*, vol. **87** , no. 6, p. 061107, (2005).

[37] K Tomoda S. Noda and A Chutinan, *Science*, vol. **289** , p. 604, (2000).

[38] D Englund, I Fushman, and J Vučković, "General recipe for designing photonic crystal cavities," *Optics Express*, vol. **13** , p. 5961, (2005).

[39] B Song, S Noda, T Asano, and Y Akahane, *Nature*, vol. **4** , p. 207, (2005).

[40] Steven G Johnson, Attila Mekis, Shanhui Fan, and John D Joannopoulos, *Molding the Flow of Light*. Piscataway, NJ, USA: IEEE Educational Activities Department, 2001, vol. 3.

[41] Cristo M. Yee and Mark S. Sherwin, "High-Q terahertz microcavities in silicon photonic crystal slabs," *Applied Physics Letters*, vol. **94** , p. 154104 , (2009).

[42] R. Mendis and D. Grischkowsky, "Undistorted guided-wave propagation of subpicosecond terahertz pulses," *Optics Letters*, vol. **26** , p. 846, (2001).

[43] Andrei Faraon, Waks Edo, Dirk Englund, Ilya Fushman, and Jelena Vučković, "Efficient photonic crystal cavity-waveguide couplers," *Applied Physics Letters*, vol. **90** , no. 7, p. 073102, (2007).

[44] Waks Edo and Jelena Vučković, "Coupled mode theory for photonic crystal cavity-waveguide interaction," *Optics Express*, vol. **13** , no. 13, p. 5064, (2005).

[45] Mohamed Nurul Afsar and Chi Hua, "Millimeter wave complex refractive index, complex dielectric permittivity and loss tangent of extra high purity and compensated silicon," *International Journal of Infrared and Millimeter Waves*, vol. **15** , no. 7, p. 1181, (1994).

[46] C. J. M. Smitha et al., "Coupled guide and cavity in a two-dimensional photonic crystal," *Applied Physics Letters*, vol. **78** , p. 1487, (2001).

[47] Edward D Palik, Ed., *Handbook of Optical Constants of Solids*. New York: Academic Press, 1985, vol. 1.